REPORT DOCUMENTATION PAGE

Form Approved
OMB No. 0704-0188

1. REPORT DATE *(DD-MM-YYYY)*	2. REPORT TYPE	3. DATES COVERED *(From - To)*
10-05-2011		

4. TITLE AND SUBTITLE
Directed Energy Beam Jitter Mitigation Using the Line-of-Sight Reference Frame

5a. CONTRACT NUMBER

5b. GRANT NUMBER

5c. PROGRAM ELEMENT NUMBER

6. AUTHOR(S)
Dunn, Nicholas Connor

5d. PROJECT NUMBER

5e. TASK NUMBER

5f. WORK UNIT NUMBER

7. PERFORMING ORGANIZATION NAME(S) AND ADDRESS(ES)

8. PERFORMING ORGANIZATION REPORT NUMBER

9. SPONSORING/MONITORING AGENCY NAME(S) AND ADDRESS(ES)
U.S. Naval Academy
Annapolis, MD 21402

10. SPONSOR/MONITOR'S ACRONYM(S)

11. SPONSOR/MONITOR'S REPORT NUMBER(S)
Trident Scholar Report no. 398 (2011)

12. DISTRIBUTION/AVAILABILITY STATEMENT
This document has been approved for public release; its distribution is UNLIMITED

13. SUPPLEMENTARY NOTES

14. ABSTRACT

This research developed a beam control system that reduces the root mean square jitter angle by 50% and the jitter angle standard deviation by 60% using on-platform orientation sensors against a moving target. This system demonstrates the necessary subsystems for isolated-platform, feed forward beam control in the line-of-sight and has the potential to minimize source laser power and engagement time requirements in practical directed energy weapon systems.

15. SUBJECT TERMS
laser, directed energy, line-of-sight, beam control, jitter

16. SECURITY CLASSIFICATION OF:			17. LIMITATION OF ABSTRACT	18. NUMBER OF PAGES	19a. NAME OF RESPONSIBLE PERSON
a. REPORT	b. ABSTRACT	c. THIS PAGE		137	19b. TELEPHONE NUMBER *(Include area code)*

U.S.N.A. --- Trident Scholar project report; no. 398 (2011)

DIRECTED ENERGY BEAM JITTER MITIGATION USING THE LINE-OF-SIGHT REFERENCE FRAME

by

Midshipman 1/C N. Connor Dunn
United States Naval Academy
Annapolis, Maryland

_____
(signature)

Certification of Adviser Approval

CDR R.J. Watkins, USN
Mechanical Engineering Department

_____
(signature)

_____
(date)

Acceptance for the Trident Scholar Committee

Professor Carl E. Wick
Associate Director of Midshipman Research

_____
(signature)

_____
(date)

Abstract

Directed energy weapons will dramatically increase naval capability by offering extreme precision, scalable power, speed-of-light engagement, and a nearly limitless magazine. Precise beam control is essential for maximizing the energy on target and damaging the target structure. Directed energy weapon systems operating in a maritime combat environment, however, will be mounted on dynamic platforms that are subject to jitter-inducing mechanical vibrations. Jitter is any deviation of the beam from its intended path due to platform induced vibrations or atmospheric effects. Jitter dramatically decreases the energy on target by displacing the beam from the aimpoint. The Office of Naval Research (ONR) Directed Energy Weapon Program has tasked researchers at the United States Naval Academy (USNA) to address this issue. Trident Scholar Ensign Matt Roberts developed a feed forward jitter compensation beam control system with the USNA Directed Energy Research Center that calculates and mitigates beam jitter due to platform vibrations. The purpose of this research is to increase the technology readiness level of this beam control system. Outside of the laboratory environment, off-platform orientation references are unavailable. In order to isolate the platform, on-platform angular rate sensors and linear accelerometers are used to determine platform orientation. Once platform orientation is determined, the first fast steering mirror (FSM) in the optical train can be controlled by the jitter compensation system to mitigate jitter. In maritime combat environments, targets are also rarely stationary. The line-of-sight reference frame is established to allow the second FSM to direct the beam at targets moving relative to the source platform. This research developed a beam control system that reduces the root mean square jitter angle by 50% and the jitter angle standard deviation by 60% using on-platform orientation sensors against a moving target. This system demonstrates the necessary subsystems for isolated-platform, feed forward beam control in the line-of-sight and has the potential to minimize source laser power and engagement time requirements in practical directed energy weapon systems.

Acknowledgements

As with any technical undertaking of this magnitude, there are countless people that played a vital role in making my Trident Scholar research project such a rewarding experience. I would first like to thank Commander Joe Watkins, my primary research adviser. He has been the driving force behind directed energy research at USNA and spent countless hours in the lab helping me sort out problems. The excitement he displays and the encouragement he offers helped me tackle all of the frustrating and unexpected technical difficulties that arose during my research. I hope to model his technical leadership throughout my career. I would next like to thank Jesse Baldwin and Curtis Mayes of the USNA Technical Support Division. Their efforts to construct the beam control laboratory made this research possible. I would like to thank Ensign Matt Roberts who introduced me to the directed energy world. His Trident research provided the foundation without which my research would not have been possible. I would also like to thank the Office of Naval Research and especially Michael Deitchman, Deputy Chief of Naval Research, and Quentin Saulter, Directed Energy Program Manager, for funding directed energy research at USNA. I would also like to thank Rear Admiral Craig Steidle (Ret.) who has served as my mentor for the past three years. I am also very grateful to the Trident Scholar Committee here at USNA who have made this project possible. I would especially like to thank Professor Carl Wick, Commander Dave Myre, and Professor Mitchell Baker. I would also like to thank Cindi Gallagher of MSC for offering her artistic help in preparing my Trident poster. Lastly, I would like to thank my family and friends who have supported me in all of my endeavors.

Table of Contents

List of Figures

List of Tables

List of Symbols

α …… Angular acceleration

θ …… Angular position

……. Angular velocity

a …… Linear acceleration

d ……... Linear displacement

K_{cr} ……. Critical gain

K_p ……. Proportional gain

$\underline{n}$ …… Mirror normal vector

P_{cr} ……. Critical period

r …… Range

r_{AB} ……. Linear distance from point A to point B

t ……. Time

Δt ……... One time step

T_d …… Derivative time

T_i …… Integral time

v ……. Linear velocity

[M] …… Mirror transformation matrix

[O] ……. Optical transformation matrix

[P] ……. Platform LOS reference frame matrix

[Q] ……. Incoming LOS reference frame matrix

[R] ……. Outgoing LOS reference frame matrix

[S] ……. Laser outgoing LOS reference frame matrix

List of Acronyms

ARS ……. Angular rate sensor

FSMX …….. Fast steering mirror X

IA- # ……. Inertial actuator number #

LMS ……. Least mean square

LOS …….. Line-of-sight

NPS …….. Naval Postgraduate School

ONR ……. Office of Naval Research

OT- # …… On-Trak position sensing module number #

PI …….. Proportional integral

PSD …….. Position sensing detector

PSM ……. Position sensing module

RMS ……. Root mean square

USNA …….. United States Naval Academy

1 Introduction

1.1 Motivation

Directed energy systems will dramatically increase naval capabilities by offering scalable power, extreme precision, speed-of-light engagement, nearly limitless magazines, and low cost per shot. The ability to scale the power of directed energy systems for specific targets and environments, combined with the extreme precision necessary to make directed energy systems viable weapons, allows warfighters to minimize collateral damage. Directed energy systems deposit energy on the target at the speed of light, unlike missiles or bullets which require significant flight time to reach the target. This ability to engage targets nearly instantaneously is optimal for defensive situations during which the engagement time window is severely limited. Critical situations such as air defense often require that several missiles or bullets be fired before the first projectile nears the target to ensure a hit. Instantaneous indications of a target hit from directed energy systems minimize excess firing of the system. This permits more targets to be engaged in a shorter period of time. Furthermore, directed energy weapons have a magazine limited only by the platform's electrical power supply and are much less expensive per shot than current defensive missiles. Directed energy systems can also be used for free space optical communications. Currently, the Department of Defense relies heavily on radio frequencies to transmit information. The available bandwidth, however, is shrinking rapidly. Optical communications increases the range of frequencies available for information transmission.

The Directed Energy Weapons Program at the Office of Naval Research (ONR) is currently developing technology to allow the Navy to fight at the speed of light. Like all other weapons systems, a directed energy weapon must impart sufficient energy to a target to exceed a certain target damage threshold, generally about 10 kJ/cm^2,[1] or an optical communication sensor detection threshold. Therefore, maximizing energy on target is crucial. Researchers have battled with the countless factors that influence energy on target including beam source power, beam propagation in turbulent and maritime environments, and beam control in dynamic

[1] Nielsen, Philip E., *Effects of Directed Energy Weapons.* Directed Energy Professional Society: Albuquerque, NM. 2009. p. 16.

environments. With platform size limiting beam source size and power, minimizing losses by understanding atmospheric propagation and beam control in dynamic environments is crucial. ONR is funding researchers investigating these challenges at the Naval Postgraduate School (NPS), the United States Naval Academy (USNA), and other government laboratories and universities. It is the purpose of this research project to address aspects of the beam control challenge that apply specifically to U.S. Naval platforms.

The Navy intends to implement directed energy weapons on tactical fighters, helicopters, and ships. These dynamic platforms and their inherent mechanical vibrations induce jitter, or deviations of the beam from its intended path, that dramatically reduces the power on target. For example, 10 μ radians of jitter will reduce the intensity of a large 10 cm diameter beam by a factor of 400 at 100 km.[2] Jitter must be reduced as much as possible to minimize the power required or maximize the range of the system. The U.S. Air Force Airborne Laser (ABL) solution uses visual feedback from the target obtained with high-resolution cameras. This system is optimized for use in the upper atmosphere where the ABL will engage ballistic missiles in the boost phase. In the lower atmosphere and maritime environments, atmospheric conditions and limited platform size may inhibit accurate feedback using such a system. The ideal system should be able to fire a stabilized beam using only the known platform orientation and the target line of sight. Trident Scholar ENS Matt Roberts developed a feed-forward jitter error calculation algorithm for the USNA Directed Energy Beam Control and Effects Laboratory in 2009-2010 that was used as a starting point for this research project. In addition, this research investigated the control algorithms necessary to track a moving target using a line-of-sight (LOS) mode while removing platform jitter. In the maritime environment, targets are rarely stationary, and any practical system must be able to engage these moving targets. The USNA Directed Energy Beam Control system at the completion Robert's work used a fixed reference frame with a stationary target of known position and calculated the firing platform position for every time step. In the current research, the LOS reference frame is implemented in which only the target position relative to the firing or laser source platform must be known. This information is readily available from optical or radar target tracking systems. Additionally, the previous system

[2] Watkins, R. Joseph, "The Adaptive Control of Optical Beam Jitter," Ph.D. dissertation, U.S. Naval Postgraduate School, December 2004. pp. 1, 28-34.

required diode lasers that were fixed relative to the moving source platform pointed at on-platform Position Sensing Modules (PSMs) to determine platform position and orientation in the fixed reference frame. Such off-platform references are not available outside of the laboratory environment. Therefore, on-platform sensors, such as accelerometers and angular rate sensors, must be used to determine the source platform orientation. The goal of this project was to integrate the previous jitter correction algorithm with on-platform orientation sensors and target tracking capabilities to create a more realistic directed energy beam control system for Naval platforms. The USNA Directed Energy Beam Control and Effects Laboratory is used to implement these improvements to develop a directed energy beam control system capable of engaging targets moving in the LOS reference frame while minimizing platform-induced jitter. The resulting beam control system may serve as the proof of concept for future systems seeking to minimize the source laser power and the dwell time required to destroy a target or maximize the range at which a target may be engaged.

1.2 Background

Department of Defense research into directed energy systems began in the 1970s and 1980s for free space optical communication between satellites. In the 1980s, the Reagan administration created the Strategic Defense Initiative, better known as Star Wars, which called for satellite based directed energy weapons to shoot down Soviet ballistic missiles. However, lasers powerful enough to destroy a ballistic missile were too large to be mounted on satellites. The Air Force began the next generation of missile defense with the ABL program in the mid 1990s to shoot down ballistic missiles in the boost phase, culminating in the destruction of a missile in flight in 2010. The Army developed the Tactical High Energy Laser (THEL) in the late 1990s. This platform is a stationary, ground based system and requires large quantities of toxic chemicals to produce the powerful source laser. The Air Force has recently developed the Airborne Advanced Tactical Laser (ATL) for use against ground targets, however the system also uses a toxic chemical source for the laser and was prohibitively heavy for a tactical fighter or helicopter. The Navy has expressed increased interest in directed energy weapons with the advent of free electron lasers (FELs) and smaller, more powerful solid state lasers. FELs allow

operators to change the beam wavelength to minimize losses due to absorption as the beam propagates through the atmosphere. This is extremely important in the maritime environment in which absorption losses are a significant contributor to propagation losses. Solid state lasers compact enough to fit on tactical naval platforms with sufficient power for tactical applications are in development and show great promise. Researchers continue to develop smaller, more powerful lasers, and it is critical that the beam control systems necessary to employ them be ready once the power level is appropriate for operational use.

2 Experimental Setup and Procedure

2.1 Description of Major Components

Research for this project was conducted in the USNA Directed Energy Research Center's Beam Control and Effects Laboratory shown in Figure 1. It is configured for safe use of Class III-IV laser devices.

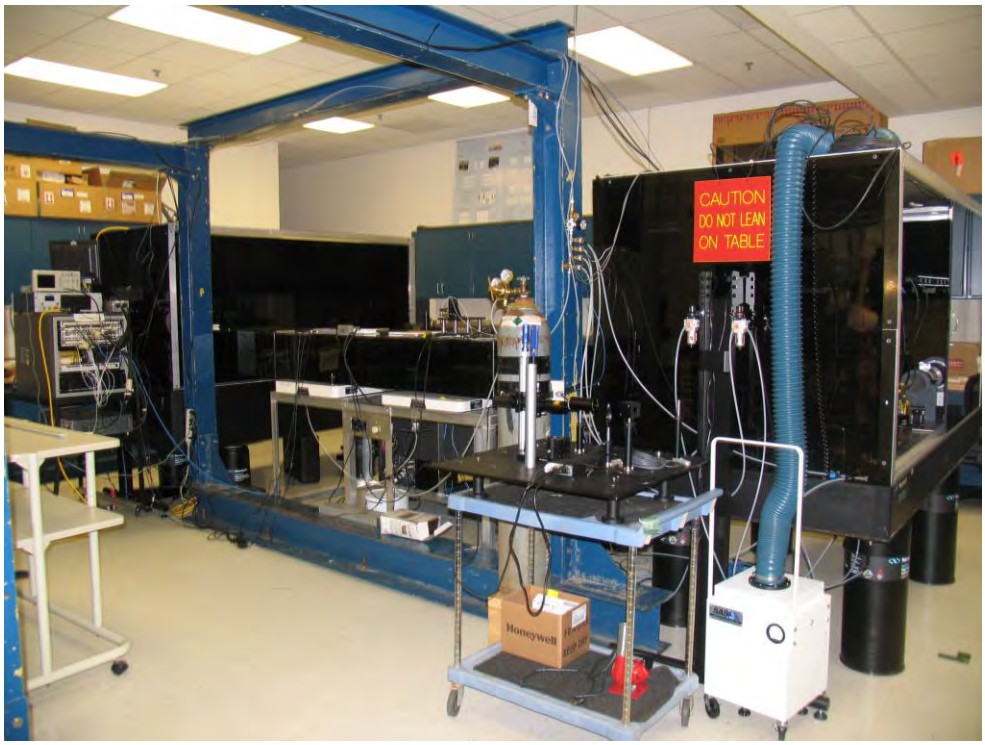

Figure 1. USNA Directed Energy Beam Control and Effects Laboratory

This research uses the configuration shown in the schematic in Figure 2 and the laboratory pictures in Figure 3 and Figure 4. Additional technical information for the hardware items used in the Directed Energy Beam Control and Effects Laboratory can be found in the appendices.

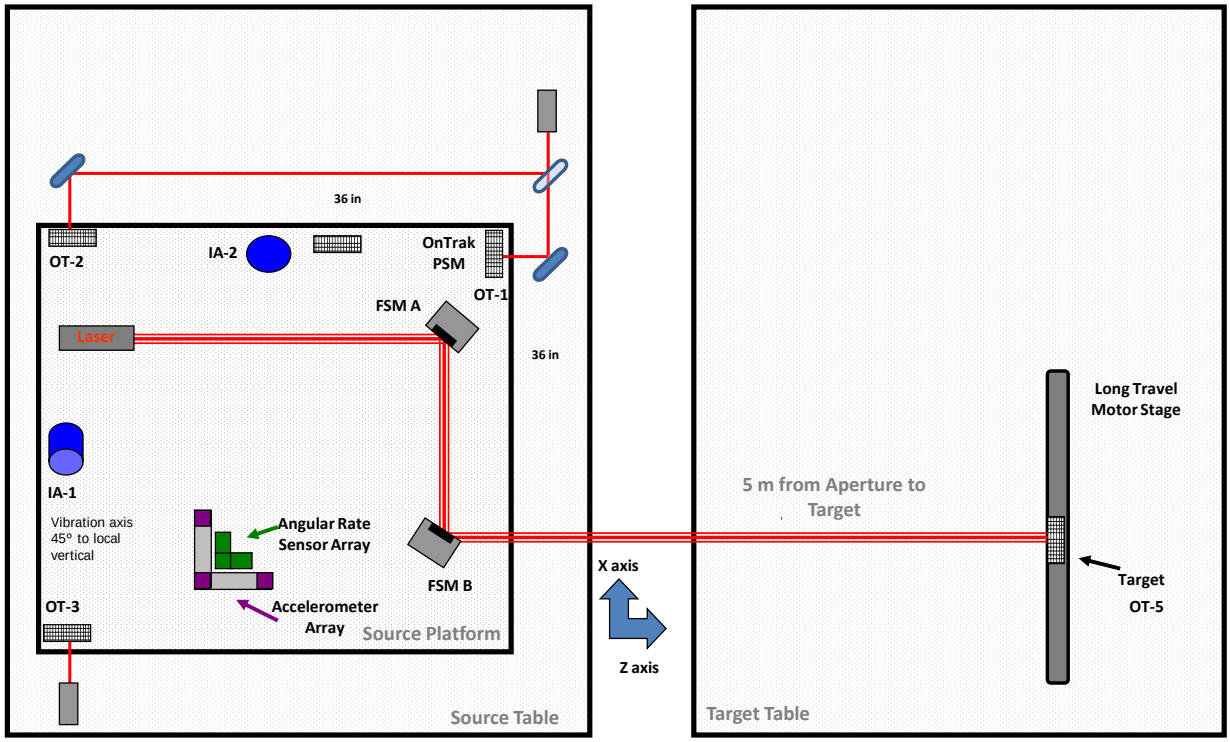

Figure 2. Experiment Configuration Schematic

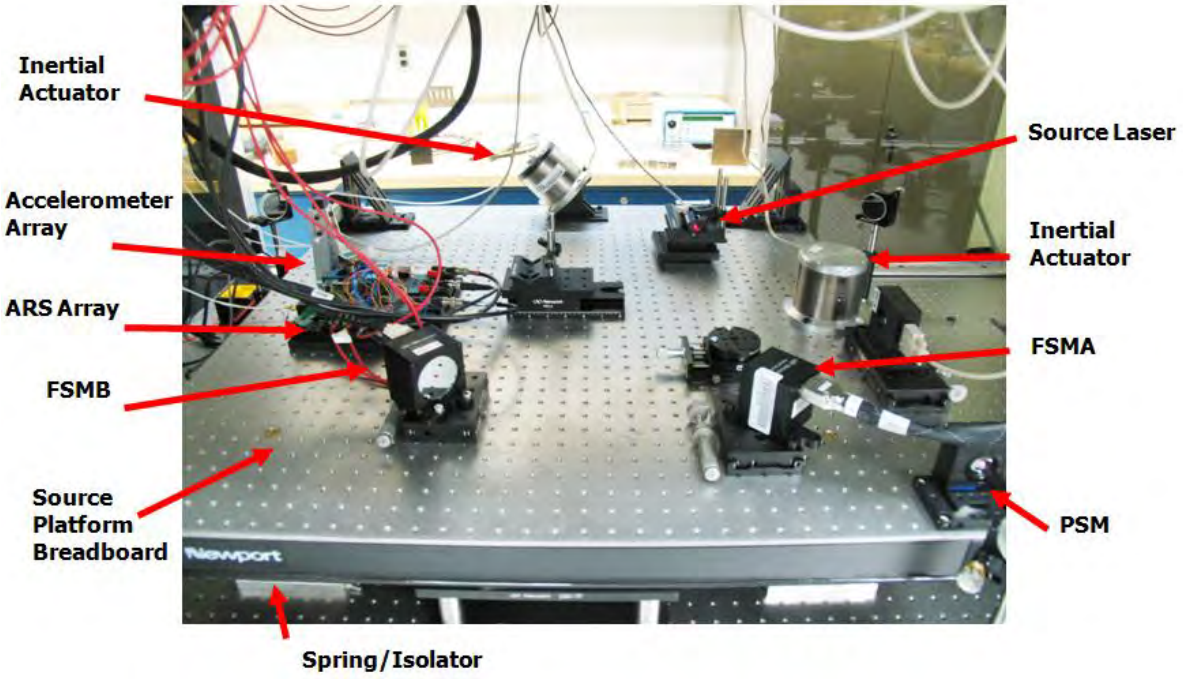

Figure 3. Source Platform Configuration

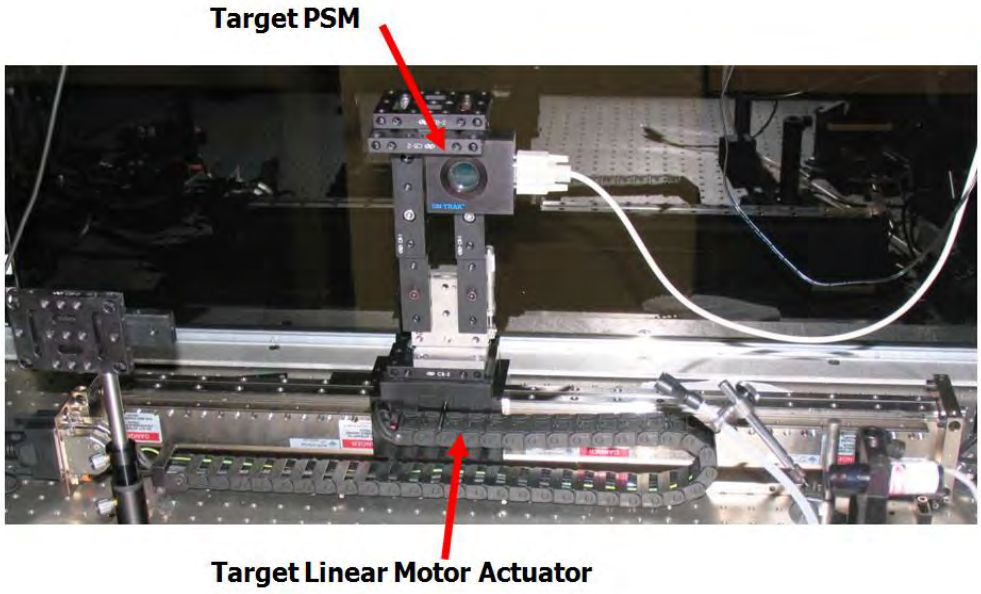

Figure 4. Target Platform

The platform reference frame used in this research is defined with the z-direction being downrange, the y-direction up, and the x-direction to the left of the platform.

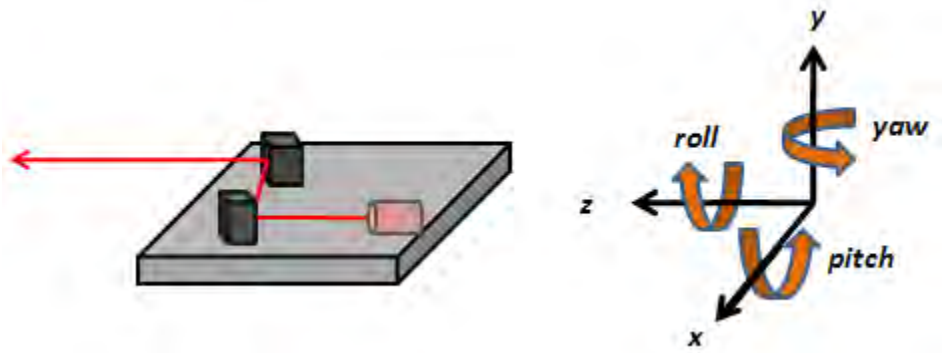

Figure 5. Platform Axis System

2.1.1 Angular Rate Sensors (ARS) Array

In order to isolate the platform from references not available outside of the laboratory, Applied Technology Associates (ATA) ARS-14 angular rate sensors (ARSs) mounted to the platform are used to measure the rate of platform rotational motion. The angular rate sensors are mounted in a mutually orthogonal configuration shown in Figure 6 and used to measure platform pitch, roll, and yaw. The array has a resolution of ±5 μrad/sec rms and a bandwidth of 2 to 1,000 Hz.[3] The ARS array is used are used as the primary internal instrument for measuring platform rotational motion.

[3] Applied Technology Associates, "ARS-14 MHD Angular Rate Sensor." 29 December 2009. <http://www.aptec.com/ATAWeb/ars-14_mhd_angular_rate_sensor.htm>.

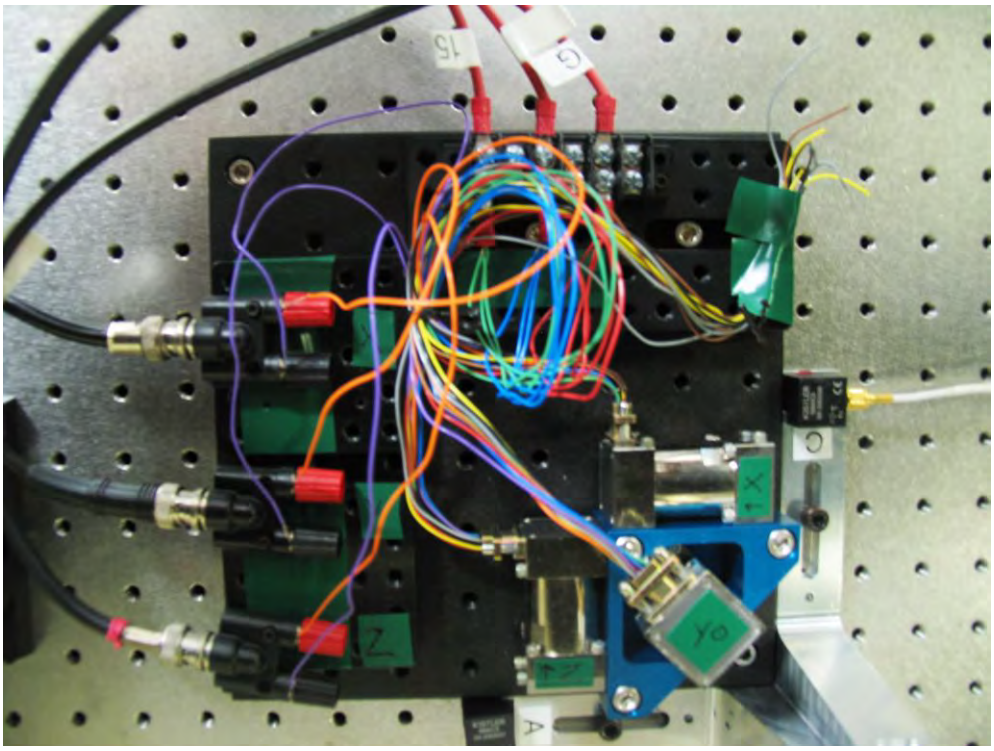

Figure 6. Angular Rate Sensor (ARS) Array

2.1.2 Accelerometer Array

Four Kistler 8690C5 linear accelerometers are mounted in a three dimensional array with each leg measuring 10 cm as shown in Figure 7. The accelerometers are capable of detecting up to ±5 *g* at between 1 and 3000 Hz with a sensitivity of 120 μ*g*.[4] The three dimensional array allows linear accelerations to be converted into rotational acceleration so that platform rotational motion may be measured. The accelerometer array is used as a secondary instrument for detecting platform rotational motion.

[4] Kistler, "PiezoBeam Accelerometer: Type 8690C." 24 April 2011.
< http://www.kistler.com/mx_en-us/925_Datasheets_dyn/productDatasheets.A1000.archive/Kistler.html>

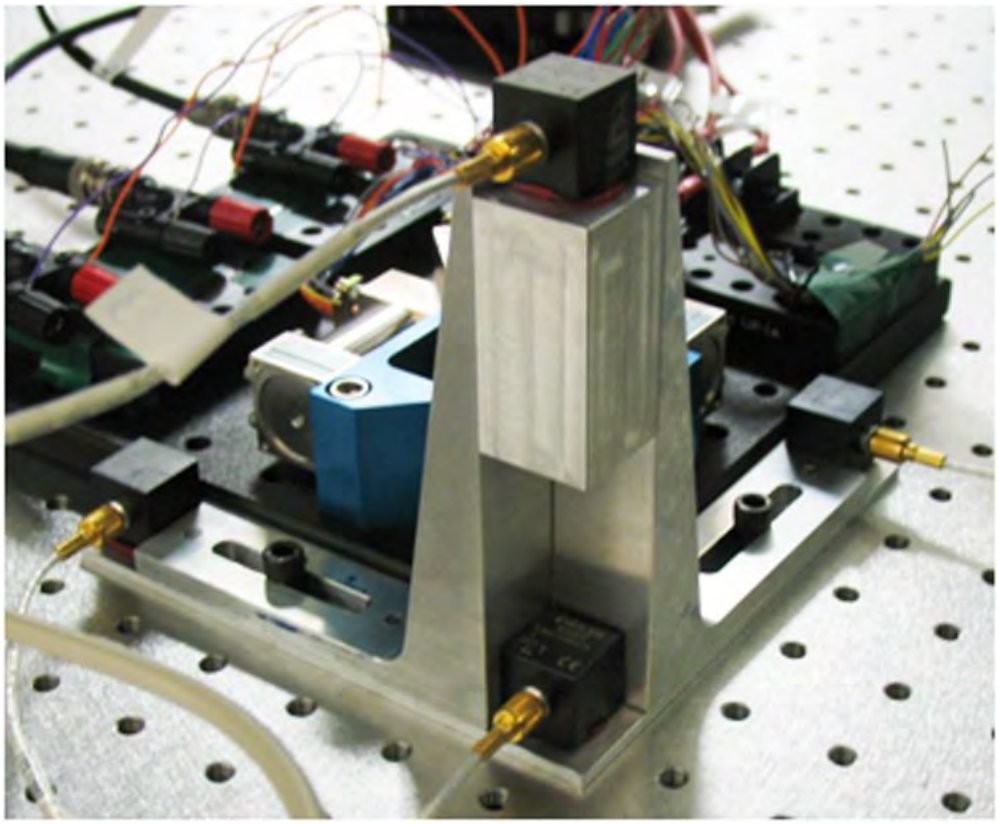

Figure 7. Accelerometer Array

2.1.3 Position Sensing Modules (PSM)

On-Trak PSM 2-10 Position Sensing Modules (PSMs) shown below are each composed of a quadrilateral Position Sensing Detector (PSD) semiconductor chip connected to an On-Trak OT301 position sensing amplifier. PSMs detect the geometric centroid of the irradiance incident on the semiconductor face. The PSMs have a detection area of 10 mm x 10 mm and provide the position of the center of the laser beam in two dimensions. The minimum resolution of the PSM is approximately 0.5 micrometers when combined with the OT301 amplifier.[5] PSMs are used to determine the position and orientation of the platform in the off-platform motion sensing configuration and to determine the beam's position on the target.

[5] On-Trak Photonics Inc., "Position Sensing Modules-Position Sensing Instruments." 23 April 2011. <http://www.on-trak.com/psm/html>.

Figure 8. Position Sensing Module[6]

2.1.4 Fast Steering Mirror (FSM)

Newport Corporation Fast Steering Mirrors (FSMs) are used to reflect the beam in the desired direction to correct for platform-induced jitter or track the moving target. A one inch diameter mirror FSM-300 is used for jitter mitigation and named FSMA. A two inch diameter mirror FSM-320 is used for target tracking and named FSMB. FSMs offer high bandwidth, sub-microradian resolution, two-axis "tip-tilt" rotation control using four voice coil actuators acting in push pull pairs. FSMA has a control bandwidth of 800 Hz making it suitable for jitter correction and FSMB has a bandwidth of 350 Hz, making it suitable for target tracking.[7] A FSM-300 is shown in Figure 9.

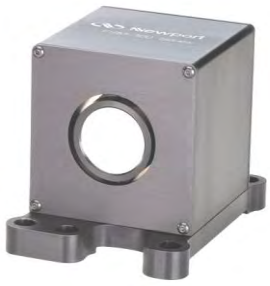

Figure 9. Newport Corporation FSM-300[8]

---

[6] On-Trak Photonics Inc., "Position Sensing Modules-Position Sensing Instruments."
[7] Newport Corporation, "Fast Steering Mirrors." 19 December 2009. <http://www.newport.com/Fast-Steering-Mirrors/847119/1033/catalog.aspx>.
[8] Newport Corporation, "Fast Steering Mirrors."

2.1.5 Linear Motor Actuator

An Aerotech model LMAC-095R-635 Linear Motor Actuator controlled by an Aerotech Soloist™ single-axis motion controller is capable of moving the target PSM 635 mm with an accuracy of ±1 μm and a repeatability of ±0.5 μm at speeds up to 5 m/s.[9]

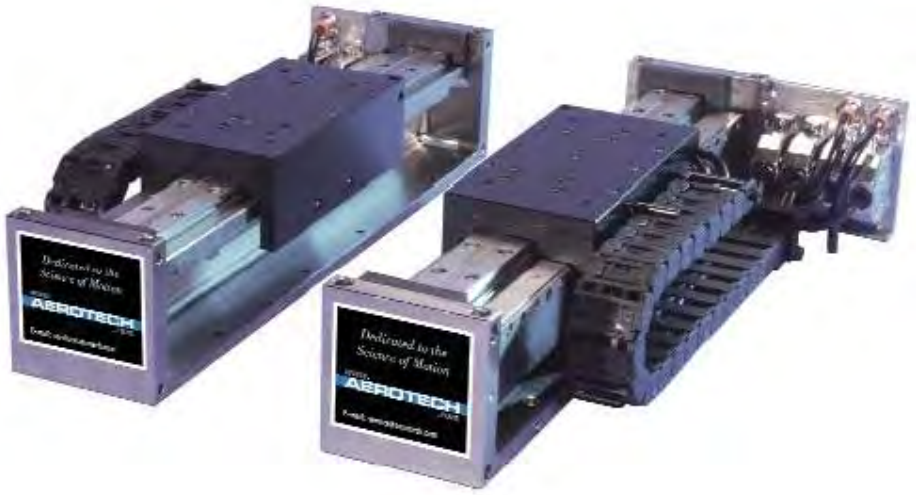

Figure 10. Aerotech Linear Motor Actuator[10]

2.1.6 Breadboard

A Newport RG-33-2-ML research grade breadboard (shown in Figure 11) with constrained layer damping is used as the source laser platform. The platform measures 91.44 cm x 91.44 cm x 60 cm (36 in x 36 in x 2.4 in) and has a mass of 71.3 kg. The breadboard was designed with a honeycombed structure to eliminate torsional and bending modes below 300 Hz.[11]

---

[9] Aerotech Inc., "LMA/LMAC Series Linear Motor Actuators." 23 April 2011. <http://www.aerotech.com/products/pdf/lms.pdf>.

[10] Aerotech Inc., "LMA/LMAC Series Linear Motor Actuators."

[11] Newport Corporation, "Optical Breadboard." 23 April 2011. <http://search.newport.com/?q=*&x2=sku&q2=RG-33-2-ML>.

Figure 11. Newport Breadboard[12]

2.1.7 Isolation System

The source table Newport RS2000-48-18 and target table Newport RS4000-48-8 optical tables are isolated from the ground by Newport I-2000 Pneumatic Isolators with automatic leveling. The source table is 4 ft. x 8 ft. x 18 in. and the target table is 4 ft. x 8 ft. x 8 in. The source laser platform breadboard is isolated from the optical table by four springs and four pneumatic isolators. The stainless steel springs are approximately 3.8 cm long with an outer diameter of 2.8 cm and a stiffness of 20 kN/m. The pneumatic isolators are Newport SLM-3A air mounts and are pressurized to 275 kPa resulting in a natural frequency of 3.5 Hz.[13]

2.1.8 Inertial Actuators

Disturbances are imposed by two CSA Engineering SA-10 Inertial Actuators mounted on the source platform with rated force outputs of up to 10 lb_f for frequencies up to 1,000 Hz. Inertial actuator 1 (IA1) is mounted at a 45 degree angle to the local vertical at the aft portion of the platform so as to impart both a pitch and a yaw motion. Inertial actuator 2 (IA2) is mounted vertically as shown in Figure 2 so as to impart a rolling motion to the platform.

---

[12] Newport Corporation, "Optical Breadboard."
[13] Newport Corporation, "Compact Air Mount." 23 April 2011. <http://search.newport.com/?x2=sku&q2=SLM-1A>.

2.1.9 Lasers

The Stocker Yale Canada Inc. Lasiris™ lasers used on the platform for the source laser and off the platform for PSM platform orientation determination are 5 mW, 635 nm diode lasers, with an elliptical beam measuring 3.8 mm x 0.9 mm. The source laser is circularized by an Edmund Optics NT47-274 anamorphic prism pair beam expander, with a resulting beam diameter of 3.8 mm.

2.1.10 Computer System and Software

The control system was developed using Mathworks MATLAB R2010a with SIMULINK version 7.5 (R2010a) and experiments were run using the SpeedGoat xPC Targetbox. The main computers for control implementation and experiment supervision are two Dell Precision 690 work stations running Microsoft Windows XP 2002 with service pack 3 on Intel Xeon CPUs with clock speeds of 3.40 GHz and 3.00 GB RAM each. The xPC Targetbox is an Intel Core 2 Duo running at 2.13 GHz.

2.2 Experimental Method

2.2.1 Experimental Assumptions

In this research, the platform is assumed to act as a rigid body. The source platform is designed to remain rigid below 300 Hz and the inertial actuators are not operated above 60 Hz.

Jitter due to platform translational motion is assumed to be small compared to that induced by platform rotational motion. Also, any large translational motion of the source platform will be detected by the beam control system as target motion in the platform LOS reference frame.

The angular velocity of the target relative to the source laser platform is assumed to be small. The angular motion of the target is described by equation 1 where r is the range to the target, v is the target velocity, and is the angular rate of motion of the target relative to the platform. Even at tactical ranges of 10 km, a target moving rapidly at 400 kph represents a only a small 0.64°/s rate of relative angular motion. Therefore, a relatively slow moving target at the 5 m range of the lab is sufficient to model a real target.

(1)

2.2.2 Beam Control System

The laboratory components are arranged as shown in the experiment configuration schematic reproduced below.

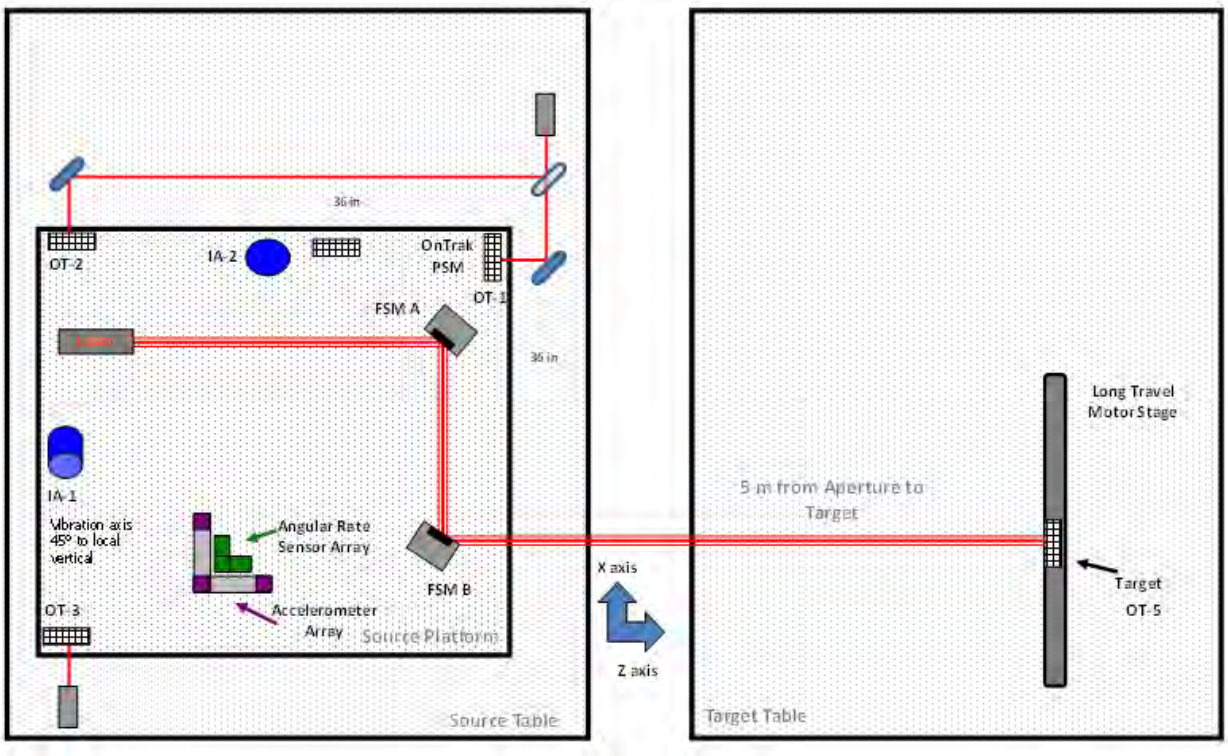

Figure 12. Experiment Configuration Schematic

The Newport breadboard is mounted on the isolator and spring combination which permits the source platform to have six limited degrees of freedom. Inertial actuator one (IA1) is mounted to the aft upper surface of the source laser platform at a 45° angle to the horizontal in order to pitch and yaw the platform. Inertial actuator 2 (IA2) is mounted vertically on the left side of the platform to roll the platform. The external reference system uses three reference PSMs (OT-1, OT-2, and OT-3) mounted to the platform facing outward toward their corresponding reference diode lasers that are fixed to the optical table. The three PSMs move with the source laser platform while the reference diode lasers remain stationary. The platform

orientation is determined by measuring the position of the reference lasers on the PSMs. These positions provide three points to define the platform orientation in a fixed reference frame. This system provides baseline platform orientation determination so that the ARS system can be evaluated. The ARSs are also mounted to the platform and directly measure the rate at which the platform rolls, pitches, and yaws. By integrating the output of the ARSs, the orientation of the platform relative to inertial space can be determined. The platform motion measured by the ARS array is compared to that measured by the PSM system to evaluate the accuracy of the ARS system of the rate determination and the method of integration. Because the internal ARS system is intended to replace the external PSM system that has been used in previous research, it is assumed that the PSM based external reference system is accurate. The three dimensional array of linear accelerometers may be used to determine the angular acceleration of the platform in all three axes using the conversion method presented by Algrain and Quinn.[14] This information may then be used to improve the accuracy of the ARS system. The accelerometer array is physically aligned to the ARS array using the three dimensional array bracket.

The fifth PSM (OT-5), mounted 4.9 m in the z-direction from the face of FSMB, is used to detect the motion of the beam at the target. The line-of-sight for target tracking was established using feedback from OT-5.

The previous jitter mitigation system used one FSM (FSMA) mounted at a 45º angle to the source laser to control platform induced jitter. A second FSM (FSMB) was mounted at a 45º to FSMA as shown in Figure 12 to allow the system to point the jitter-stabilized beam at a moving target. The jitter correction and target tracking systems are treated as isolated systems and use independent controllers as they would in applications outside of the laboratory. In order to ensure that the feedback target tracking system does not detect and remove residual jitter uncorrected by FSMA, the feedback from OT-5 used to steer FSMB was filtered using a 2-8Hz lowpass filter. Future and practical systems may use an optical means of tracking the target with the optical detector boresighted with the source laser.

Knowing the platform orientation relative to the stationary external reference frame and knowing the FSM orientations in real time, the path of the beam in the platform LOS reference

---

[14] Algrain, Marcelo C. and James Quinn. "Accelerometer Based Line-of-Sight Stabilization Approach for Pointing and Tracking Systems." *Second IEEE Conference on Control Applications*, Sep 1993.

frame can be determined. Therefore, the expected position of the beam at the target can be predicted, and the error between the predicted and desired beam position can be calculated. The jitter and target tracking system use independent proportional-integral (PI) controllers. In the jitter mitigation system, the PI controller is used to minimize the error between the predicted beam position at the target and the desired beam position at OT-5. In the target tracking system, OT-5 provides feedback to the controller indicating the error between the beam LOS and the platform-target LOS. The PI controller steers FSMB to minimize this error. The desired beam position is defined as (0,0) on OT-5 for both cases. The jitter system requires calibration to define the rest position of the source platform. All platform motion measurements are defined relative to this calibration. The beam is electronically aligned to the target by subtracting the target miss distance in both x and y-axes measured in the calibration run from the experiment results.

2.2.3 Experimental Procedure

Experiments were run to separately evaluate the platform motion sensing, jitter mitigation, and target tracking subsystems. The entire beam control system, formed by combining the subsystems, was then evaluated. In each experiment, the platform was vibrated by IA1 at 10 Hz to produce a pitch/yaw motion or by IA1 and IA2 at multiple frequencies (pitch/yaw: 10, 13, 27, 47 Hz; roll: 17, 23, 41, 51 Hz) to produce pitch/roll/yaw motion. Data was collected at 1 kHz (time step of 0.001 seconds). For each data run with each beam control system, the inertial actuators begin shaking the platform one second after the start of the run. The jitter mitigation control system starts 3.1 seconds after the start of the run. For cases with target motion, the target tracking control system starts 2.5 seconds after the start of the run. Once the target tracking system has locked onto the target, target motion is manually started using a separate computer. Relative to the source platform, the target moves to the right 30 mm, stops, moves to the left 60 mm, stops, and then returns to its original position by moving 30 mm to the right. The target moves at a maximum of 5 mm/s with a profile velocity when starting (ramp up), stopping (ramp down), or changing direction in order to eliminate discontinuities in the target velocity profile. A velocity profile demonstrating parabolic ramp up is shown below.

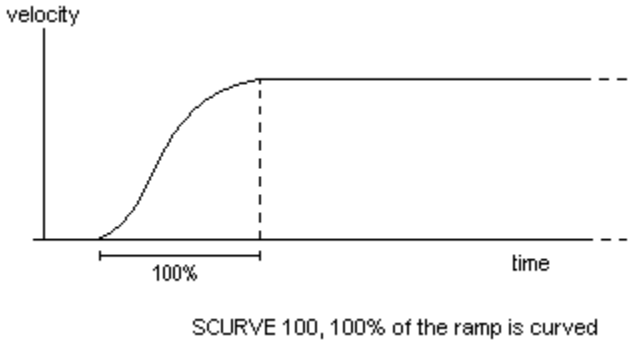

Figure 13. Parabolic Target Acceleration[15]

[15] Aerotech Inc., "Soloist Help: SCURVE Command."

2.3 Tunnel and Isolator Effects on Jitter

As the beam propagates through the atmosphere, turbulence creates changes in the index of refraction of the propagation medium that cause the beam to refract. To minimize the atmospheric propagation influences so that the beam control system alone may be analyzed, the source and target optical tables and beam propagation path are surrounded by acrylic panels. The optical table isolators effectively isolate the source platform from any motion that would be transferred through a hard mount, so that only the inertial actuators provide the disturbance. The influence of the closed tunnel is highlighted in green in Figure 14, which indicates that the noise floor of the system is 2.11 µrad. This noise floor was calculated by taking the root-mean-square of the jitter angle. This is the noise in the system caused by the natural frequencies of the objects in the system. The FSMs were fixed at zero and the source platform was floated to permit platform motion. This is considered the minimum level of jitter the beam control system is capable of achieving.

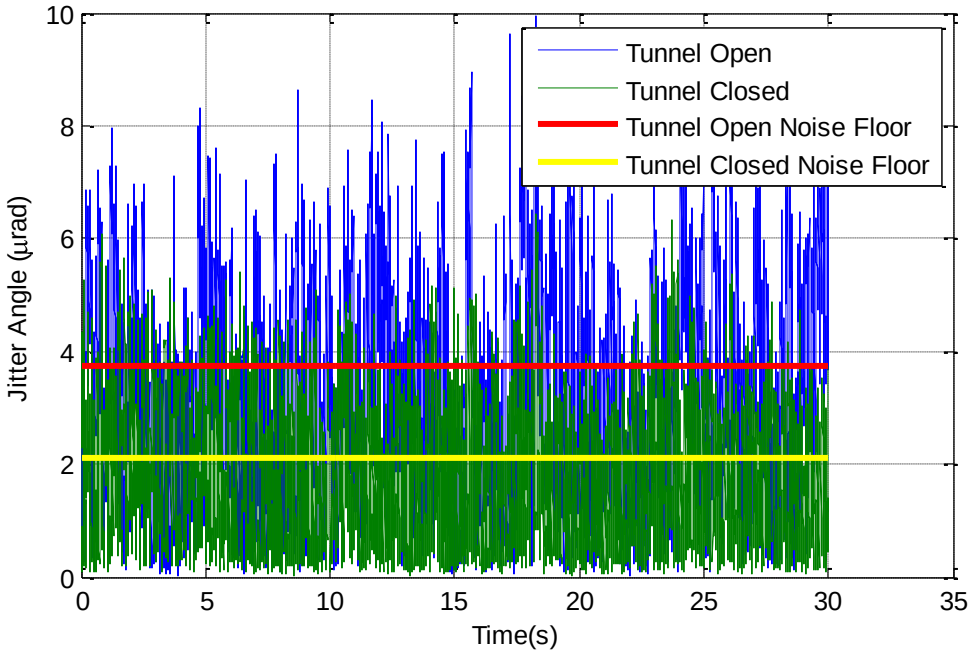

Figure 14. Tunnel Effect on Noise Floor

Power spectral density analysis for the tunnel closed noise floor is shown in Figure 15.

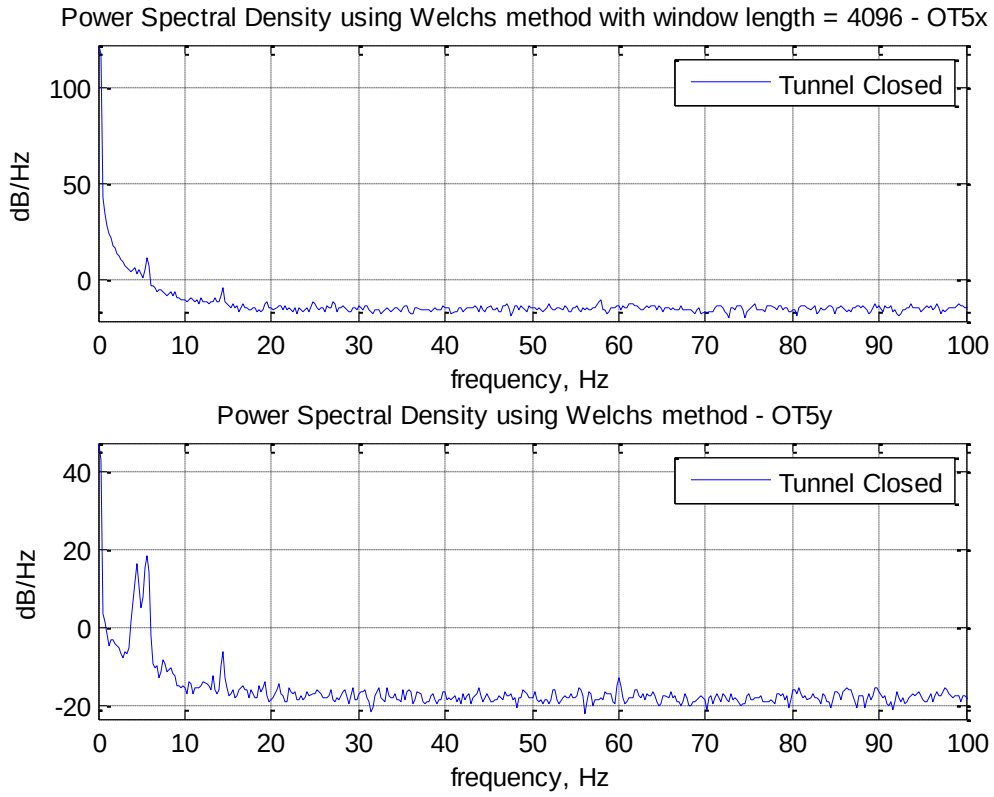

Figure 15. Tunnel Closed Power Spectral Density

The 5 Hz platform rigid body transverse mode and the 13 Hz platform rigid body rotational mode are prevalent in both the x and y-directions. Though small in magnitude, the 60 Hz AC current electrical noise is seen in the y-direction as expected.

3 Theory

3.1 Jitter

Jitter is any deviation of the beam from its intended path due either to platform motion or atmospheric propagation effects. An angular displacement of the platform θ radians in one axis relative to the target will cause a linear displacement of the laser impact point at the target *d* as follows:

$$d = r \tan(\theta) \tag{1}$$

where *r* is the range to the target. A 1 μrad jitter will result in a 1 cm beam displacement at a range of 10km. At this jitter angle, a 1 cm diameter beam would have no overlap with its original incident area. Since jitter occurs in multiple axes and the angle is a function of time, the effect is to "smear" the beam over a broad area at the target, causing a loss in intensity and a corresponding increase in energy required to damage the target. This effect is shown in Figure 16. Thus, jitter greatly reduces the effectiveness of a directed energy system and must be mitigated.

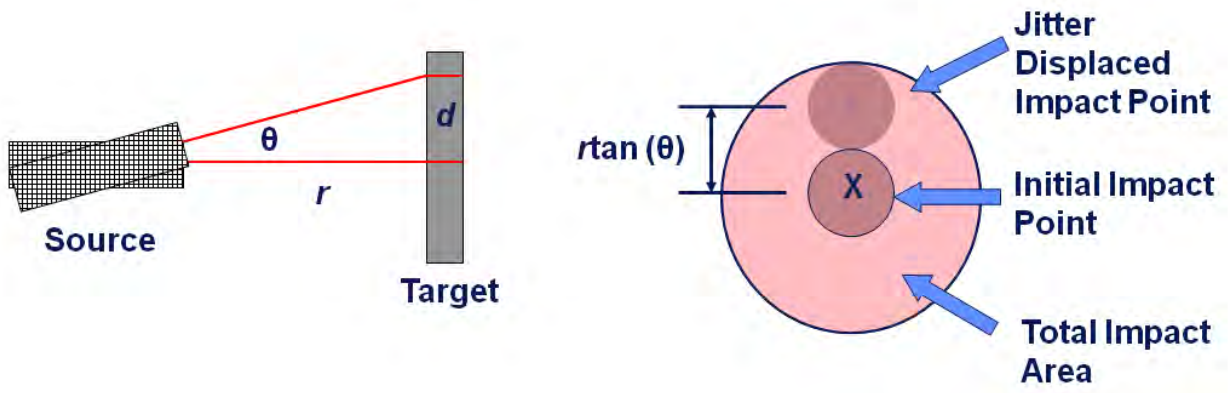

Figure 16. Jitter Displacement Diagram

3.2 On-Platform Orientation Determination

3.2.1 Position Sensing Module (PSM) Platform Orientation Determination

The plane defining the source platform is determined by measuring the position of the laser on each orientation PSM relative to the calibrated center position. With the distances between the actual and calibrated positions known, the pitch roll and yaw angles of the platform are determined by using equations 2-4 respectively. These equations use the small angle approximation, .

The notation ot1y indicates the displacement of the reference laser on OT-1 in the y direction. $z_{2,1}$ indicates the distance from OT-2 to OT-1 in the z direction (see Figure 12).

(2)

(3)

(4)

3.2.2 Angular Rate Sensor Platform Orientation Determination

The angular rate output from the ARS array was integrated to give an angular position relative to the rest position determined during the calibration routine as shown in equation 5.

(5)

When applied to each axis of rotation, this equation gives the orientation of the platform for use by the beam prediction algorithm and jitter mitigation system. As is the case with all inertial sensors, the ARS system "drifts" away from the original zero. Two methods were devised to correct this problem. The first method resets a two second running mean of ARS array output for each axis. The second method uses a lowpass filter at 8 Hz with a magnitude reduction of 10

dB to filter out the platform oscillations caused by the inertial actuators (>10 Hz), thereby leaving only the "drift" signal. This drift was then subtracted out from the original signal. To account for the one time step required to integrate the angular rates, the platform orientation is predicted one time step ahead by summing the integrated rates and the product of the calibrated rates and the sample time.

3.2.3 Linear Accelerometer Based Platform Orientation Refinement

The four linear accelerometers are arranged in a three dimensional array to permit transformation of the measured linear accelerations into angular accelerations. The equations for converting from linear accelerations to angular accelerations presented by Algrain and Quinn and adapted for use in this system are shown in equations 6-8.[16]

(6)

(7)

(8)

The notation $a_{B,z}$ indicates the linear acceleration of accelerometer B in the z-direction and r_{OB} indicates the position vector from accelerometer O to accelerometer B in the y-direction.

[16] Algrain and Quinn, 1993.

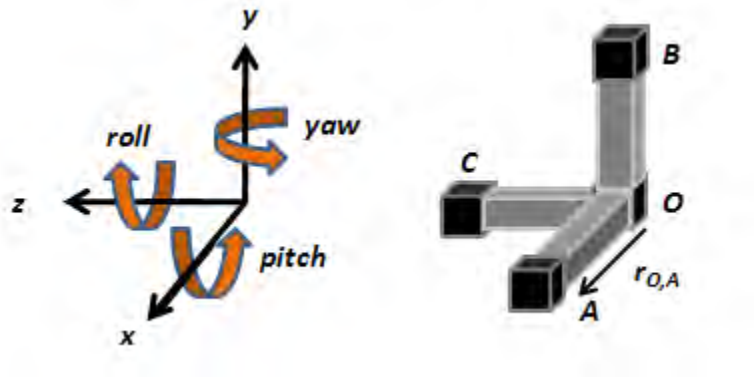

Figure 17. Accelerometer Array Schematic

These angular accelerations (⎯⎯) would be added to the angular rates measured by the ARS array (⎯ in a manner equivalent to adding the second order term to the Taylor Series as shown in equation 9.

⎯ ⎯⎯ (9)

In practice, however, the ARS-accelerometer platform orientation calculation produced results nearly identical to those produced by the ARS array alone. This result is believed to be due to measurement and mounting inaccuracies in the accelerometer array. The error resulting from imprecise measurement of the distance between accelerometers, combined with the inability to precisely align the array with a platform axis in addition to the vertical yaw axis, is sufficient to negate any improvement that the accelerometers may have offered.

3.3 Line-of-Sight (LOS) Reference Frame

The LOS reference frame is a type of reference frame that is not fixed in space. A point on a platform, in this case the center of the FSMB face in its zeroed orientation, is arbitrarily defined as the origin. Everything else in the reference frame is defined relative to the origin by a range, an azimuth, and an elevation. The LOS reference frame theory developed here is derived from that presented by DeBruin and Johnson in *Line-of-Sight Reference Frames: A Unified*

Approach to Plane-Mirror Optical Kinematics.[17] A LOS vector set, consisting of the LOS vector from a source to a target and two mutually-orthogonal image plane vectors, defines a LOS reference frame. As a result, LOS reference frames provide orientation but not position information. This is of little concern, however, because only the position of the target relative to the source is necessary for successful engagement with a directed energy weapons systems. Target tracking systems, whether they be electro-optical or radar based, define the target position in a LOS reference frame. As a result, a LOS reference frame must be used in the USNA Directed Energy Beam Control System to be operationally relevant.

To predict beam position on a target, the beam path through the optical train must be determined using the LOS reference frame. When applied to the source laser, the LOS vector $\underline{q}_1$ defines the optical axis and $\underline{q}_2$ and $\underline{q}_3$ define the image plane to form the LOS reference frame matrix [Q] as shown in Figure 18.

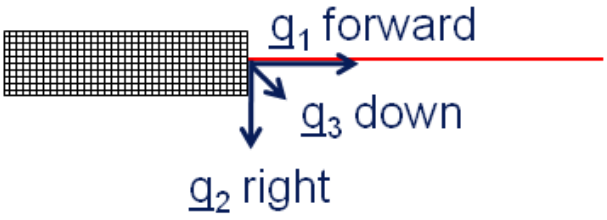

Figure 18. Source Laser LOS Reference Frame

For a single mirror, the incoming LOS reference frame matrix [Q] can be transformed into the outgoing LOS reference frame [R] through the use of a mirror transformation matrix [M].

$$[R]^T=[M][Q]^T \tag{10}$$

[17] DeBruin, James C. and David B. Johnson, Line-of-Sight Reference Frames: a Unified Approach to Plane-Mirror Optical Kinematics. *SPIE* vol. 1697, p. 111-129, 1992.

The transformation matrix [M] is defined using the scalar components of the mirror normal vector $\underline{n} = (n_1,n_2,n_3)$ as follows:

$$[M]=\begin{bmatrix} 1-2n_1n_1 & -2n_1n_2 & -2n_1n_3 \\ -2n_2n_1 & 1-2n_2n_2 & -2n_2n_3 \\ -2n_3n_1 & -2n_3n_2 & 1-2n_3n_3 \end{bmatrix} \quad (11)$$

In optical systems with n mirrors, the mirror transformation matrices may be combined to form a system optical transformation matrix [O] as follows:

$$[O]=[M_n][M_{n-1}]\ldots[M_2][M_1] \quad (12)$$

These vectors and transformation matrices must all be represented in terms of the same reference frame or vector basis, which in practical applications will be the platform LOS reference frame [P]. A transformation basis is an orthonormal vector triad that can be used to define any three dimensional vector. Vector orientations and positions remain unchanged when represented in a different vector basis. Transferring components of a vector from the arbitrary basis A to basis B can be achieved through a transformation matrix as follows:

$$[B]={}^{B}T^{A}\,[A] \quad (13)$$

where [A] is a vector triad in basis A and [B] is a vector triad in basis B.

The FSMs used to control the beam rotate about two axes. Each axis must have a reference frame defining its zeroed orientation and an angle defining changes relative to that reference frame. For (M_1) shown in Figure 19, reference frame [A] and its angle φ and reference frame [B] and its angle θ define pan and tilt respectively.

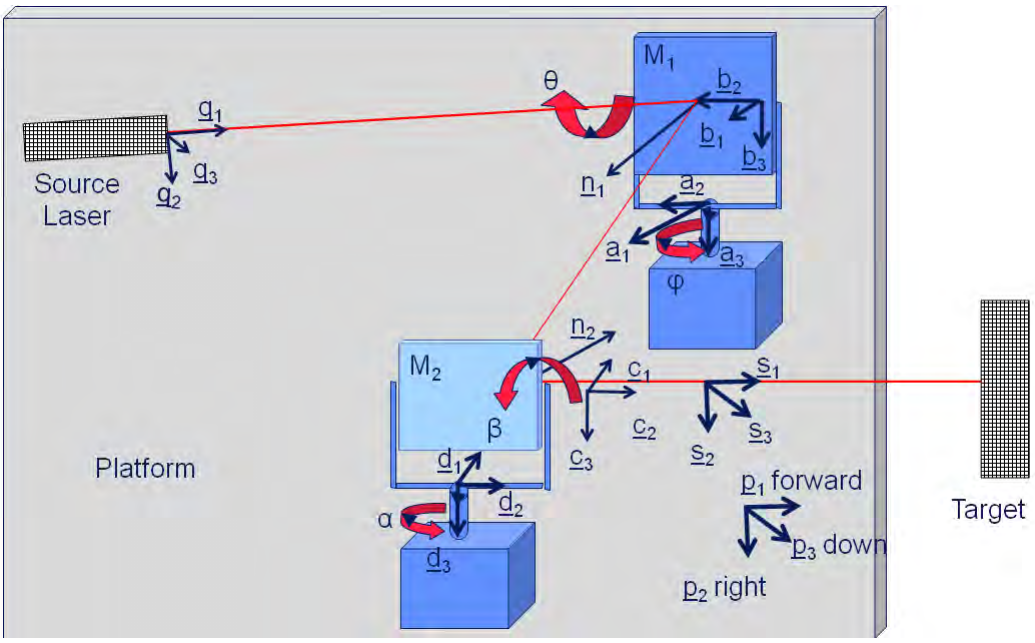

Figure 19. Platform Diagram

Using the basis transformation from equation 13, the source laser LOS reference frame [Q] can be defined in the platform LOS reference frame basis [P] to create $[Q^P]$. Similarly, the outgoing LOS reference frame [S] can be described in the [P] basis to form $[S^P]$. With $[Q^P]$ known by the source laser configuration on the platform and $[S^P]$ provided by the target tracking system and with jitter corrections added by the jitter correction algorithm, the optical transformation matrix in the [P] basis $[O^P]$ may be solved for using equation 14.

$$[O^P]=[S^P][Q^P]^{-1} \tag{14}$$

With the $[O^P]$ necessary to hit the target and mitigate jitter determined, the angles required for each mirror can be solved for using equation 15 where S and C represent sine and cosine respectively.

$$[O^P] = \begin{bmatrix} 1-2S_\beta^2 S_\alpha^2 & 2S_\beta C_\beta S_\alpha & -2S_\beta^2 S_\alpha C_\alpha \\ 2S_\beta C_\beta S_\alpha & 1-2C_\beta^2 & 2S_\beta C_\beta C_\alpha \\ -2S_\beta^2 S_\alpha C_\alpha & 2S_\beta C_\beta C_\alpha & 1-2S_\beta^2 C_\alpha^2 \end{bmatrix} \begin{bmatrix} 1-2S_\theta^2 S_\varphi^2 & 2S_\theta C_\theta S_\varphi & -2S_\theta^2 S_\varphi C_\varphi \\ 2S_\theta C_\theta S_\varphi & 1-2C_\theta^2 & 2S_\theta C_\theta C_\varphi \\ -2S_\theta^2 S_\varphi C_\varphi & 2S_\theta C_\theta C_\varphi & 1-2S_\theta^2 C_\varphi^2 \end{bmatrix} \quad (15)$$

With the required angles determined, the mirrors can be directed to move as required to mitigate jitter and hit the target.

3.3.1 Controllers

3.3.1.1 Proportional-Integral (PI) Control

A proportional-integral (PI) controller is used to control both FSMA and FSMB. A PI controller seeks to minimize the error between the actual value and the desired value the of system variable being controlled. Proportional control action produces a control output that is an amplification of the error signal. Integral control action changes the control output at a rate proportional to the error signal. Thus, the proportional gain determines the magnitude of the control response and the integral gain determines the rate in order to minimize system response overshoot.[18]

3.3.1.2 PI Controller Gains

Because the mathematical model governing the plant (the beam control system) is not easily determined and a step function cannot be applied to determine system response, the FSMA PI controller was initially tuned using Ziegler-Nichols tuning rules based on critical gain and critical period. The controller was tuned for the for multiple frequency vibration case with gains shown in Table 1.[19]

---

[18] Ogata, K., *Modern Control Engineering,* 4th ed, Prentice Hall, Upper Saddle River, NJ, 2002, p.65.
[19] Ogata, K., 2002, p. 685.

Table 1. Zeigler-Nichols Tuning Rules Based on Critical Gain and Critical Period

Controller	K_p	T_i	T_d
P	$0.5K_{cr}$	∞	0
PI	$0.45K_{cr}$	$(1/1.2\ )P_{cr}$	0
PID	$0.6K_{cr}$	$0.5\ P_{cr}$	$0.125P_{cr}$

The proportional and integral gains determined by this method, however, caused an unstable control response, so they were scaled to 45% of their original value. From this stable value, the proportional and integral gains were manually optimized for the multiple frequency vibration case to produce the minimum jitter and are shown in Table 2.

Table 2. FSMA PI Gains

		Control Method		
FSM Axis	**Gain**	**Feedback**	**PSM**	**ARS**
X	Proportional	0.018	0.0135	0.00315
	Integral	21.6	18.9	5.985
Y	Proportional	0.045	.018	0.00225
	Integral	54	27	6.975

The proportional and integral gains for FSMB were determined in the same manner.

Table 3. FSMB PI Gains

FSM Axis	**Gain**	**Feedback**
X	Proportional	0.02
	Integral	2
Y	Proportional	0.01
	Integral	1

3.4 SIMULINK Model

Experiments conducted in the USNA Directed Energy Beam Control and Effects Laboratory are designed and run using the SIMULINK virtual environment in MATLAB. The SIMULINK model for the beam control system is shown below in Figure 20.

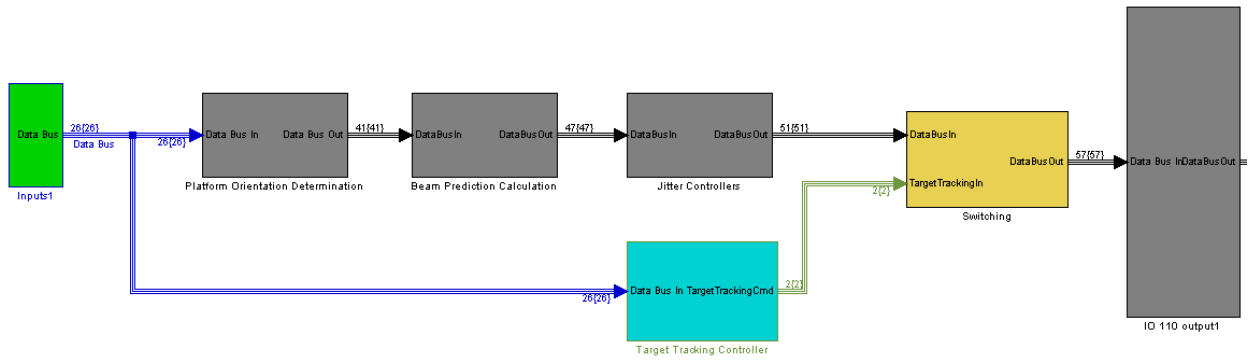

Figure 20. Beam Control System SIMULINK Model

Every operation required to conduct experiments is defined by a separate block. The first block (green) receives input signals from the sensors and equipment in the beam control system. The last gray box sends command signals to the beam control system and outputs all the signals from the model to MATLAB. The first gray block is the platform orientation calculation block. The second gray block predicts the beam position at the target. The third gray block contains the PI controller for FSMA. The turquoise block contains the PI target tracking controller. The yellow block allows the user to turn controllers on and off. Each block has several sub-blocks necessary to perform platform motion sensing, beam position prediction, FSM control, and test case selection. Several of the blocks are discussed below. The rest are included in Appendix N.

Within the second block are the blocks that calculate the platform orientation using the PSMs, ARS array, and ARS array-accelerometer array combination shown below in Figure 21.

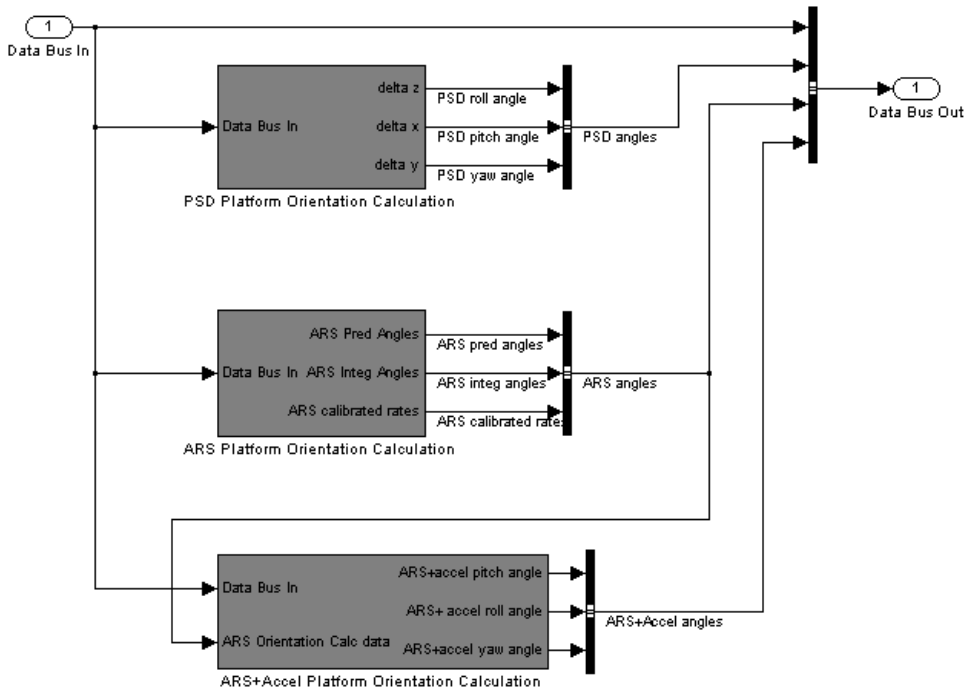

Figure 21. Platform Orientation Calculation SIMULINK Model

The middle gray block calculates the platform orientation using ARS inputs supplied by the data bus. The calculation blocks are shown below.

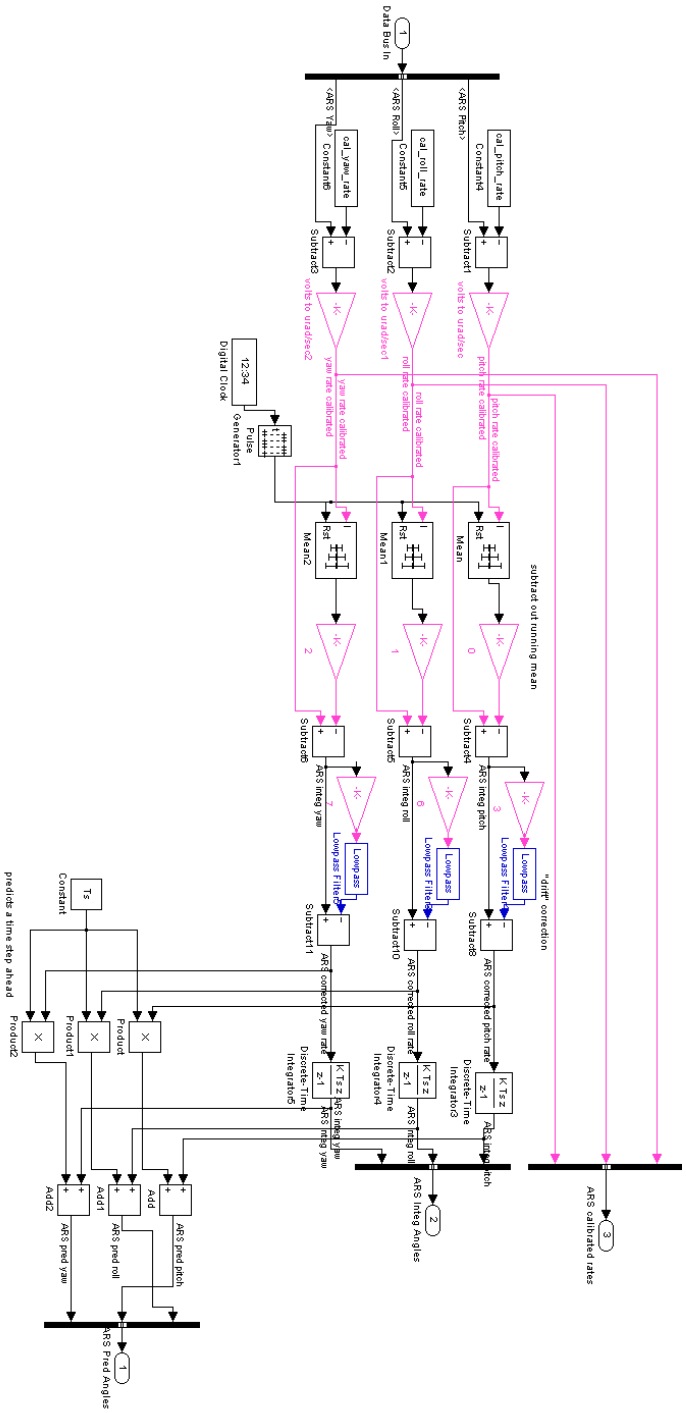

Figure 22. ARS Platform Orientation Calculation SIMULINK Model

The first group of black boxes obtains ARS supplied voltage data from the data bus and calibrates the rate sensors. The pink blocks convert the ARS supplied voltages into angular rates. The second group of black boxes allows the option of subtracting out the running mean from the ARS signals every two seconds to remove "drift." The blue lowpass filters are a second option for removing ARS signal drift. The last group of black boxes integrates the angular rates and predicts the platform orientation one time step ahead.

The target tracking PI controller block diagram is shown below.

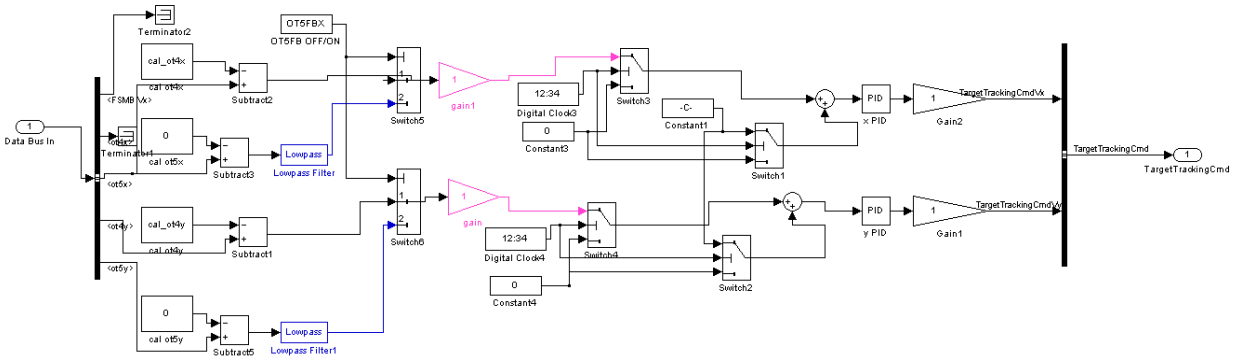

Figure 23. Target Tracking PI Controller SIMULINK Model

The first column of black boxes determines the error between the actual and desired beam position on the target. The blue lowpass filters allow the PI controller boxes at the right to minimize the error in the low frequency target motion without influencing the high frequency residual jitter.

4 Experimental Results

4.1 ARS and PSM Platform Motion Sensing Comparison

4.1.1 Internal Platform Motion Sensing

The ARS based method for determining the orientation of the source laser platform compared favorably to that of the PSM method. Because performance of the jitter mitigation has been evaluated previously using the PSM method,[20] the PSM method was used as the baseline to which all other methods were compared. As shown in Figure 24 and Figure 25, the percent error between the mean of the two methods remained below 1% for all axes for both the 10 Hz pitch/yaw vibration and the multiple frequency vibration cases. The difference between purely integrating the output from the ARSs to determine platform orientation and adding the one time step prediction to the pure integration was negligible.

[20] Roberts, Watkins, and Barton, "Development of a Feed-Forward Compensation Technique to calculate Beam Position in the Mitigation of Platform-Induced Jitter," 2010.

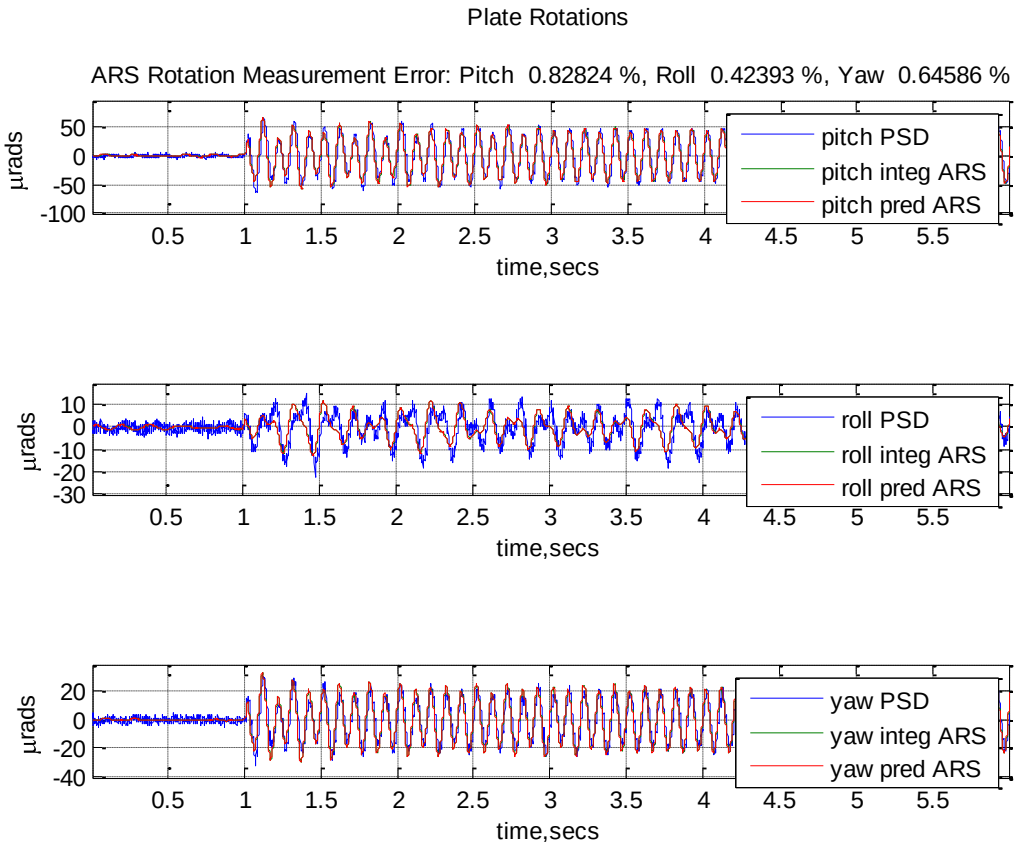

Figure 24. ARS vs. PSM Platform Orientation Determination for 10Hz Excitation

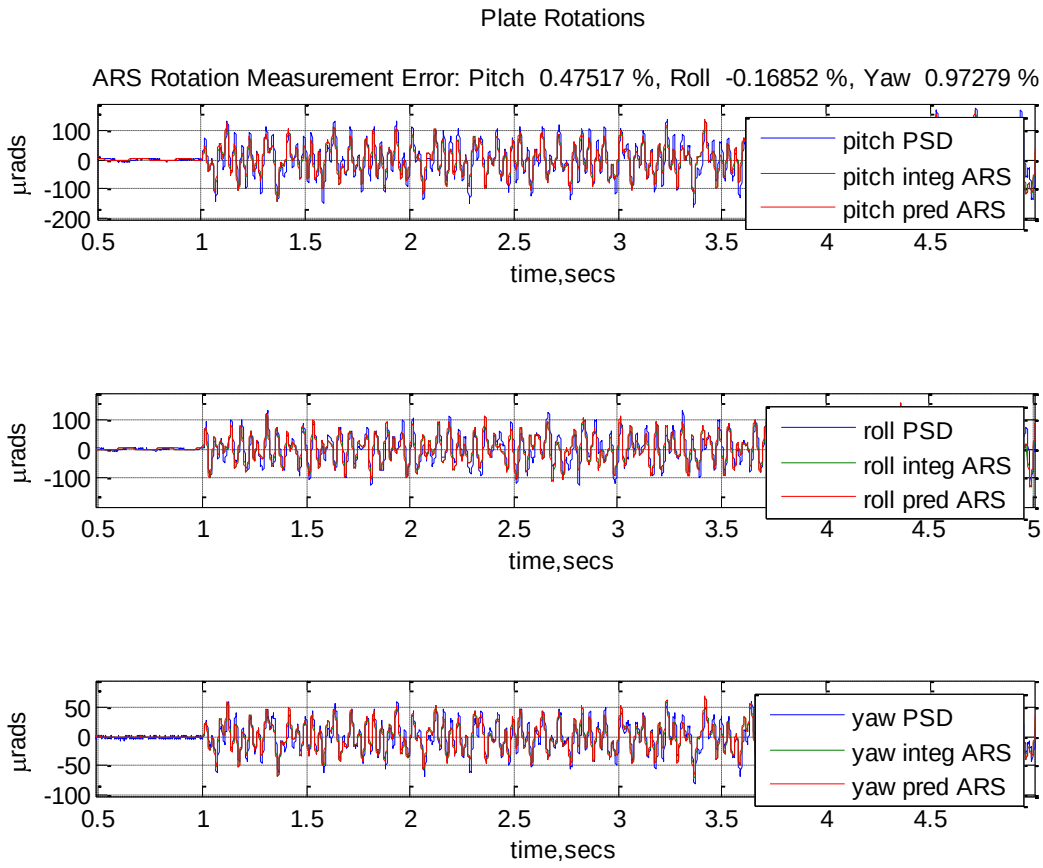

Figure 25. ARS vs. PSM Platform Orientation Determination for Multiple Frequency Excitation

The root mean square (RMS) error between the platform orientation determined by the PSM method and the ARS array method was taken as well. The RMS errors for all vibrations in all axes were less than 0.1%. This indicates that the PSM and ARS methods produce consistent calculations of platform orientation.

4.1.2 Error Analysis

While the PSM and ARS methods of platform motion sensing proved comparable, two significant sources of error exist in both of these methods. Neither the ARS method nor the PSM method accounts for translation along an axis. As a result, even perfect rotational orientation

determination will result in an error at the target. However, translational jitter is independent of range, so it is negligible compared to rotational jitter at ranges longer than those used in the laboratory environment. Applying a target tracking system in the LOS reference frame resolves large translational movements as relative target motion. However, the target tracking system used in this research relies on feedback. In order to ensure that the target tracking system does not remove jitter, as is the case in real world applications, the feedback data is filtered. As a result, any translational motion with a spectral excitation greater than 8 Hz is not removed and could result in errors at the target.

A second source of error exists in the inability to align the ARS and PSM reference frames with the platform reference frame. Small angular differences in the reference frames would indicate coupled rotational motion in one reference frame while another may indicate a pure axial rotation. A known rotational motion in only one axis is nearly impossible to create due to inertial actuator mounting limitations and changes in the platform center of rotation with new configurations. As a result, the platform reference frame must be defined relative to the motion sensing instruments.

4.2 Jitter Mitigation Controller Performance Comparison

4.2.1 Statistics Used

The statistics used in this research to evaluate the beam control system jitter mitigation performance are the following:

- x and y measurement of the beam position on the target
- Power spectral density of the beam position at the target in the x and y directions
- Jitter angle
- Root mean square (RMS) of the jitter angle
- Percent improvement of the RMS jitter angle
- 300 ms running mean of the jitter angle
- Standard deviation of the jitter angle
- Percent improvement of the jitter angle standard deviation

The x and y measurement of the beam position at the target is an effective means to visually observe the magnitude of the jitter reduction and the accuracy of the system relative to

the calibrated target center. This measurement also indicates the jitter control in each axis for easy diagnostics during system development.

The power spectral density of the beam position at the target in the x and y directions was determined using Welch's method[21] with a 4096 sample window and a window overlap of 50%. This plot indicates the frequency content of the jitter measured at the target and the power in each frequency. It serves as a means of determining the magnitude of jitter reductions and the frequencies that the beam control system detects and effectively corrects.

Jitter angle is the angular error as a result of jitter. It is calculated for each time step using the small angle approximation by taking the radial miss distance from the calibrated target center and dividing by the distance to the target. The jitter angle characterizes the jitter independent of target range, allowing for system comparison.

The RMS jitter angle is a good indicator of the accuracy of the beam control system. The RMS jitter angle indicates the RMS miss distance at the target from the calibrated value. For cases with moving targets, this statistic was calculated for the longest period of constant target velocity (the 60 mm target movement to the left relative to the source platform).

The percent improvement of the RMS jitter angle indicates the improvement in the accuracy of the system once control is engaged. For moving targets, this value was calculated for the longest period of constant target velocity.

The 300 ms running mean of the jitter angle reduces the clutter of the jitter angle plot, so variations in jitter angle may be observed and system accuracy qualitatively evaluated.

The standard deviation of the jitter angle is an indicator of the beam control system precision about the mean value. For moving targets, this value was calculated for the longest period of constant target velocity.

The percent improvement of the standard deviation indicates the improvement of the jitter angle precision with the control system engaged. For moving targets, this value was calculated for the longest period of constant target velocity.

---

[21] Welch, P.D. "The Use of Fast Fourier Transform for the Estimation of Power Spectra: A Method Based on Time Averaging Over Short, Modified Periodograms." *IEEE Trans. Audio Electroacoust*. Vol. AU-15 (June 1967). p.70-73.

4.2.2 Jitter Mitigation Performance for 10 Hz Pitch/Yaw Vibration

The jitter mitigation system using the PI controller is evaluated with a stationary target for the three cases: target feedback, feed forward using PSM platform motion sensing, and feed forward using ARS platform motion sensing. The case in which the PI controller receives feedback from the target PSM is considered the best possible jitter mitigation the system is capable of achieving for the 10 Hz pitch/yaw vibration (shown below in Figure 26).

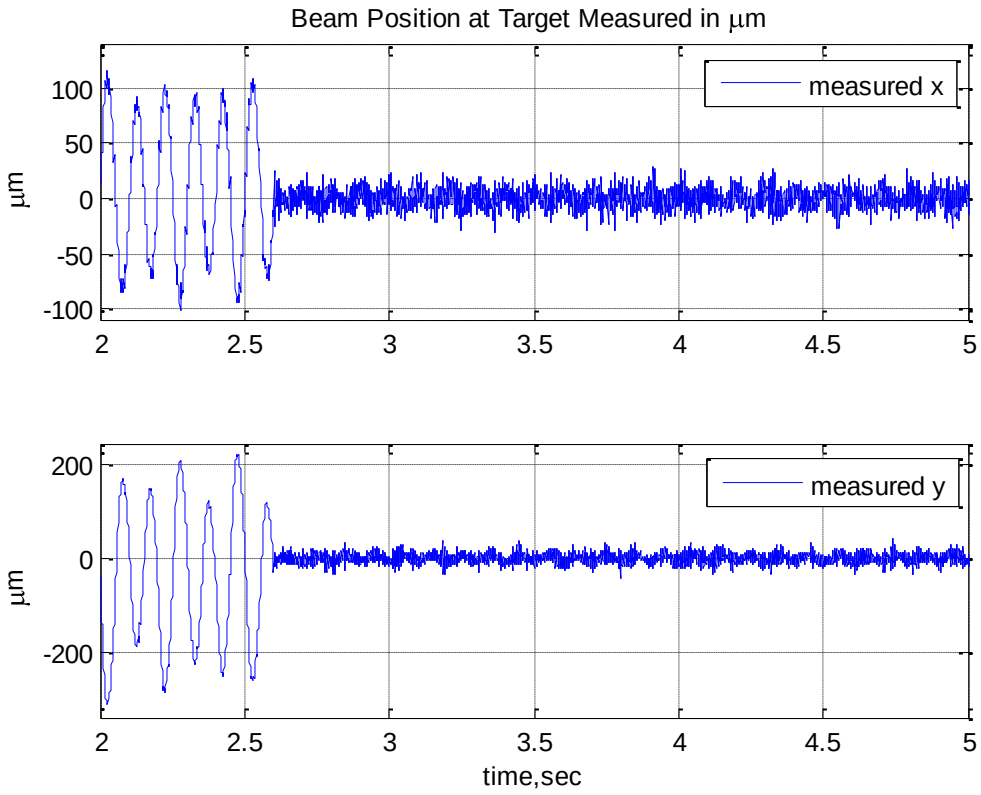

Figure 26. Jitter Mitigation Using Feedback PI Control for 10 Hz Vibration

Under control, the jitter angle, depicted in Figure 27, is reduced to less than ±15 μrad. The RMS jitter angle is reduced 75.2% from 29.2 μrad to 7.2 μrad. The standard deviation of the jitter angle is reduced 82.73% from 12.56 μrad to 2.1 μrad.

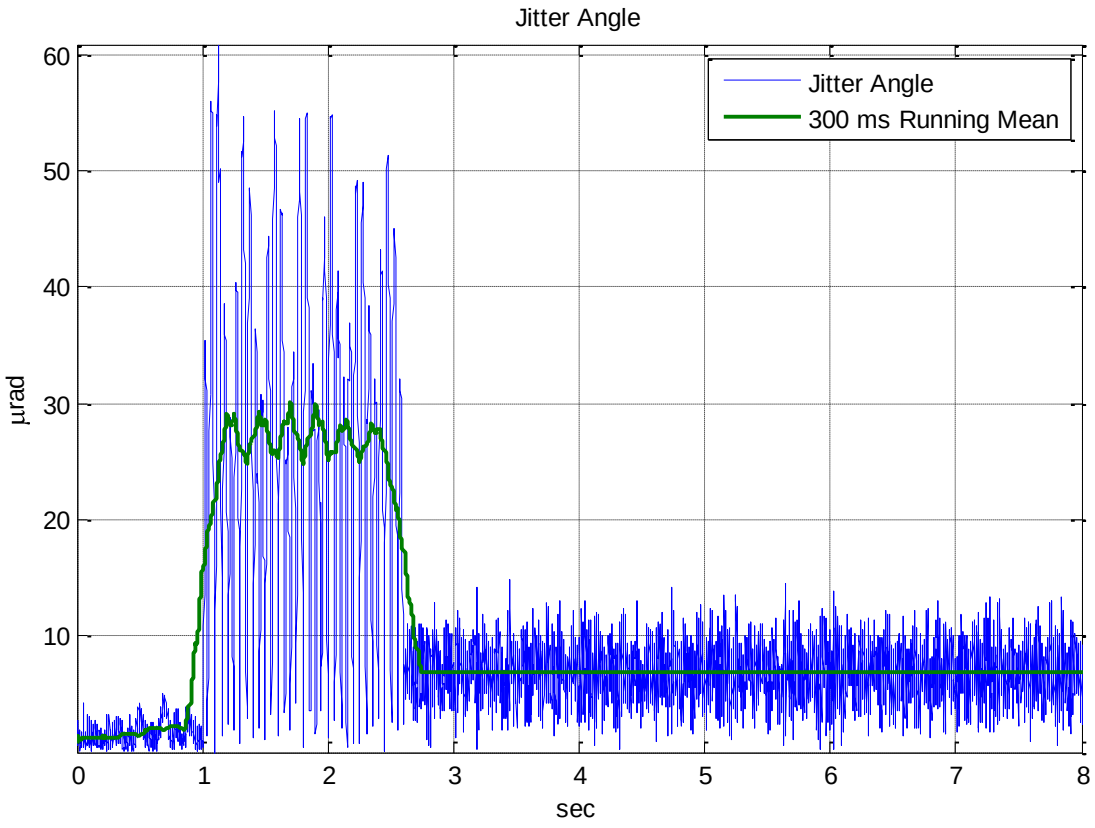

Figure 27. Jitter Angle for Feedback PI Control for 10 Hz Vibration

As indicated in Figure 28, the feed forward PSM method reduces jitter measured at the target to less than ±60 µm in the x-direction and ±75 µm in the y-direction. The decrease in jitter mitigation performance for feed forward control compared to feedback control is expected.

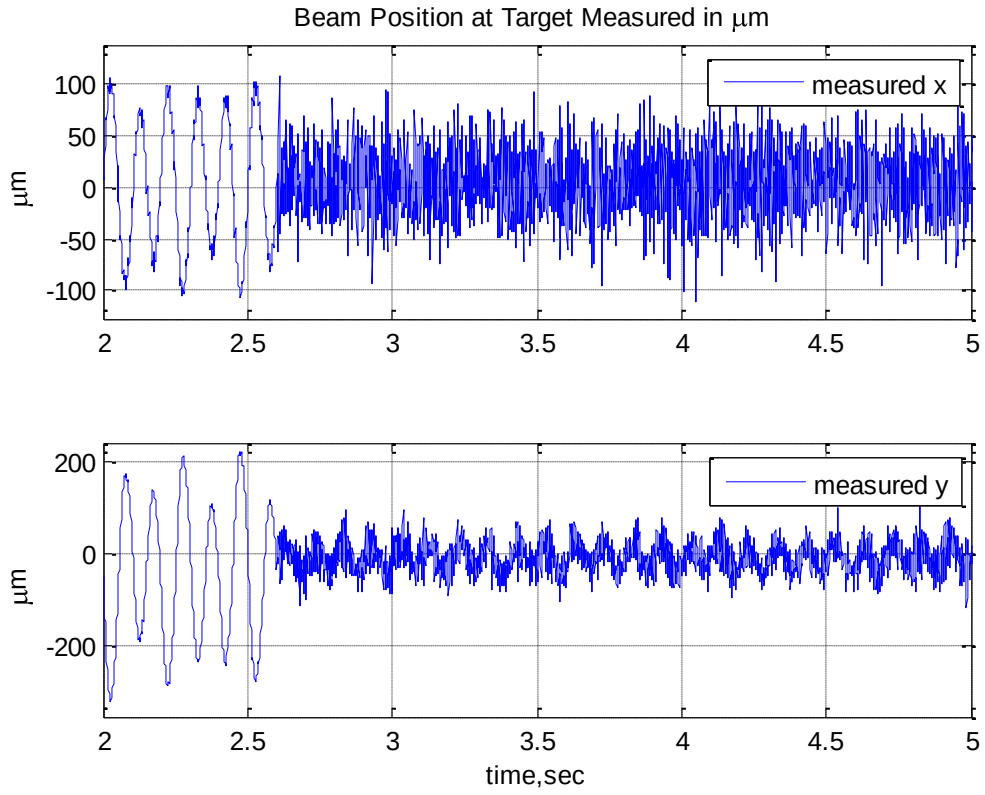

Figure 28. Jitter Mitigation Using PSM PI Control for 10 Hz Vibration

Figure 29 shows that the feed forward jitter mitigation control method using off-platform PSM motion sensing reduces the maximum jitter angle to less than ±25 μrad. The RMS jitter angle is reduced 66.15% from that of the uncontrolled beam to 9.9 μrad. The standard deviation of the jitter angle is reduced 64.02% from 12.56 μrad to 4.52 μrad.

.

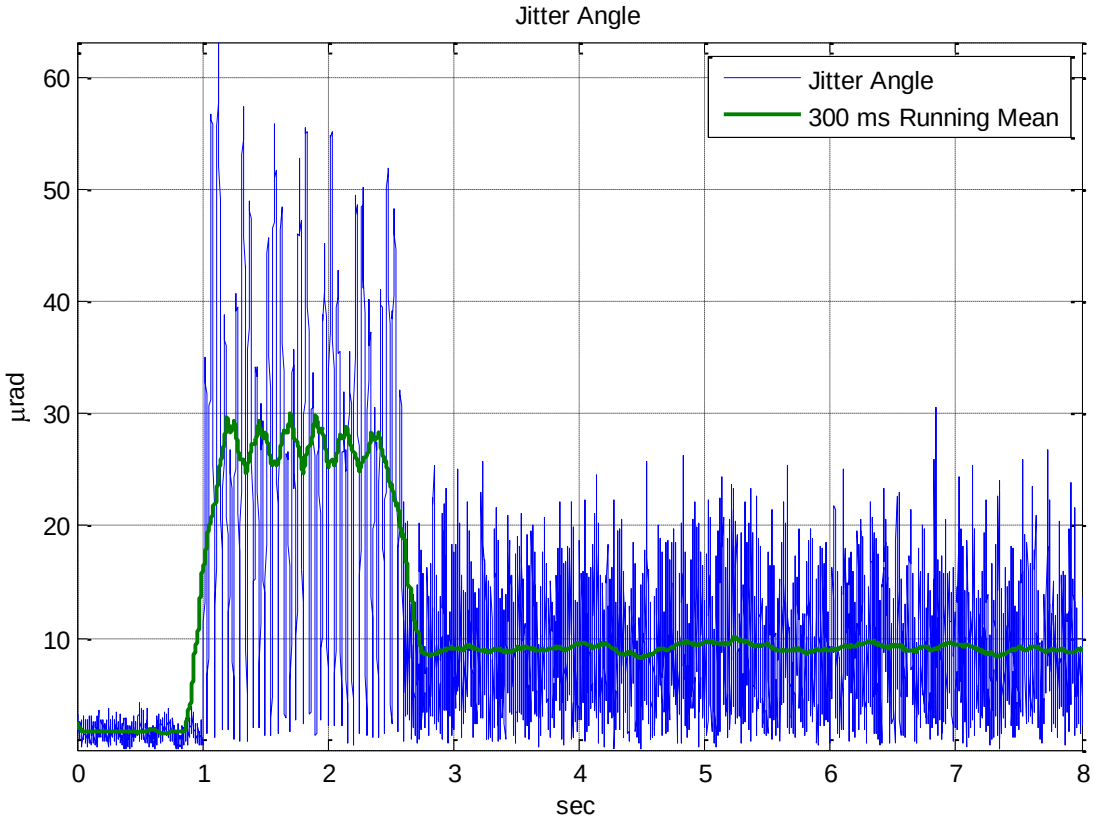

Figure 29. Jitter Angle for PSM PI Control for 10 Hz Vibration

The performance of the jitter mitigation system using ARS and PSM platform motion sensing is very similar in terms of jitter angle. As seen in Figure 30, the ARS based system also reduced beam jitter at the target to less than ±60 µm in the x-direction but was slightly less effective in the y-direction, reducing jitter to ±85 µm. The 10 Hz frequency of the beam motion remains visible after control, indicating the ARS based control system does not effectively remove this frequency of jitter. It should be noted, however, that the jitter control gains were tuned for the multiple frequency case.

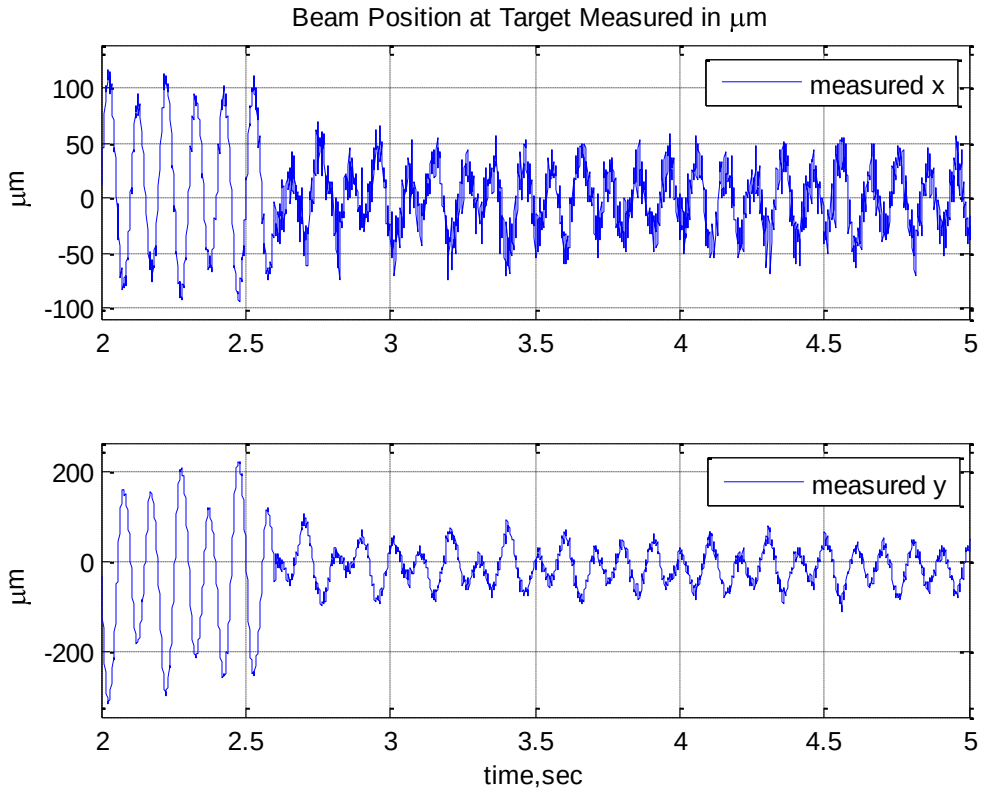

Figure 30. Jitter Mitigation Using ARS PI Control for 10 Hz Vibration

Similar results are also seen in Figure 31. The jitter angle is reduced to less than 25 μrad with an RMS jitter angle of 10.7, a 63% reduction from that of uncontrolled beam. The standard deviation of the jitter angle is reduced 57.01% to 5.40 μrad.

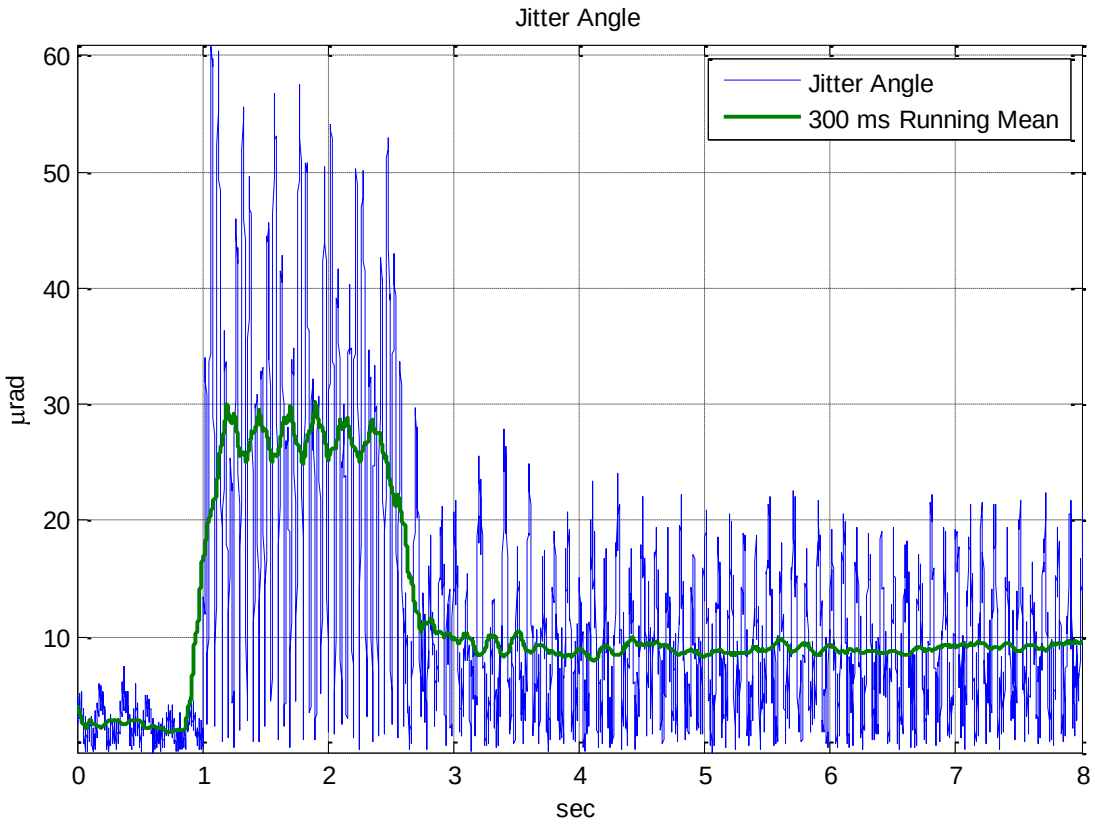

Figure 31. Jitter Angle for ARS PI Control for 10 Hz Vibration

The similarity between the performance of the PSM and ARS based jitter mitigation systems is highlighted by Figure 32 and Table 4, though the PSM system consistently slightly outperforms the ARS system.

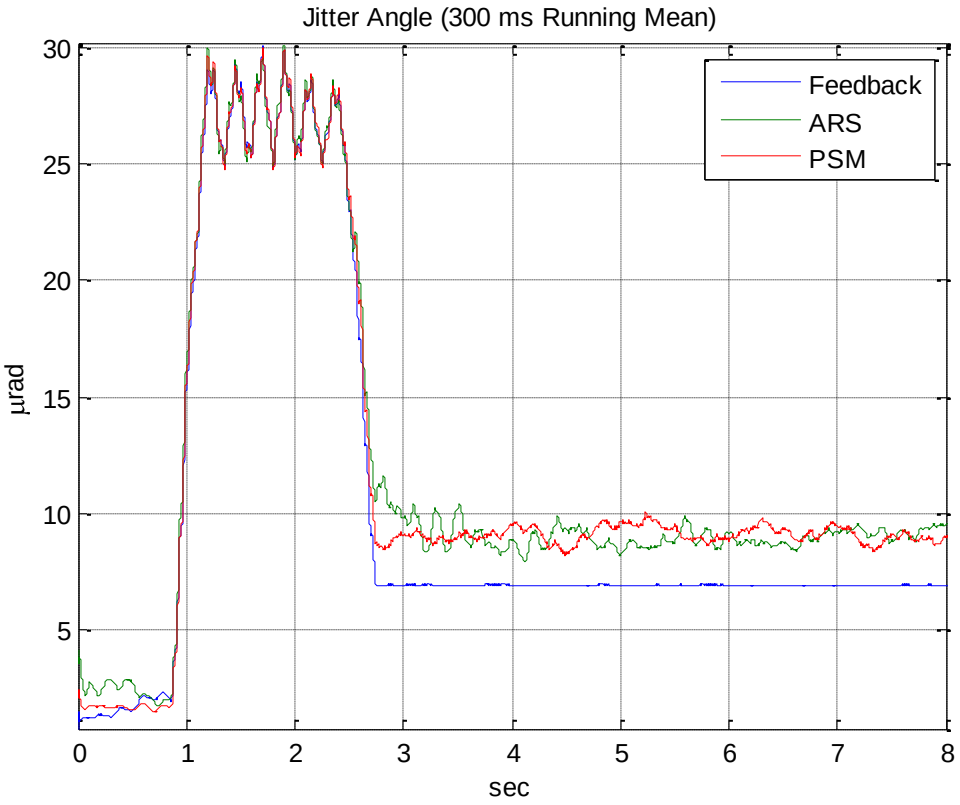

Figure 32. Running Mean Comparison of 10 Hz Vibration Jitter Mitigation Systems

Table 4. Jitter Mitigation System Performance Comparison for 10 Hz Vibration

Control Scheme	**RMS Jitter Angle (µrad)**	**Improvement in RMS Jitter Angle**	**Standard Deviation (µrad)**	**Improvement in Standard Deviation**
Uncontrolled	29.21	—	12.56	—
Feedback	7.24	75.23%	2.17	82.73%
PSM	9.89	66.15%	4.52	64.02%
ARS	10.72	63.30%	5.40	57.01%

The power spectral density below most prominently displays the 10 Hz vibration frequency in the motion of the uncontrolled beam at the target. The third harmonic of this frequency contains more power than that of the second harmonic because the resonant frequency of the inertial actuator is a broad band around 30 Hz. The peak at 5 Hz is the platform transverse mode. Its third harmonic is also visible at 15 Hz. At 60 Hz, detector electrical noise can be seen in the PSM results for the y-axis of the target detector.

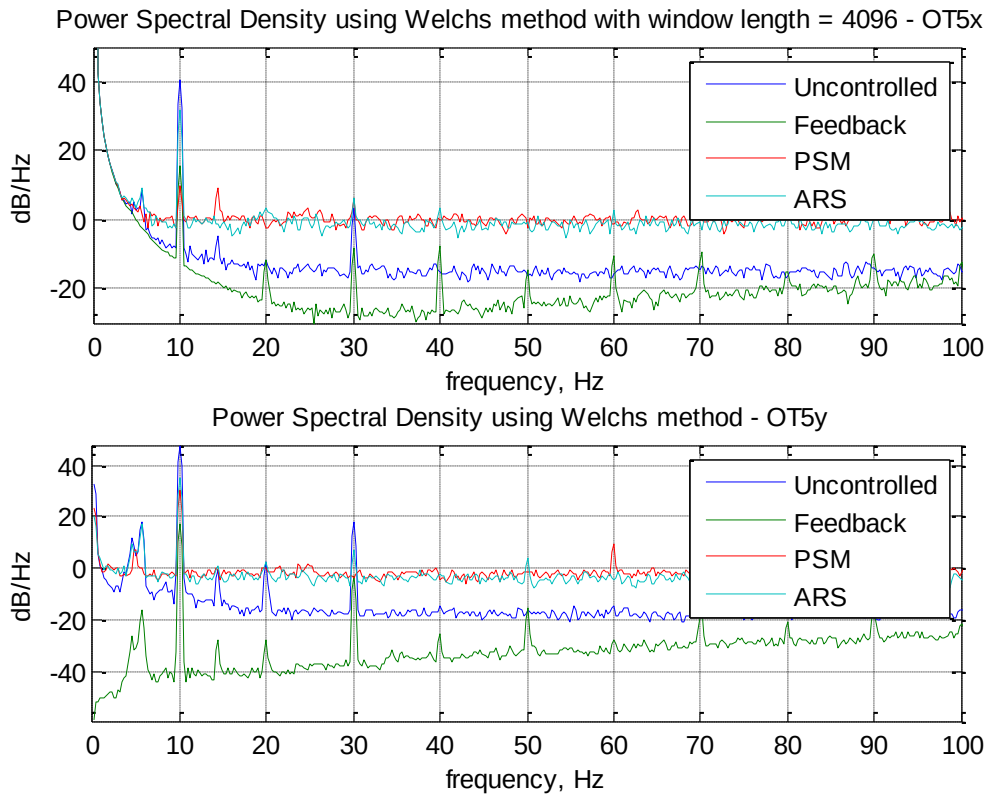

Figure 33. Power Spectral Density Comparison for 10 Hz Vibration Jitter Mitigation

The feedback system response most effectively reduces the vibration energy at all frequencies with an average power spectral density below -20 dB. The feedback system reduces the supplied 10 Hz pitch/yaw vibration 30 dB to 17 dB in the y-direction. By comparison, the ARS and PSM systems reduce this supplied frequency to 35 and 30 dB respectively. The ARS and PSM systems had small effects on the 5 Hz platform-isolator system transverse mode. Neither system is capable of detecting platform translation. Surprisingly, the PSM system is

more effective than feedback at reducing the 40 dB of 10 Hz motion in the x-direction, reducing it by 30 dB while the feedback system reduced it by only 25 dB. Of note, the ARS and PSM system PI controller increases the spectral power to 0 dB for the entire frequency spectrum. This controller response to frequencies not also present in the uncontrolled case is attributed to misalignments of the platform motion sensing systems and error introduced by integrating angular rates in the ARS system. A relatively large magnitude of disturbance is required for the beam prediction calculations to work properly. This is why actuated frequencies, their harmonics, and resonant frequencies are reduced in energy but all others are amplified.

4.2.3 Jitter Mitigation Performance for Multiple Frequency Pitch/Roll/Yaw Vibration

As expected, the feedback jitter mitigation system effectively removes jitter for the multiple frequency platform vibration case. Again, the feedback case is considered the best of the jitter mitigation systems examined. Control using feedback for multiple frequency platform vibration is shown in Figure 34 below.

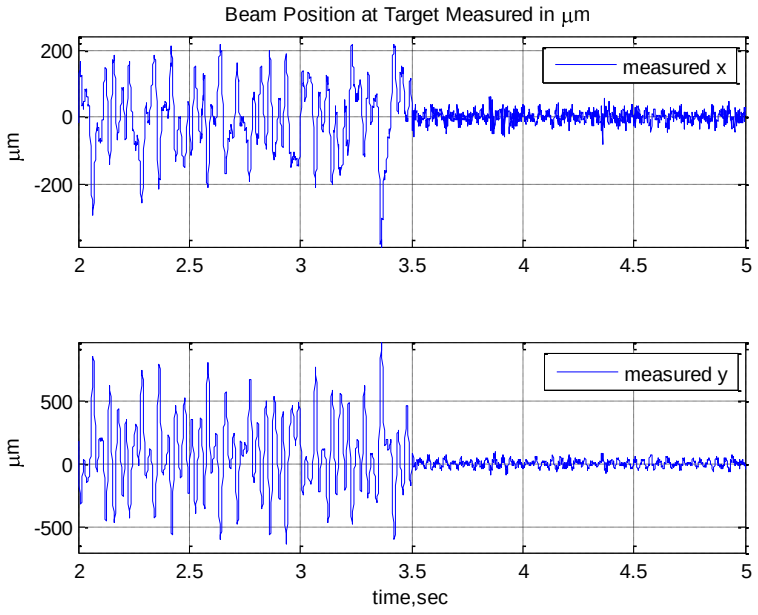

Figure 34. Jitter Mitigation Using Feedback PI Control for Multiple Frequency Vibration

Using feedback control, the jitter angle is reduced from greater than ±200 µrad in the x-direction and greater than ±500 µrad in the y-direction to less than ±50 µrad in both directions. The jitter angle standard deviation is reduced 85.98% from 40.37 µrad to 5.66 µrad.

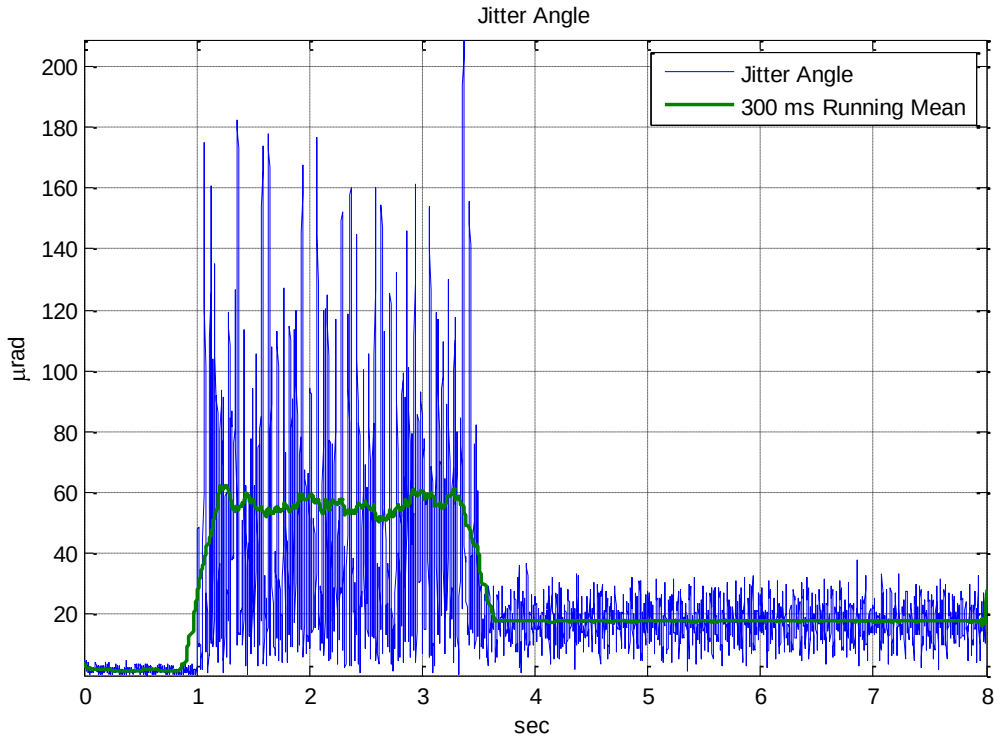

Figure 35. Jitter Angle for Feedback PI Control for Multiple Frequency Vibration

Again, feed forward jitter mitigation is not as effective as feedback, but it significantly reduces the beam jitter at the target. For multiple frequency vibration PSM jitter mitigation shown in Figure 36, jitter is reduced to ±100 µm in the x-direction and less than ±200 µm in the y-direction. This corresponds to a 64.72% reduction in RMS jitter angle and a 68.49% reduction in jitter angle standard deviation (shown in Figure 37).

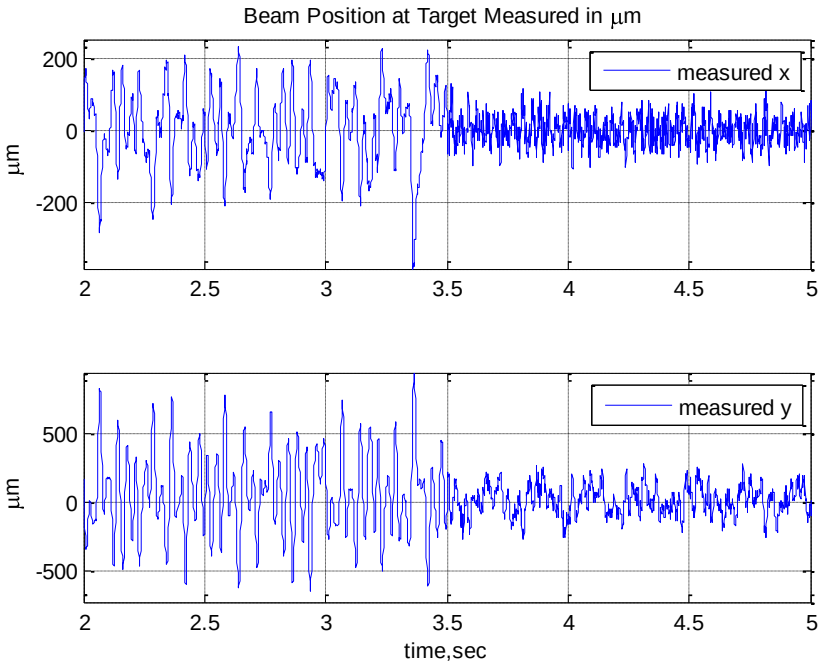

Figure 36. Jitter Mitigation Using PSM PI Control for Multiple Frequency Vibration

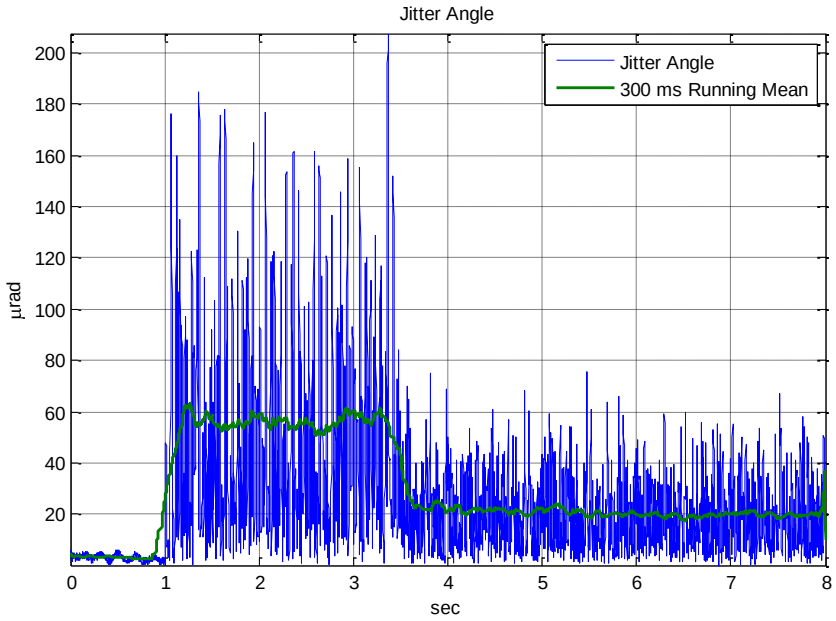

Figure 37. Jitter Angle for PSM PI Control for Multiple Frequency Vibration

Unlike in the 10 Hz pitch/yaw platform vibration case, the PSM system is significantly more effective at reducing jitter than the ARS system for the multiple frequency platform vibration case. The ARS system slightly reduced the ±200 µm jitter in the x-direction to less than ±150 µm. However, the ARS system proved nearly as effective as the PSM system in y-direction jitter mitigation, also reducing y-direction jitter to less than ±200 µm.

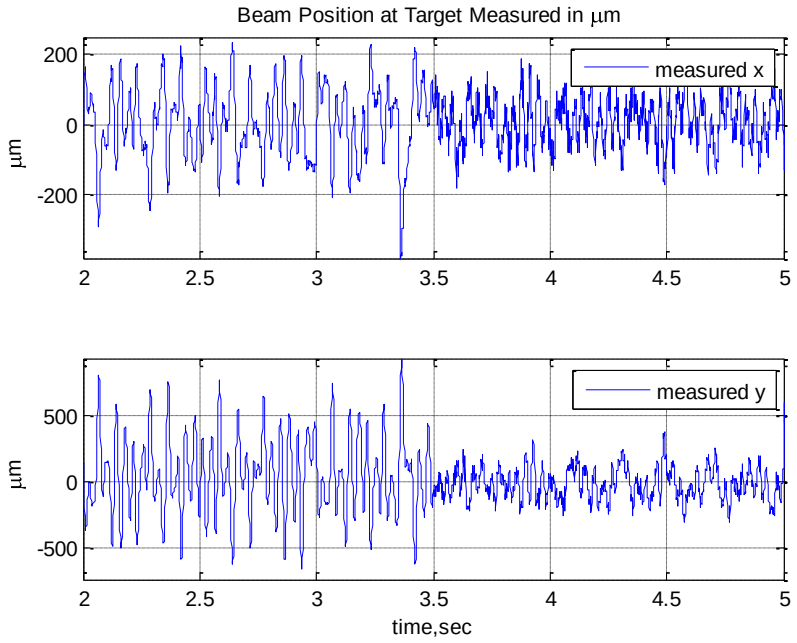

Figure 38. Jitter Mitigation Using ARS PI Control for Multiple Frequency Vibration

When combined, however, the reduction in RMS jitter angle remained significant at 53.40% with a 58.94% reduction in standard deviation as shown in Figure 39.

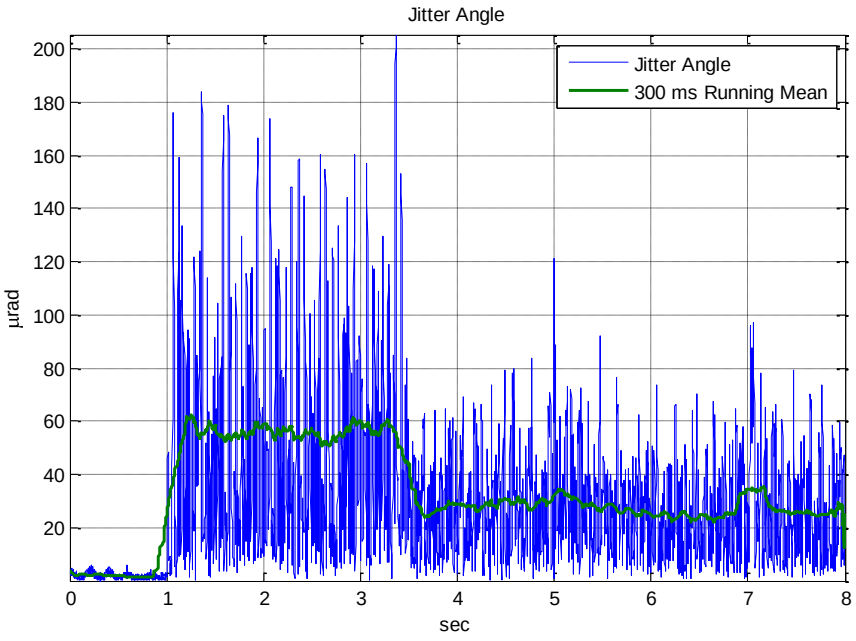

Figure 39. Jitter Angle for ARS PI Control for Multiple Frequency Vibration

Figure 40 highlights the performance comparison between the systems. The large spike in the ARS mean jitter angle at 5 seconds and 7 seconds is the result of resetting the running mean of the ARSs to zero every two seconds beginning at 3 seconds in order to remove the sensor drift. The 0.5 Hz running mean reset frequency is the frequency experimentally determined to best reduce sensor drift. Other cases using the ARS system to determine platform orientation apply a lowpass filter to the ARS outputs to create the sensor drift signal. This drift signal is subtracted from the ARS outputs as discussed in section 3.2.2.

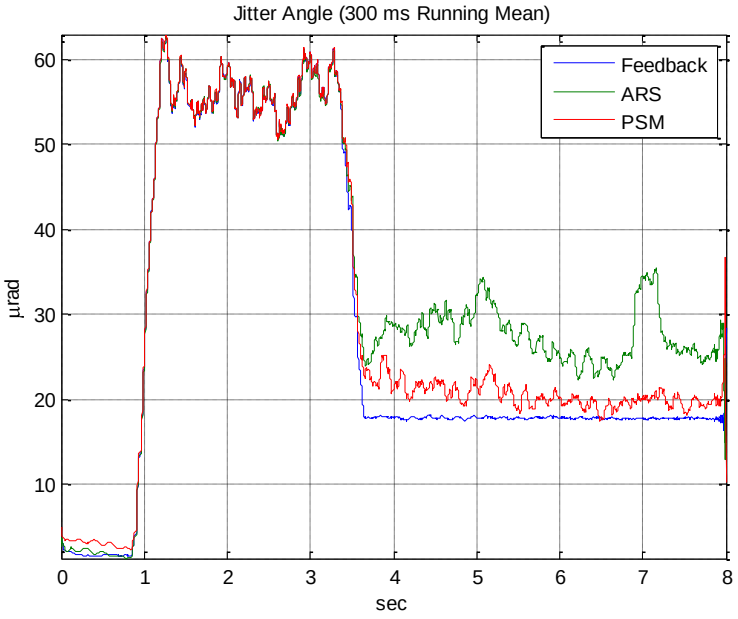

Figure 40. Running Mean Comparison of Multiple Frequency Vibration Jitter Mitigation Systems

General system performance statistics are presented in Table 5.

Table 5. Jitter Mitigation System Performance Comparison for Multiple Frequency Vibration

Control Scheme	RMS Jitter Angle (μrad)	Improvement in RMS Jitter Angle	Standard Deviation (μrad)	Improvement in Standard Deviation
Uncontrolled	68.77	—	40.37	—
Feedback	18.72	72.78%	5.66	85.98%
PSM	24.26	64.72%	12.72	68.49%
ARS	32.05	53.40%	16.58	58.94%

The power spectral density in Figure 41 reveals the complexity of the disturbance that the source platform experiences. The frequencies with high energy are primarily represented by the vibration frequencies of 10, 13, 29, and 47 Hz pitch/yaw and 17, 23, 41, and 51 Hz roll. The harmonics are not as prevalent as they were in the 10 Hz pitch/yaw case. However, large "hump" at 30 Hz indicates that significant energy remains uncontrolled as a result of the broad actuator resonance band at 30 Hz. Furthermore, the 5 Hz platform transverse mode and 13 Hz rotational mode show much increased energy. The PSM system removes the jitter that results from the platform transverse mode at 5 Hz, reducing the x-translation induced jitter 20 dB from 30 dB to 10 dB and the y-translation induced jitter 13 dB. Although neither the ARS system nor the PSM system is capable of detecting platform translation, the power spectral density indicates that PSM system is more effective at removing the 5 Hz translation-induced jitter. This reduction in spectral power for a motion that neither the ARS system nor the PSM system can detect results from the control system mitigating the 10 Hz actuation frequency. This disturbance is at a harmonic interval of the 5 Hz translational mode. The systems are equally effective at measuring the platform 13 Hz rotational mode and mitigating the resulting jitter. The ARS and PSM systems both reduced the 13 Hz rotational mode 17 dB in the x-direction and 20 dB in the y-direction.

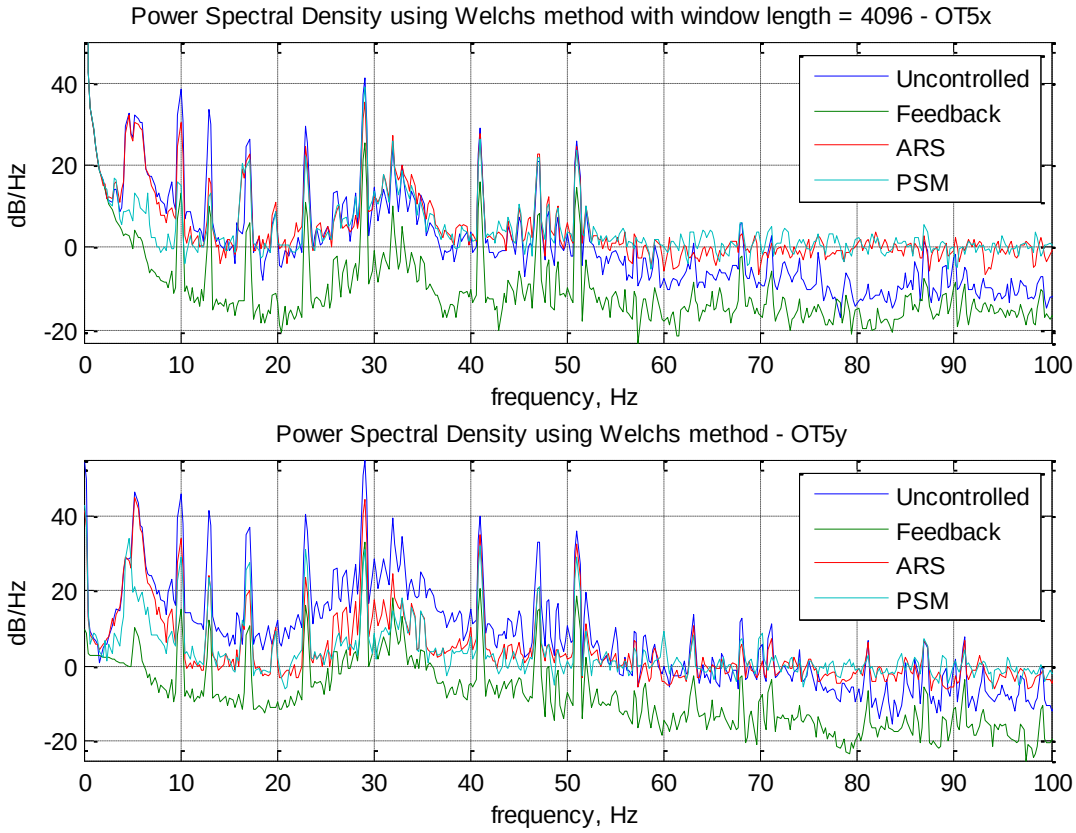

Figure 41. Power Spectral Density Comparison for 10 Hz Vibration Jitter Mitigation

4.2.4 Jitter Mitigation System Error Analysis

The results of the jitter mitigation system acting independent of target motion accurately characterize their effectiveness. The x-y plots of the beam position at the target for the ARS and PSM systems, particularly for the multiple frequency vibration case, highlight the relative effectiveness of the system in each direction. Although the magnitude of the residual jitter in the x-direction may be lower than that in the y-direction, the relative reduction of jitter in the y-direction is consistently greater than that in the x direction. This discrepancy between the x and y-directions indicates FSM alignment errors in the x-direction. The beam prediction algorithm predicts the position of the beam at the target using the technique of geometrical optics assuming that the FSMs are mounted at a 45º angle to the beam path. However, the mounting mechanism cannot guarantee these angles and they cannot be easily determined. The misalignment error

compounds because of the multiple FSMs in the system. FSM alignment error is not experienced in the y-direction because the platform surface serves as a mounting reference to ensure that the beam intersects the mirror y-axis perpendicularly. The power spectral density plots also reveal a consequence of PI control. Compared to the high frequencies for the uncontrolled case, the high frequencies for the feed forward control cases carry much more energy. This is expected because the PI controller is tuned to control the low frequency response of the system so that the steady state error is zero. This comes at the price of introducing high frequency noise as the system oscillates rapidly about the steady state value. This "waterbed effect" is seen for all vibration cases, with and without target motion. As observed in Figure 40, resetting the running mean of the ARS signals every two seconds introduces significant jitter. As a result, a superior means of removing the ARS drift signal was devised using a lowpass filter. This lowpass filter is used in the ARS system for all vibration cases with target motion.

4.3 Target Tracking Controller Performance Comparison

The PI feedback target tracking system effectively controlled FSMB to track the moving target, and thus keep the beam line-of-sight aligned with the platform-to-target line-of-sight. The decrease and increase in x-position of the beam on the target at 10 and 23 seconds, respectively shown in Figure 42, denotes target acceleration as it slows, pauses, and reverses direction. The target tracking system converges onto an aimpoint on the target within a second of the acceleration period and maintains that aimpoint until the next acceleration period. The displacement from zero is not a concern, because it does not reduce the power on target. It only slightly changes the location where the laser's energy is deposited. These offsets are small and would not result in a miss. The overall effect is still the deposition of energy at a single point on the target while the target is in motion. Further work is necessary to maintain the desired aimpoint during acceleration periods. The jitter induced by the target tracking system is less than ±25 μm in the x-direction and ± 50 μm in the y-direction throughout the target's motion. Much of this jitter results from the target platform itself (see Figure 14), which is not floated, and from the target PSM, which is elevated and cantilevered to align with the source platform in the y-direction.

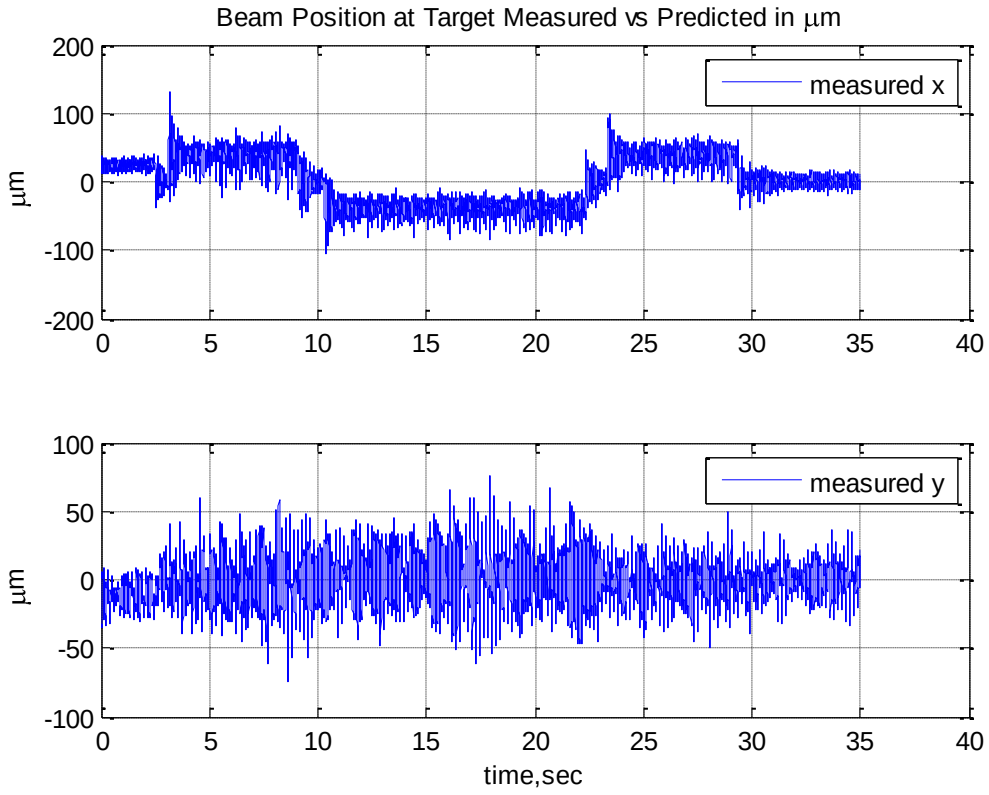

Figure 42. PI Control Target Tracking With No Vibration

Figure 43 and Figure 44 indicate that the lowpass filter used to decouple the target tracking and jitter mitigation systems functions properly. The same 200 μm jitter in the y-direction seen in Figure 43 is also seen in Figure 26 before jitter mitigation starts. The x-direction is similar.

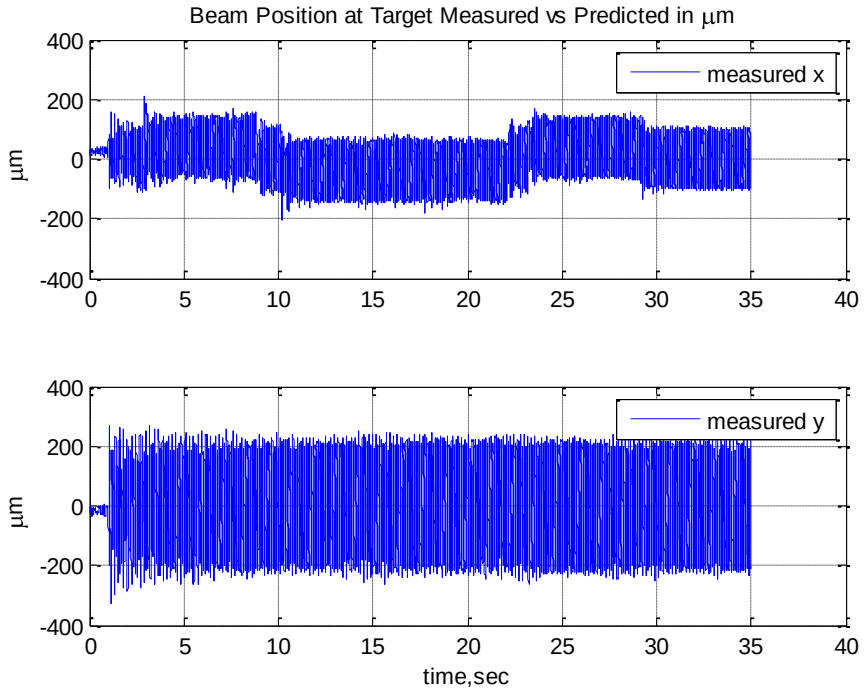

Figure 43. PI Control Target Tracking With 10Hz Vibration

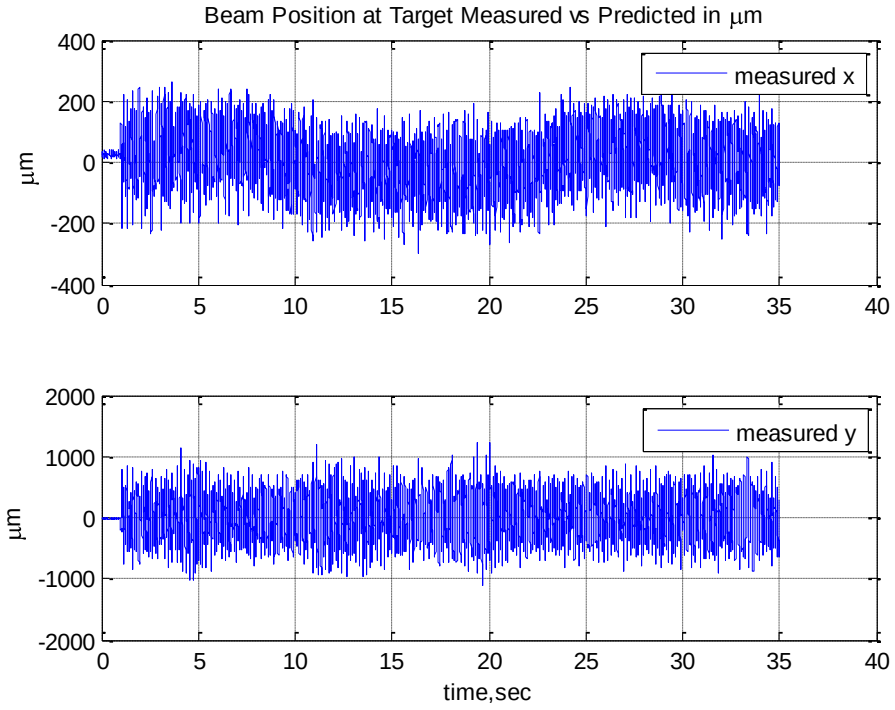

Figure 44. PI Target Tracking With Multiple Frequency Excitation

4.4 System Performance Evaluation

4.4.1 Beam Control System Performance for 10 Hz Pitch/Yaw Vibration with Target Motion

Combining the jitter mitigation and target tracking systems produces a beam control system that effectively mitigates platform-induced jitter while engaging a moving target. As was the case for the jitter mitigation studies, the feedback target tracking and jitter mitigation in Figure 45 and Figure 46, also represents the best beam control system performance currently achievable in the laboratory and serves as a baseline for comparison. This feedback based system reduces the jitter angle from 60 μrad to below 15 μrad for the 10 Hz case. The PSM and ARS feed forward systems compare favorably to this standard. The feedback system reduced RMS jitter angle by 69.98% while the PSM and ARS systems reduced RMS jitter angle by 55.88% and 52.08% respectively. The PSM system slightly outperformed the ARS system by reducing the jitter angle standard deviation 58.31% compared to 42.38%.

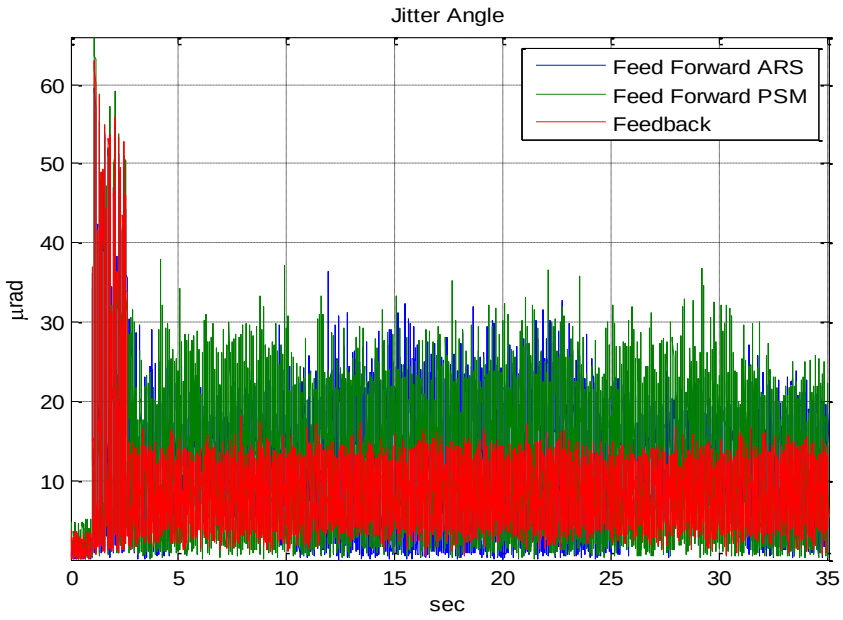

Figure 45. Jitter Mitigation System Jitter Angle Comparison for 10 Hz Vibration with Target Motion

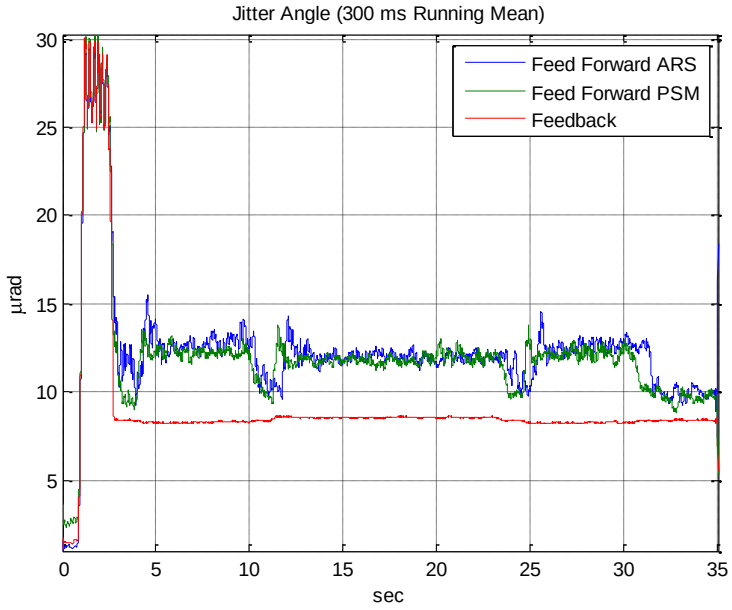

Figure 46. Jitter Mitigation System Running Mean Comparison for 10 Hz Vibration with Target Motion

The power spectral density plot in Figure 47 indicates that the PSM and ARS systems performed almost identically at frequencies above 10 Hz. At 10 Hz, the PSM system performed nearly as well as the feedback system in the x-direction, reducing the jitter by 25 dB. The ARS system reduced the 10 Hz frequency x-direction jitter by 8 dB. In the y-direction, the ARS and PSM systems performed very similarly over the frequency spectrum, reducing the 10 Hz y-direction jitter 13 dB and 18 dB respectively.

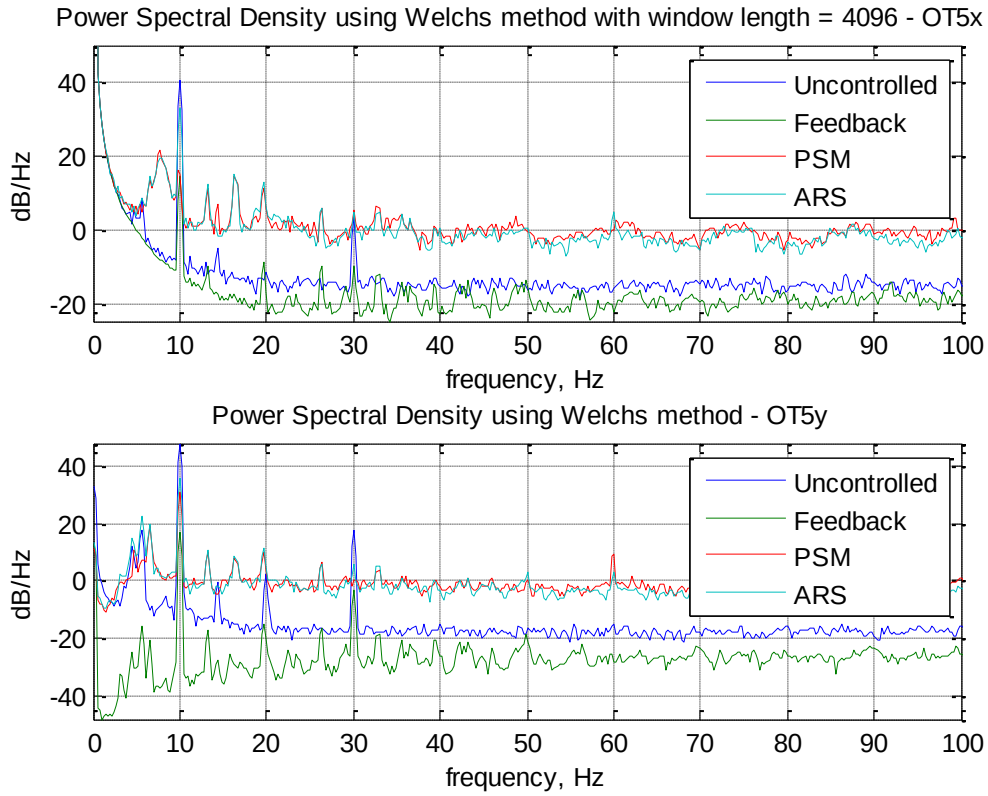

Figure 47. Jitter Mitigation System Power Spectral Density Comparison for 10 Hz Vibration with Target Motion

Table 6. Jitter Mitigation System Performance Comparison for 10 Hz Vibration with Target Motion

Control Scheme	RMS Jitter Angle (μrad)	Improvement in RMS Jitter Angle	Standard Deviation (μrad)	Improvement in Standard Deviation
Uncontrolled	29.56	—	13.00	—
Feedback	8.87	69.98%	2.41	81.47%
PSM	13.04	55.88%	5.42	58.31%
ARS	14.17	52.08%	7.49	42.38%

4.4.2 Beam Control System Performance for Multiple Frequency Pitch/Roll/Yaw Vibration with Target Motion

The multiple frequency pitch/roll/yaw vibration with target motion case is the case most representative of a real world scenario in which a jitter-mitigating, target-tracking beam control system will be used. The results indicate that, while not as effective as feedback or PSM based systems, an ARS based system is viable. Figure 48 shows that all systems examined reduced the initial 160 μrad jitter angle to below 80 μrad. The feedback and PSM system reduced the RMS jitter angle by 73.42% and 70.66% respectively, while the ARS system reduced the RMS jitter angle by 54.67%. However, the jitter angle standard deviations for the PSM and ARS systems are much larger than that of the feedback system. The feedback system reduced the standard deviation from 38.69 μrad to 3.07 μrad. The PSM system reduced the standard deviation to 9.73 μrad, and the ARS system reduced the standard deviation to 14.12 μrad.

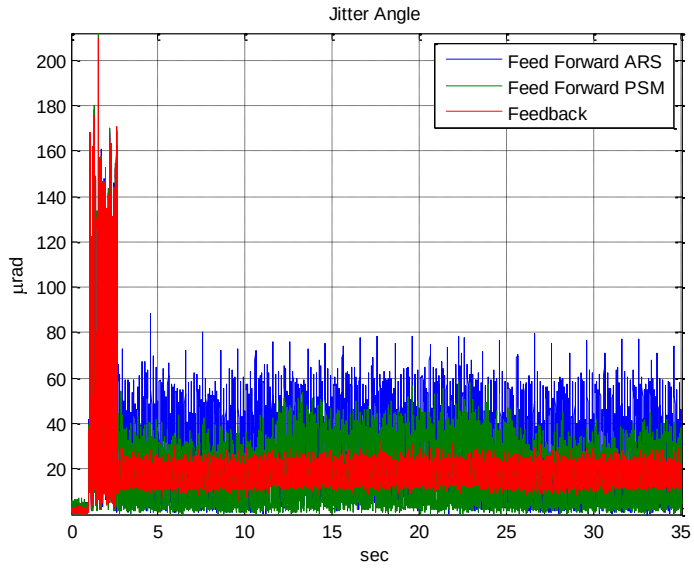

Figure 48. Jitter Mitigation System Jitter Angle Comparison for Multiple Frequency Vibration with Target Motion

In the jitter angle running mean plot shown below, the PSM system reduces jitter more than the feedback system. The mechanism of this anomaly is unknown, but it is believed to be a result of target motion and calibration between runs resetting the jitter angle.

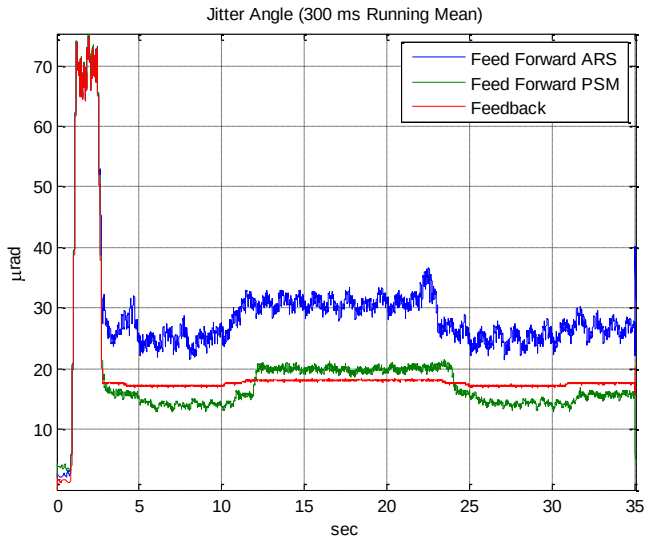

Figure 49. Jitter Mitigation System Running Mean Comparison for Multiple Frequency Vibration with Target Motion

The power spectral density, as expected, indicates that the ARS system is unable to detect and control the jitter due to the 5 Hz platform transverse mode. Except for the 10 Hz x-direction jitter, the ARS and PSM system performed very similarly, with the PSM system reducing the power across the frequency spectrum slightly more than the ARS system. The ARS system reduced the 10 Hz x-direction jitter 8 dB while the PSM system almost matched the feedback system, reducing the power 23 dB. As was the case with the stationary target multiple frequency power spectral density plot, the broad inertial actuator resonance around 30 Hz introduces a large amount of jitter to the system.

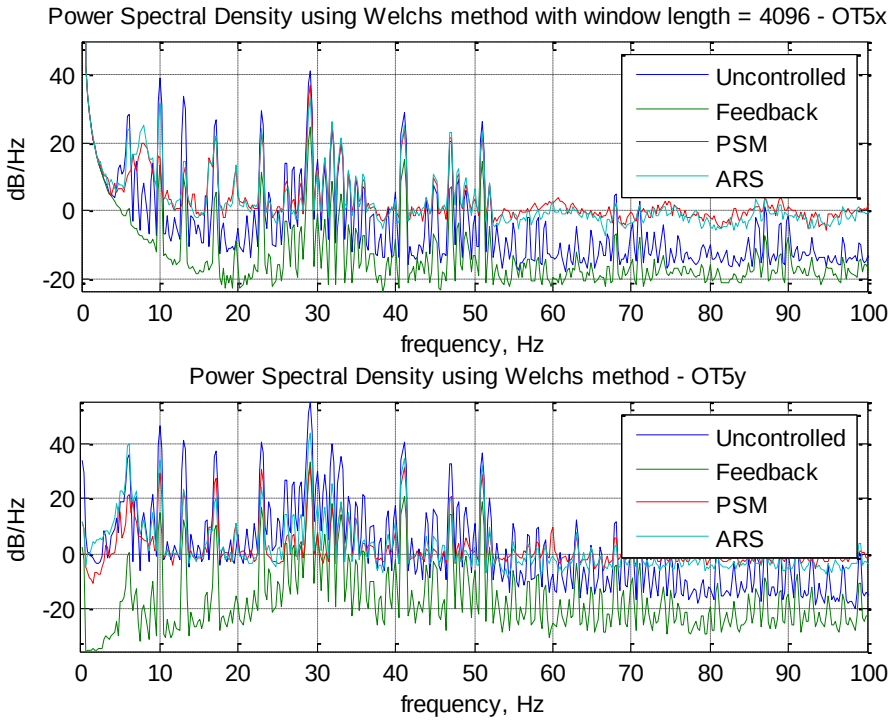

Figure 50. Jitter Mitigation System Power Spectral Density Comparison for Multiple Frequency Vibration with Target Motion

Table 7. Jitter Mitigation System Performance Comparison for Multiple Frequency Vibration with Target Motion

Control Scheme	RMS Jitter Angle (μrad)	Improvement in RMS Jitter Angle	Standard Deviation (μrad)	Improvement in Standard Deviation
Uncontrolled	78.32	—	38.69	—
Feedback	18.37	73.42%	3.07	92.06%
PSM	21.92	70.66%	9.73	74.85%
ARS	34.07	54.67%	14.12	63.49%

4.4.3 Beam Control System Error Analysis

Several significant sources of error exist in this research. The primary source of error is the construction of the beam control system. As noted previously, despite using research grade equipment, optics mounting angles will have some inaccuracy associated with them as they are mechanical systems and the desired tolerances are measured in micrometers. The resulting error in the x-direction at the target is significant because the calculation of the beam position at the target, the centerpiece of feed forward jitter mitigation, is no longer accurate. Furthermore, the distance between optical elements and between the source platform and the target must be measured manually, thereby introducing additional error to the jitter mitigation system.

Another significant source of error results from reference frame misalignments. The ARS array, accelerometer array, and PSM reference frames are not aligned with that of the platform. In order to accurately sense platform motion sensing and comparison and compare sensing systems, these reference frames must coincide. As is the case with the optics, the tolerances for the motion sensing systems are small. Small rotations of the ARS array, accelerometer array, or PSM reference frames relative to the platform reference frame can cause large errors in motion sensing by coupling axes of rotation. Rotational differences between the platform motion sensing system reference frames and the platform reference frame may be corrected electronically using a rotation matrix. However, the platform axes of rotation must be known. This is not easily measured because a pure pitch, roll, or yaw motion is nearly

impossible to create. Additionally, the FSM reference frames are not aligned with that of the target PSM. This can be seen by sweeping FSMA in the x-direction with all else stationary, and by sweeping FSMB in the x-direction with all else stationary. Both cases result in beam motion in y-directions at the target. Despite repeated attempts, the cross coupling could not be completely corrected. Future models will require accurate knowledge of the FSM and target reference frames to correct these misalignments.

Additionally, the PSM array, like the accelerometer array, relies on hand measured distances between detectors to calculate platform rotations. Small measurement errors reduce the performance of the system.

5 Conclusion

5.1 Results

This research successfully developed a directed energy beam control system that is capable of mitigating platform-induced jitter using internal sensors while engaging targets moving in the LOS reference frame. The ARS array proved comparable to the PSM array at sensing base platform motion and determining platform orientation with error less than 1%. The accuracy with which the ARS array senses actual platform motion can be improved by aligning the platform axes of rotation with those of the ARS array. The PI jitter mitigation system effectively removed jitter for 10 Hz pitch/yaw motion and multiple frequency pitch/roll/yaw motion. System performance can be enhanced with improved system construction and calibration precision. The PI target tracking system effectively maintained a slightly offset aimpoint on targets of constant velocity. Combining the jitter mitigation and target tracking systems into a beam control system, created an effective means to mitigate jitter while engaging moving targets. Though not as effective as the feedback system or the PSM system, the ARS system reduced RMS jitter angle by over 50% and jitter angle standard deviation by over 60%. To characterize the effectiveness of the jitter mitigation system in a real world application the jitter effect on beam radius is determined as shown in Figure 51.

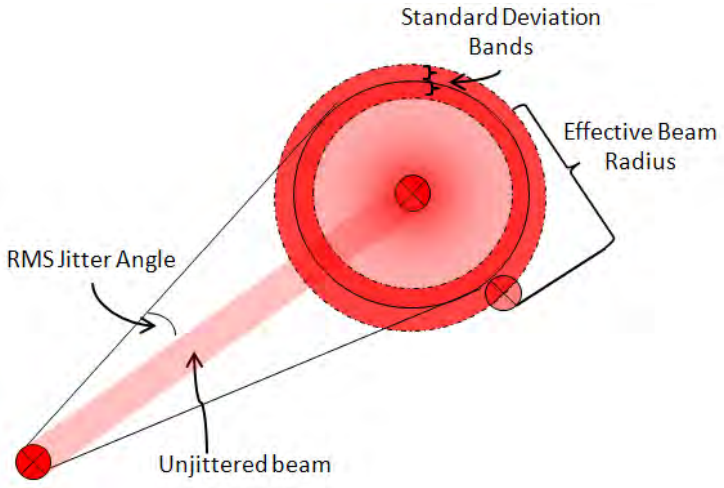

Figure 51. Jitter Effect On Beam Radius Diagram

Assuming a directed energy weapon system with a 1 meter aperture, 1 µm wavelength and 10 kW/cm^2 irradiance, the effective irradiance at the target for the no jitter case, the ARS controlled case, and the uncontrolled case are shown in Figure 52.

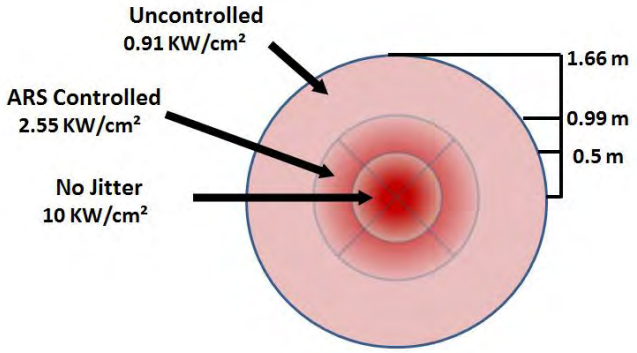

Figure 52. Jitter and Control Effects on a 1m Aperture 1µm Wavelength 10 kW/cm^2 Beam at 10km

Experiments have determined that 10 kJ of energy will burn through a cubic centimeter of almost any substance. Therefore, the 180% increase in irradiance at the target using the ARS beam control system dramatically reduces the source laser power and the dwell time required to destroy a target. The ARS system is a viable means of improving the performance of a directed energy weapon system.

5.2 Future Work

Though effective, the beam control system developed in this research can be improved in several areas to achieve the microradian to sub-microradian jitter budget of most directed energy systems. System performance will most be improved by aligning the accelerometer and ARS reference frames to that of the source platform electronically using a rotation matrix. This will improve platform motion sensing and thereby improve the jitter mitigation system. Jitter control could also be improved by accurately aligning the optical elements on the platform. To minimize construction, measurement, and alignment errors, a prototype platform cut using computer controlled machines should be built. However, this type of system is not practical during a research phase of development which requires varying configurations. Alignment of the existing system will greatly improve jitter mitigation performance in the x-direction and should

be performed before the system is expanded to include a beam director and adaptive optics. Adding optical elements adds to the complexity of the system and allows errors to compound further. Platform-induced jitter can be further reduced by applying an adaptive controller, such as a least-mean-squares (LMS) controller.

The PI feedback target tracking system is a first step in developing a practical beam control system. Future work should explore improved target tracking algorithms, such as H_∞ control, to permit tracking of accelerating targets and reduced displacement from zero on the target. To move outside of the laboratory environment target feedback should be replaced by an optical target tracking system boresighted with the source laser. With these systems in place, the target should be moved in two degrees of freedom relative to the source platform to simulate a target in real applications.

APPENDIX A: Newport Fast Steering Mirrors

FSM System

	FSM-300	FSM-320
Number of Axes	2 (tip-tilt)	2 (tip-tilt)
Angular Range from ±10 V	± 26.2 mrad (± 1.5°), mechanical(1)	± 26.2 mrad (± 1.5°), mechanical(1)
Resolution	≤ 1 µrad rms, mechanical(1)	≤ 1 µrad rms, mechanical(1)
Repeatability	≤ 3 µrad rms, mechanical(1)	≤ 3 µrad rms, mechanical(1)
Accuracy From ±26.2 mrad, 20°C(1,2)	≤ 0.262 mrad (0.015°), mechanical(1)	≤ 0.262 mrad (0.015°), mechanical(1)
Linearity From ±26.2 mrad, 20°C(1,2)	≤ 1.0%	≤ 1.0%
Closed-Loop Amplitude Bandwidth(2) (-3 dB)	≥ 800 Hz at 10 mV	≥ 350 Hz at 10 mV
Closed-Loop Phase Bandwidth(2) (60° lag)	≥ 400 Hz	≥ 325 Hz
Response Flatness(2)	Peaking ≤ 3 dB	Peaking ≤ 3 dB
Noise Equivalent Angle (1 Hz to 10 kHz)	≤ 3 µrad rms	≤ 3 µrad rms
Resolution of Local Position Sensor	≤ 0.5 µrad	≤ 0.5 µrad
Quiescent Power at FSM Assembly	≤ 5 W at any angle ± 26.2 mrad	≤ 5 W at any angle ± 26.2 mrad
Operating Temperature Range(2)	0 to 35°C (32 to 95°F)	0 to 35°C (32 to 95°F)
Storage Temperature Range	-20 to 55°C (-4 to 131°F)	-20 to 55°C (-4 to 131°F)
Warm-up Time for Mirror Stability(2) at 20°C	≤ 10 minutes	≤ 10 minutes
Mirror Thermal Drift(2)	≤ 5 µrad/°C, mechanical(1)	≤ 5 µrad/°C, mechanical(1)
Optical Axis Location	1.5 in. (38.1 mm) high, centered left-to-right	1.5 in. (38.1 mm) high, centered left-to-right
Mirror Head Weight with Base	15.3 oz (434 g)	15.3 oz (434 g)
Interconnect Cable Length	9.8 ft (3 m)	9.8 ft (3 m)

Standard Mirror Options

	FSM-300	FSM-320
Mirror Substrate Material	Pyrex	Fused Silica
Mirror Retaining Mechanism	Mirror bonded to aluminum carrier (user replaceable).	Mirror bonded to stainless steel carrier (replaceable).
Mirror Pivot Point (centered on mirror)	Gimbaled 12.19 mm behind mirror surface	Gimbaled 9.15 mm behind mirror surface
Mirror Diameter	25.4 mm	50.8 mm
Mirror Thickness	6.0 mm	3.0 mm
Mirror Wedge	≤ 5 arc min	≤ 5 arc min
Clear Aperture(3) at 0° angle of incidence	≥ 20.3 mm	≥ 40.6 mm
Clear Aperture(3) at 45° angle of incidence	≥ 14.4 mm	≥ 28.8 mm
Surface Flatness(3) (after coating and bonding)	≤ λ/10 at 632.8 nm over clear aperture	≤ λ/2 at 632.8 nm over clear aperture
Surface Quality(3)	15-5 scratch-dig	40-20 scratch-dig
Reflectivity, Standard Coatings(3)		
ER.1 Coating: Enhanced Aluminum	> 93%, 450-700 nm	> 93%, 450-700 nm
ER.4 Coating: Protected Gold	> 96%, 650- 1700 nm; > 98% from 1.7-2.0 µm	Please contact Newport.
Additional coating options	Please contact Newport.	Please contact Newport.

FOOTNOTES:

1) Optical angular range is equal to twice the mechanical angular range.
2) Measured under position output control. Optical closed-loop performance is also determined by external feedback electronics.
3) Optical parameters apply to central 80% of mirror aperture.

FSM-CD300B Controller/Driver

Command Input and Position Output	Analog, ±10 V = ±26.2 mrad
Peak Operating Power to Mirror	30 W
Continuous Max Operating Power to Mirror	15 W
Thermal Protection	60°C at mirror coil
Operating Temperature[2]	0 to 35°C (32 to 95°F)
Storage Temperature	-20 to 55°C (-4 to 131°F)
Use Location	Indoor use only
Relative humidity	< 95%, non-condensing
Operating altitude	< 3,000 m (10,000 ft)
Power	100-240 Vac ±10%, 47-63 Hz
Current consumption (typical)	0.40 A @ 100 Vac, 0.25 A @ 240 Vac
Fuses	2 ea, “slo-blo” (T), 5 x 20 mm, rated 2.5 A, 250 Vac
Weight	5.5 lbs (2.5 kg)
Case Dimensions (excluding connectors)	3.9” x 9.0” x 10.0” [h x w x d] (100 x 229 x 254 mm)

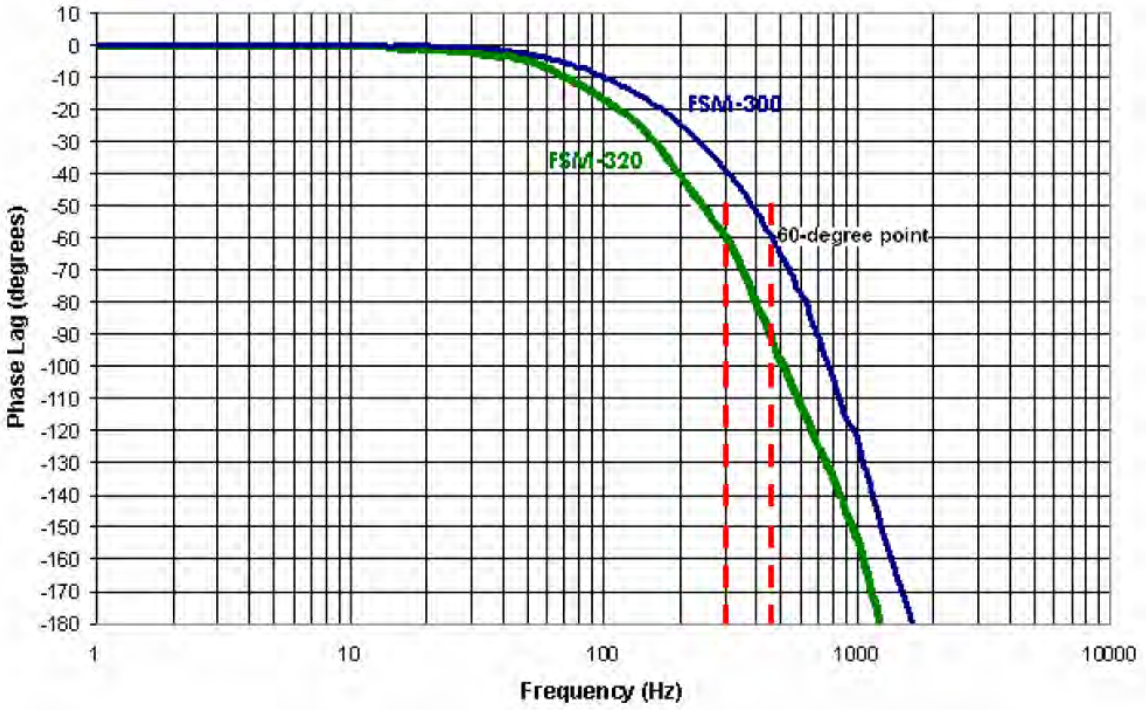

Typical phase angle Bode plot for small-angle angle excitation.
Amplitude 0.262 mrad.

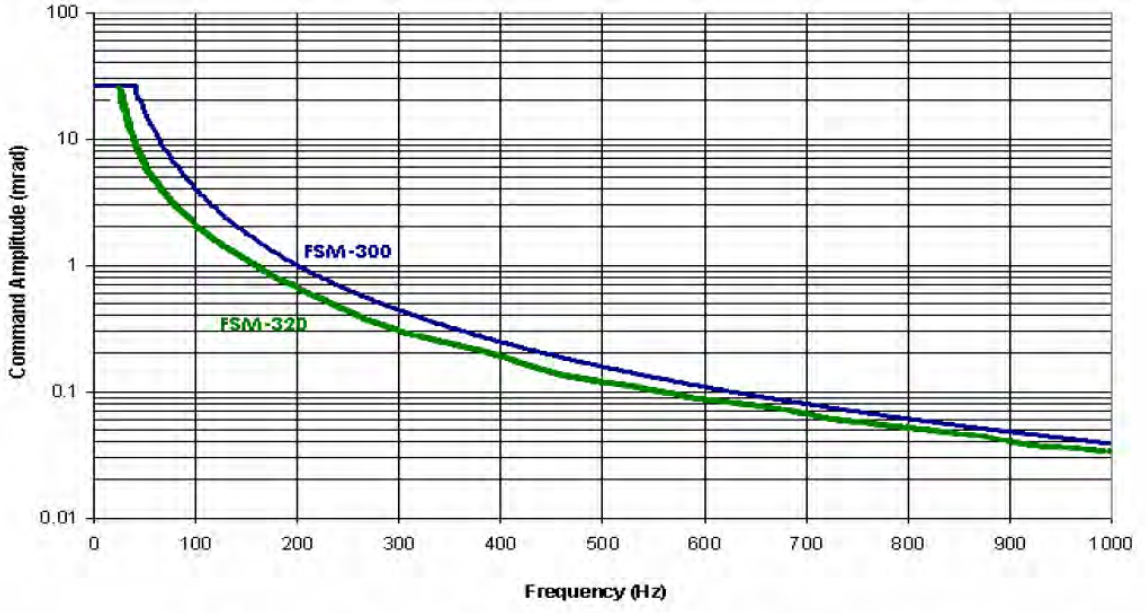

Typical shut-down curve as a function of amplitude and frequency at 20°C. Continuous operation is "safe" below the line. Derate for higher ambient temperatures.

APPENDIX B: Aerotech Inc. Linear Motor Actuator

LMA/LMAC Series SPECIFICATIONS

LMA										
Total Travel	100 mm	200 mm	300 mm	400 mm	500 mm	600 mm	700 mm	800 mm	900 mm	1000 mm
Drive System	Linear Brushless Servomotor									
Feedback	Noncontact Linear Encoder									
Resolution[5]	5 nm - 1.0 µm									
Max Travel Speed[1][6]	5 m/s									
Max Linear Acceleration[6]	3 g (30 m/s² no load)									
Max Horizontal Load[2]	40 kg									
Max Side Load[2]	20 kg									
Continuous Force[3]	207 N									
Continuous Force (20 psi)[3]	276 N									
Peak Force[3]	1106 N									
Accuracy	±1 µm/25 mm									
Calibrated Accuracy[4]	±5 µm Over Entire Length of Travel									
Repeatability	±0.5 µm									
Nominal Stage Weight	16.3 kg	18.5 kg	20.7 kg	22.8 kg	25.0 kg	27.2 kg	29.4 kg	31.6 kg	33.7 kg	35.9 kg
Moving Weight	3.28 kg (142 Motor Option)					5.18 kg (264 Motor Option)				
Material	Aluminum									
Finish	Electroless Nickel Base/Black Hardcoat Tabletop									

Notes:
1. Maximum speed based on stage capability; maximum application velocity may be limited by system data rate and resolution.
2. Maximum load based on bearing capability; maximum application load may be limited by acceleration requirements.
3. Specifications based on BLM-264-A motor. Travel increases by 20 mm when using the BLM-142-A motor.
4. Available with Aerotech controller.
5. May require encoder multiplier.
6. Consult factory on high speed and/or high acceleration applications.

LMAC										
Total Travel	100 mm	200 mm	300 mm	400 mm	500 mm	600 mm	700 mm	800 mm	900 mm	1000 mm
Drive System	Linear Brushless Servomotor									
Feedback	Noncontact Linear Encoder									
Resolution[5]	5 nm - 1.0 µm									
Max Travel Speed[1][6]	5 m/s									
Max Linear Acceleration[6]	3 g (30 m/s² no load)									
Max Horizontal Load[2]	20 kg									
Max Side Load[2]	10 kg									
Continuous Force[3]	47.9 N									
Continuous Force (20 psi)[3]	73.1 N									
Peak Force[3]	292 N									
Accuracy	±1 µm/25 mm									
Calibrated Accuracy[4]	±5 µm Over Entire Length of Travel									
Repeatability	±0.5 µm									
Nominal Stage Weight	4.5 kg	5.4 kg	6.3 kg	7.2 kg	8.1 kg	9.0 kg	9.9 kg	10.8 kg	11.7 kg	12.6 kg
Moving Weight	0.79 kg (95 Motor Option)					1.00 kg (143 Motor Option)				
Material	Aluminum									
Finish	Electroless Nickel Base/Black Hardcoat Tabletop									

Notes:
1. Maximum speed based on stage capability; maximum application velocity may be limited by system data rate and resolution.
2. Maximum load based on bearing capability; maximum application load may be limited by acceleration requirements.
3. Specifications based on BLMUC-143-A motor. Travel increases by 35 mm when using the 95 motor.
4. Available with Aerotech controller.
5. May require encoder multiplier.
6. Consult factory on high speed and/or high acceleration applications.

LMAC Series DIMENSIONS

LMAC

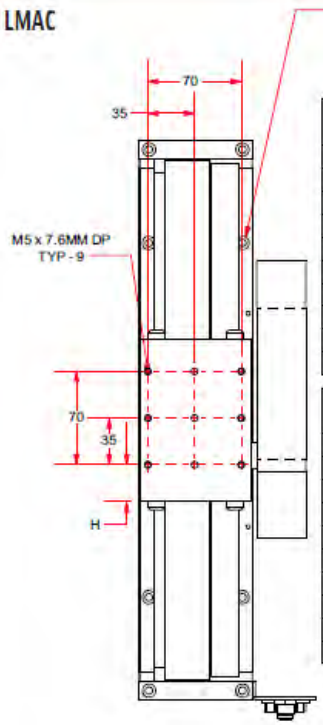

BASIC MODEL	TOTAL TRAVEL	DIMENSIONS - MILLIMETERS							
		A	B	C	D	E	F	G	H
LMAC100	100	320	305	235	188	118	291	162	46
LMAC200	200	420	405	335	238	168	391	162	46
LMAC300	300	520	505	435	288	218	491	162	46
LMAC400	400	620	605	535	338	268	591	162	46
LMAC500	500	720	705	635	388	318	691	162	46
LMAC600	600	820	805	735	438	368	791	162	46
LMAC700	700	920	905	835	488	418	891	162	46
LMAC800	800	1020	1005	935	538	468	991	162	46
LMAC900	900	1120	1105	1035	588	518	1091	162	46
LMAC1000	1000	1220	1205	1135	638	568	1191	162	46

BASIC MODEL	TOTAL TRAVEL	DIMENSIONS - MILLIMETERS							
		A	B	C	D	E	F	G	H
LMAC135	135	320	305	235	188	118	291	122	28
LMAC235	235	420	405	335	238	168	391	122	28
LMAC335	335	520	505	435	288	218	491	122	28
LMAC435	435	620	605	535	338	268	591	122	28
LMAC535	535	720	705	635	388	318	691	122	28
LMAC635	635	820	805	735	438	368	791	122	28
LMAC735	735	920	905	835	488	418	891	122	28
LMAC835	835	1020	1005	935	538	468	991	122	28
LMAC935	935	1120	1105	1035	588	518	1091	122	28
LMAC1035	1035	1220	1205	1135	638	568	1191	122	28

* ADD 40 TO WIDTH FOR B3/B4 CONNECTOR OPTIONS

RIGHT HAND MODEL SHOWN

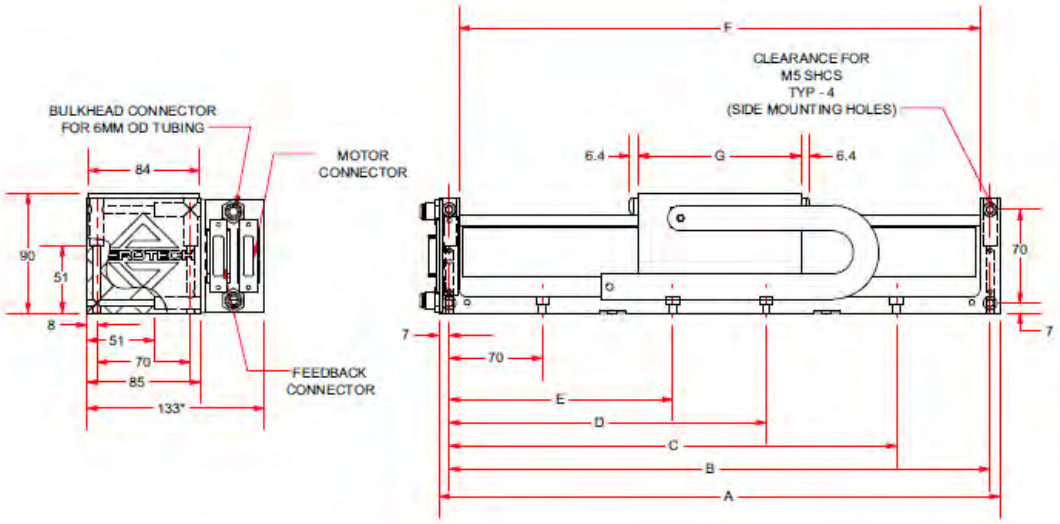

DIMENSIONS: MILLIMETERS

APPENDIX C: ATA Angular Rate Sensor

ARS-14 MHD Angular Rate Sensor

The ARS-14 is our most sensitive angular rate sensor, designed to work in a variety of high-performance applications, such as line-of-sight stabilization and precision motion control systems. The ARS-14 can measure angular motions as low as 50 nanoradians, and has low sensitivity to linear acceleration inputs, making it ideal for use in highly dynamic environments such as aerial and ground-based vehicles. The ARS-14 also features low power consumption, making it a candidate for application where power is limited. The assembly is compact, rugged, and capable of handling environmental extremes without affecting performance. The ARS-14 is also space qualifiable. The ARS-14 has a wide, usable frequency range from less than 2 Hz to more than 1,000 Hz. The scale factor of the ARS-14 is nominally 20 Volt/(rad/sec), but can be customized based on customer requirements.

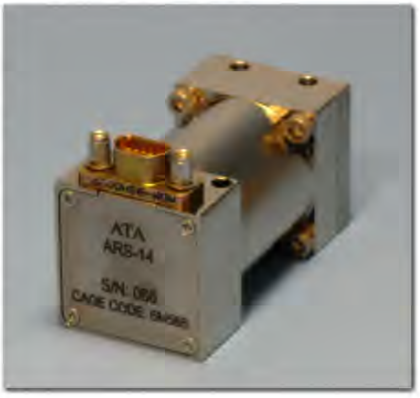

ATA's patented magneto-hydrodynamic angular motion sensors utilize the finest materials and workmanship combined in durable packages that feature:

- Dynamic range > 120 dB
- Low power consumption
- Low cross axis angular sensitivity
- Low linear acceleration sensitivity
- Integral electronics/low noise
- One-year warranty against defects in materials and workmanship on sensors, 90 days on cables.

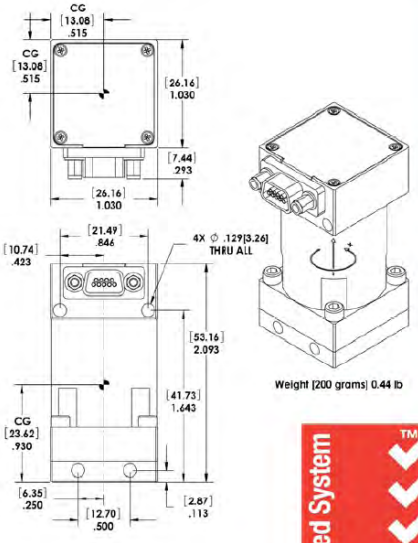

This product is subject to U.S. Government approval as required in accordance with the U.S. Government International Traffic in Arms (ITAR) Subchapter M, Title 22, Code of Federal Regulations, Parts 120 through 130 (22 CFR 120-130).

Specifications are subject to change without notice.

ATA

"Sensing ways to make the world better"®

1300 Britt St SE ♦ Albuquerque, NM 87123 USA ♦ Tel: (505) 823-1320 ♦ Fax: (505) 823-1560
E-mail: ContactATA@aptec.com ♦ Website: www.atasensors.com

Certified System™
ISO 9001
QMI-SAI Global
#1034112

ARS-14 Product Specifications

Typical ARS-14 Frequency Response

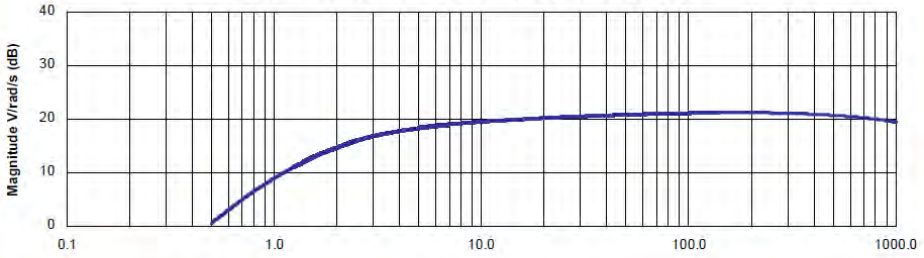

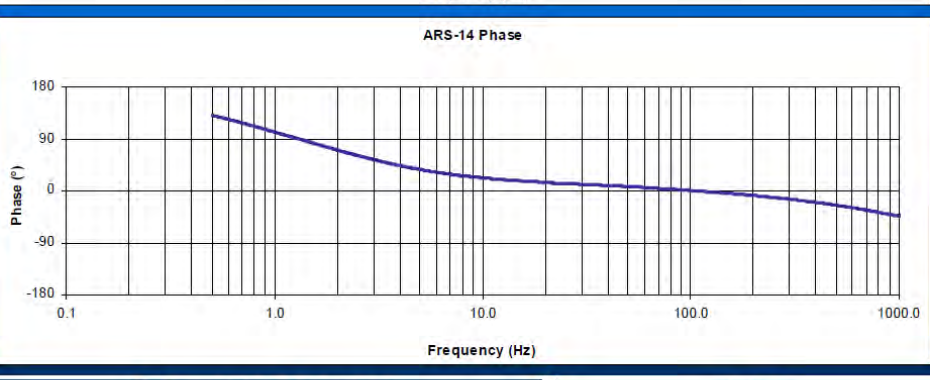

Performance / Electrical

ARS-14 Range[1]	± 0.5 radians/sec
ARS-14 Scale Factor[2]	20 Volt/(rad/sec)
Bandwidth, -3dB in testing	<2 to 1,000 Hz
Cross-axis Angular Error	< 2 %
Linear Acceleration Sensitivity	1 x 10^{-6} radians/g
Noise Equivalent Rate[3]	<5 x 10^{-6} radians/sec rms
Noise Equivalent Angle[3]	<50 x 10^{-9} radians rms
Non-linearity	< 0.25 %
Temperature Coefficient[4]	< 0.3 % Scale Factor / °C
Power Dissipation	< 0.2 Watts
Output Impedance	< 100 Ohms
Grounding[5]	Case isolated from signal common by 1MΩ minimum

Notes:
1. Based on a +/- 10V output voltage swing.
2. Measured @ 10 Hz, custom scale factors available.
3. Over 1-1000 Hz.
4. Percent change in Scale Factor per °C @ 10 Hz.
5. Signal common may be connected to case if required.
6. Analog Devices AD590 2 Terminal IC Temperature Transducer.

Wiring

ARS-14 Pin Out ITT, MDM-9S MIL-83513		
Pin	Std. Color	Connection
1	Black	Temp – [6]
2	Brown	Temp + [6]
3	Red	Power/Signal Ground
4	Orange	Signal Out
5	Yellow	N/C
6	Green	+15V
7	Blue	-15V
8	Purple	Power/Signal Ground
9	Gray	Case Ground

Environmental

Temperature-Operating	-30°C to +50°C
Temperature- Non-Operating	-40°C to +60°C

Specifications are subject to change without notice.

APPENDIX D: CSA Engineering Inertial Actuator

SA Series Inertial Actuators

CSA Engineering, Inc.

- Inertial force generator
- 1-10 lbf broadband output (0 - peak)
- Peak outputs greater than 100 lbf
- Wide bandwidth (20 to 1000 Hz)
- Self contained

SA series actuators deliver inertial force over a wide bandwidth in compact, rugged, electromagnetically efficient forms. The actuators use an electromagnetic circuit with a moving magnet that allows the coil to be thermally grounded to the housing. Magnets are suspended by specially designed long life flexures. The force is generated along the axis of the cylindical units.

Typical applications include active damping or vibration cancellation, mounts for active vibration isolation, or disturbance generation. Dynamic amplification at frequencies near the actuator resonance results in large force outputs. A rigid housing enables direct insertion of the SA into structural load paths.

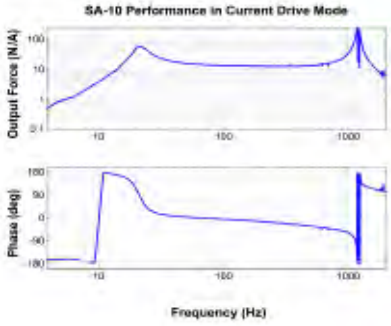

Actuators are specified by force capacity and internal suspension resonance. Standard options/accessories include alternative end caps, coils of specified impedance, a variety of cable interfaces, and current or voltage drive mode amplifiers. The overall design is easily customizable to meet the requirements of mounting configurations, drive electronics, or mass budgets.

The SA1, SA5, and SA10 are standard products. Also available are the SA2, SA35 and other non-standard models. Actuators are specified as SA*x-f* where *x* is the zero-peak force output at high frequency in pounds and *f* is the primary resonant frequency in Hz. For example, the SA5-60 produces 5 pounds force and has a 60 Hz resonance.

SPECIFICATIONS

	SA1	SA5	SA10	Units
Rated Force Output*	1	5	10	lbf (0-peak)
Bandwidth	40-1000	20-1000	20-1000	Hz
Motor Constant**	0.5	2	5	lbf/Amp
Resonant Frequency***	30-200	30-200	30-200	Hz
Resistance**	2	2	2	Ohm
Total Mass	0.25	2.9	5.5	lbm
Diameter	35	76	93	mm
Height	30	66	92	mm

* Significantly greater forces possible with good heatsinking
** Typical values
*** User-specified. Manufactured to ± 2-3%

For more information, email *actuators@csaengineering.com*

APPENDIX E: Newport Breadboard

Model	**IG-33-2**
Width	3 ft.
Length	3 ft.
Thickness	2.3 in. (58 mm)
Thread Type	1/4-20
Mounting Hole Pattern	1.0 in. grid
Surface Flatness	±0.006 in. over 2 ft. (±0.15 mm over 600 mm)
Working Surface	400 Series ferromagnetic stainless steel
Core Design	Trussed honeycomb, vertically bonded closed cell construction, 0.010 in. (0.25 mm) Steel sheet materials, 0.030 in. (0.76 mm)
Broadband Damping	Integrated Damping including constrained layer core, damped working surface and composite edge finish
Mounting Hole Type	Cut (not rolled) threads with countersink
Hole/Core Sealing	Easy clean conical cup 0.75 in. (19 mm) deep Non-corrosive high impact polymer material
Maximum Dynamic Deflection Coefficient	$<17 \times 10^{-4}$
Maximum Relative Motion Value	$<13 \times 10^{-7}$ in. ($<3.3 \times 10^{-5}$ mm)
Deflection Under Load	$<15 \times 10^{-5}$ in.
Top and Bottom Skins	0.134 (3.4 mm) thick with integrated damping layer

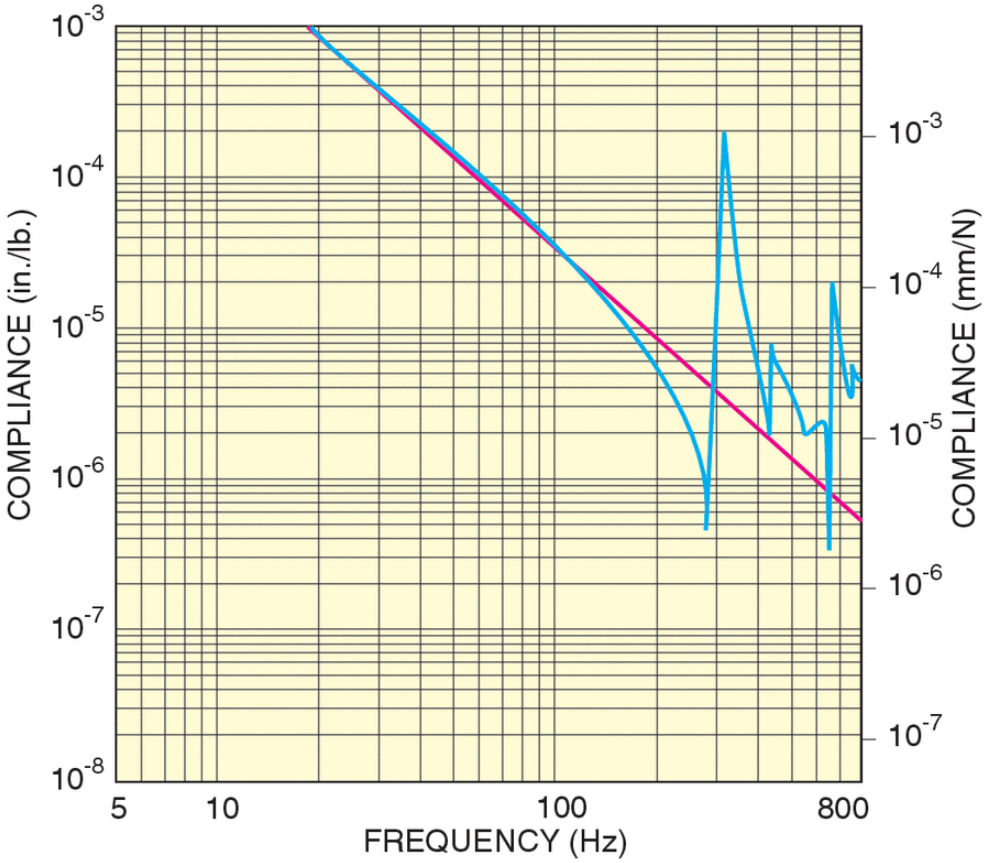
COMPLIANCE (in./lb.)
10-3
10-4
10-5
10-6
10-7
10-8
5
10
100
800
FREQUENCY (Hz)
COMPLIANCE (mm/N)
10-3
10-4
10-5
10-6
10-7

APPENDIX F: On-Trak PSD

PSD Theory (http://www.on-trak.com/theory.html)

Description

Position Sensing Detectors "PSD's" are silicon photodiodes that provide an analog output directly proportional to the position of a light spot on the detector active area. The PSD allows you to simultaneously monitor position and light intensity. The PSD is a continuous analog position sensor. Compared to discrete element devices, the PSD offers outstanding position linearity, high analog resolution, fast response time, and simple operating circuits.

Theory Of Operation

A Position Sensing Detector consists of n-type silicon substrate with two resistive layers separated by a p-n junction. The front side has an ion implanted p-type resistive layer with two contacts at opposite ends. The back side has an ion implanted n-type resistive layer with two contacts at opposite ends placed orthogonally to the contacts on the front side. On a single axis PSD, the electrodes are placed at opposite ends of the p-type resistive layer. A light spot within the spectral range of silicon will generate a photocurrent that flows from the incident point through the resistive layers to the electrodes. The resistivity of the ion implanted layer is extremely uniform so the photogenerated current at each electrode is inversely proportional to the distance between the incident spot of light and electrodes. The PSD outputs track the motion of the "centroid of power density" to an extremely high resolution and ultra-high linearity. On-Trak Position Sensing Amplifiers take the photocurrent from each electrode and process the signals to provide X, Y outputs independent of light intensity.

Position Resolution

The position resolution of a PSD is the minimum detectable displacement of a spot of light on the detector surface. The position resolution of On-Trak PSDs are proven better than one part in a million. Resolution dependent on:

- Detector Size
- Detector Noise
- Light Input Intensity
- Bandwidth of the Electronic Signal Processing Circuits

Position Linearity

Position non-linearity is defined as geometric position error divided by detector length and is measured within 80% of the detector length. Position non-linearity is typically better than 0.05% for the single axis PSD and better than 0.3% for the duolateral. The On-Trak vs competitor two-dimensional linearity plot shows the ultra linear characteristic of these PSDs.

One-Dimensional PSD

The one-dimensional PSD detects a light spot moving over its surface in a single direction. The photoelectric current generated by the incident light flows through the device and is seen as an input bias current divided into two output currents. The distribution of the output currents show the light position on the detector.

Duolateral Two-Dimensional PSD

The duolateral two-dimensional PSD detects an incident light spot position on its square surface. The photoelectric current generated by the incident light flows through the device and is seen as two input currents and two output currents. The distribution of the output currents show the light position of one dimension (Y), and the distribution of the input currents show the light position of the second dimension (X).

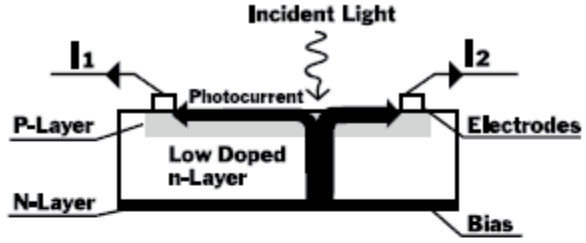

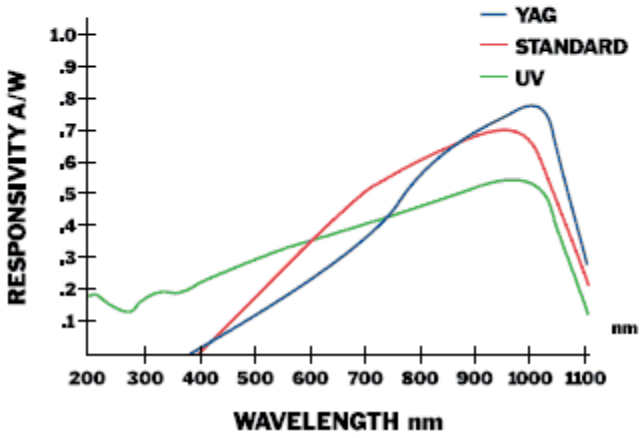

PSD Type	Spectral Range	Responsivity
Standard	400-1100 nm	0.70 A/W @ 940 nm

APPENDIX G: Newport Compact Air-Mount

Model	SLM-3A
Load per Isolator	136 kg (300 lb)
Load Capacity	136 kg (300 lb)
Max. Air Pressure	60 psi
Natural Frequency (Nominal), Max.	5
Natural Frequency (Nominal), Min.	3 Hz
Isolator Weight	0.68 kg (1.5 lb)
Operating Temperature Range	-40 to 83 °C

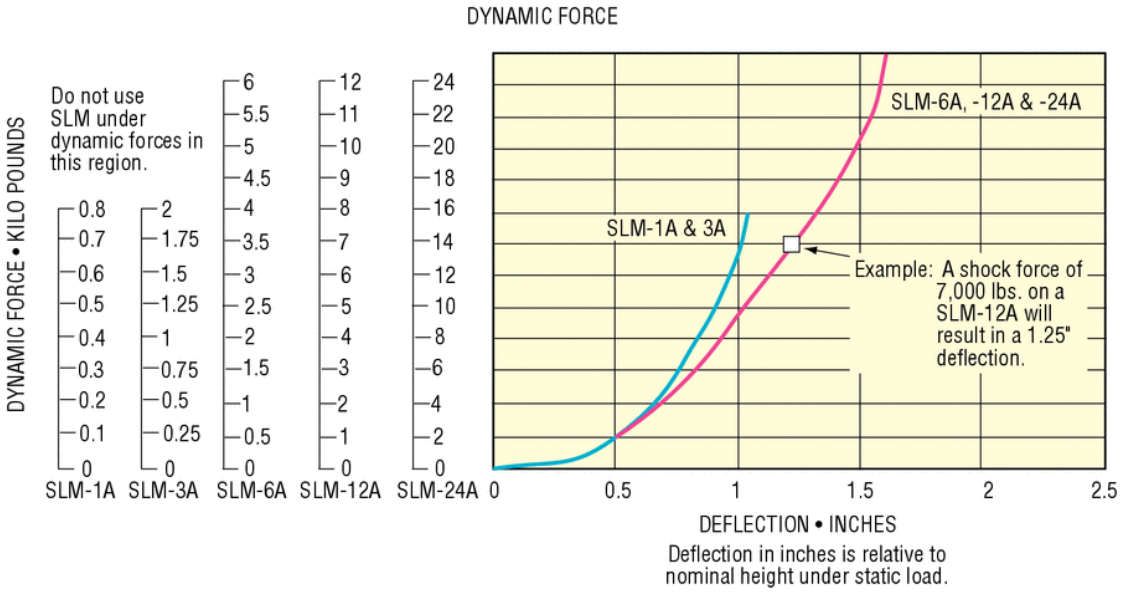

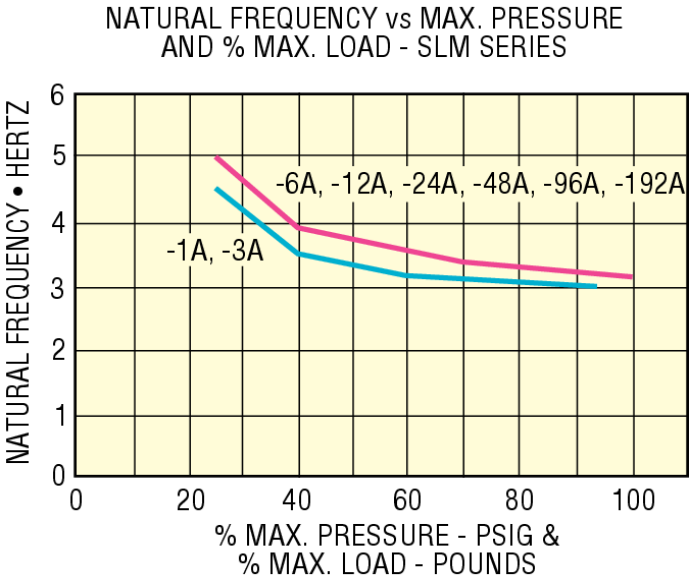
NATURAL FREQUENCY vs MAX. PRESSURE
AND % MAX. LOAD - SLM SERIES
NATURAL FREQUENCY • HERTZ
0
1
2
3
4
5
6
0
20
40
60
80
100
% MAX. PRESSURE - PSIG &
% MAX. LOAD - POUNDS
-6A, -12A, -24A, -48A, -96A, -192A
-1A, -3A

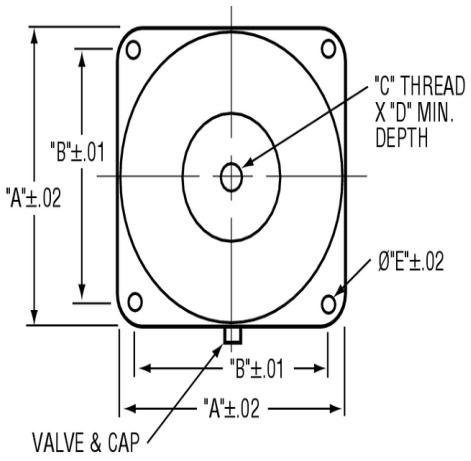
"C" THREAD
X "D" MIN.
DEPTH
"B"±.01
"A"±.02
Ø"E"±.02
"B"±.01
"A"±.02
VALVE & CAP

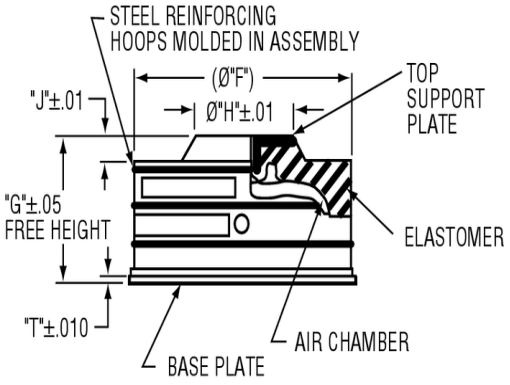
STEEL REINFORCING
HOOPS MOLDED IN ASSEMBLY
(Ø"F")
Ø"H"±.01
TOP
SUPPORT
PLATE
"J"±.01
"G"±.05
FREE HEIGHT
ELASTOMER
"T"±.010
AIR CHAMBER
BASE PLATE

APPENDIX H: Newport Optical Tables

Model	RS4000-48-8
Mounting Hole Type	1/4-20
Mounting Hole Pattern	1 in. grid
Length	8 ft.
Width	4 ft.
Thickness	8 in.
Working Surface	400 series ferromagnetic stainless steel
Deflection Under Load	$<5.0 \times 10^{-5}$ in. in. ($<1.3 \times 10^{-3}$ mm mm)
Maximum Dynamic Deflection Coefficient	0.4×10^{-3}
Core Design	Trussed Honeycomb, Vertically Bonded Closed Cell Construction, 0.010 in. Steel sheet materials, 0.030 in. triple core interface
Broadband Damping	Constrained layer core, damped working surface and composite edge finish
Hole/Core Sealing	Easy clean conical cup 0.75 in. (19 mm) deep, Non-corrosive high impact polymer material
Top and Bottom Skins	3/16 in. (4.8 mm) thick with integrated damping layer
Crated Weight	521 kg (1172 lb)

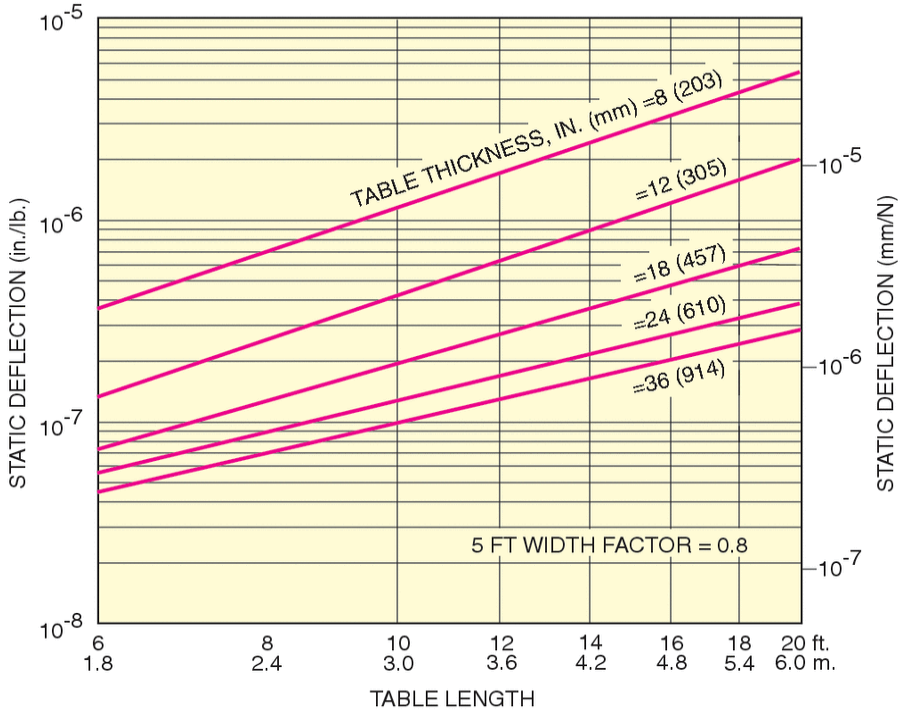
STATIC DEFLECTION (in./lb.)
STATIC DEFLECTION (mm/N)
TABLE THICKNESS, IN. (mm) =8 (203)
=12 (305)
=18 (457)
=24 (610)
=36 (914)
5 FT WIDTH FACTOR = 0.8
TABLE LENGTH

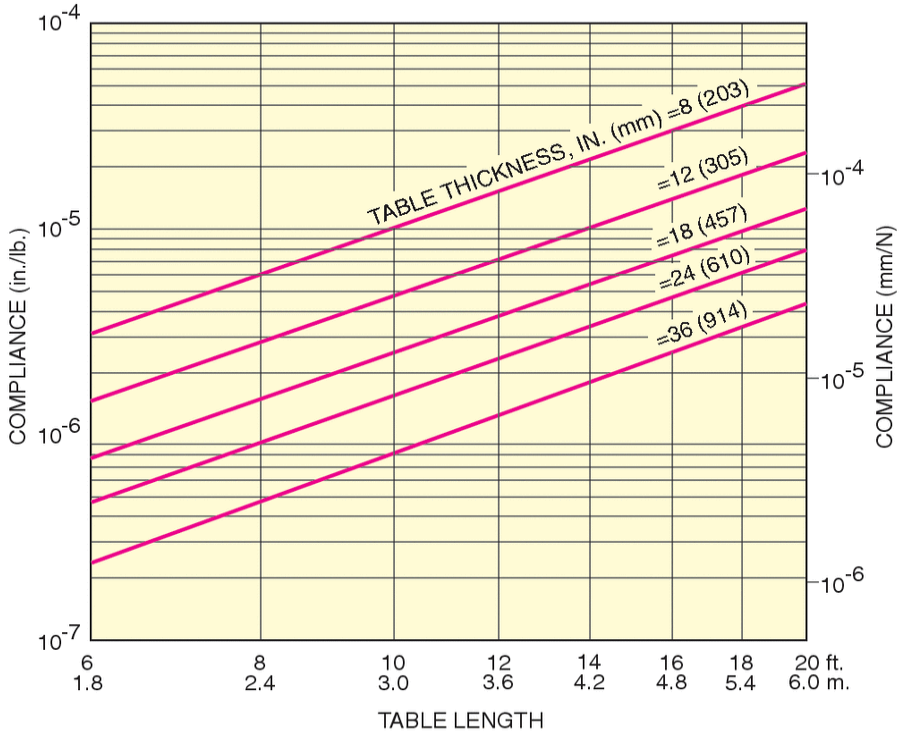
COMPLIANCE (in./lb.)
COMPLIANCE (mm/N)
TABLE THICKNESS, IN. (mm) =8 (203)
=12 (305)
=18 (457)
=24 (610)
=36 (914)
TABLE LENGTH

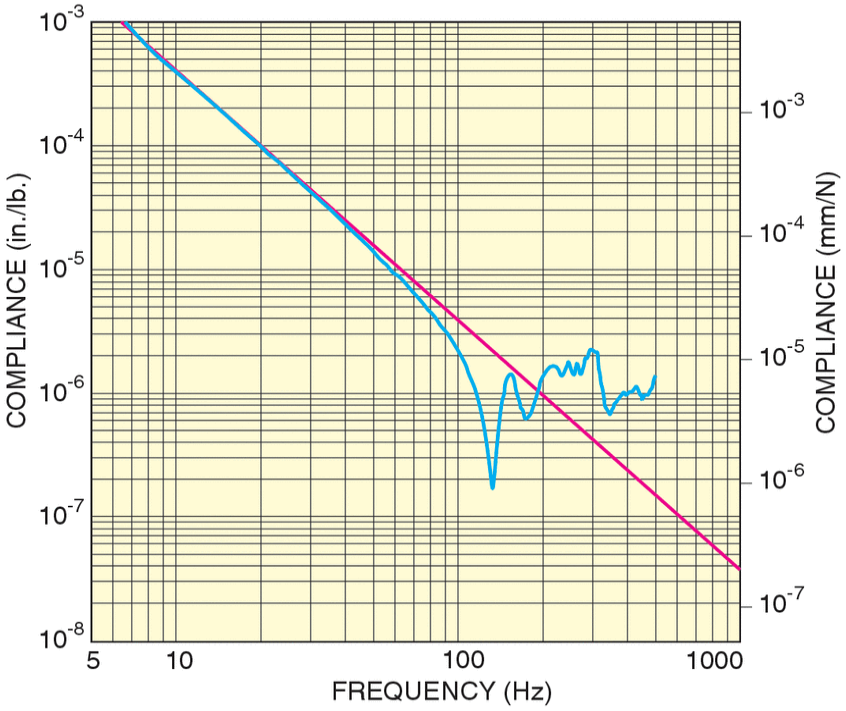
COMPLIANCE (in./lb.)
10^{-3}
10^{-4}
10^{-5}
10^{-6}
10^{-7}
10^{-8}
COMPLIANCE (mm/N)
10^{-3}
10^{-4}
10^{-5}
10^{-6}
10^{-7}
5
10
100
1000
FREQUENCY (Hz)

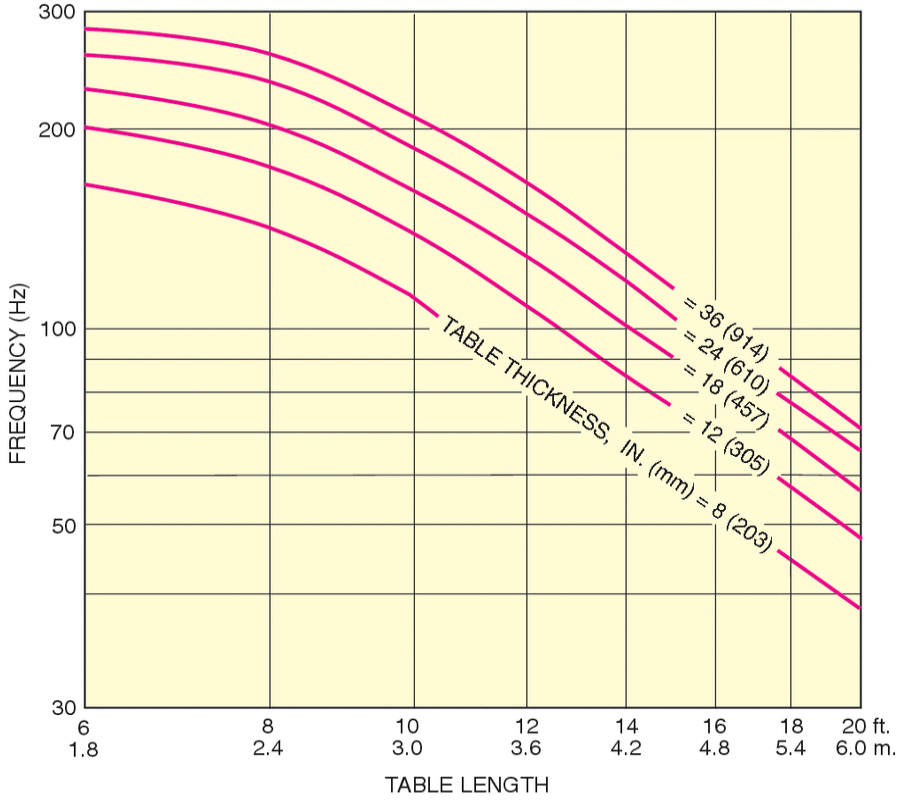
FREQUENCY (Hz)
300
200
100
70
50
30
= 36 (914)
= 24 (610)
= 18 (457)
= 12 (305)
TABLE THICKNESS, IN. (mm) = 8 (203)
6
1.8
8
2.4
10
3.0
12
3.6
14
4.2
16
4.8
18
5.4
20 ft.
6.0 m.
TABLE LENGTH

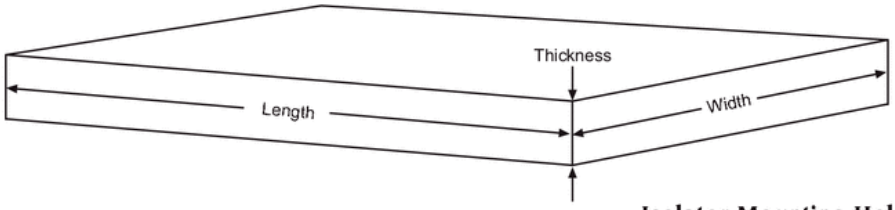

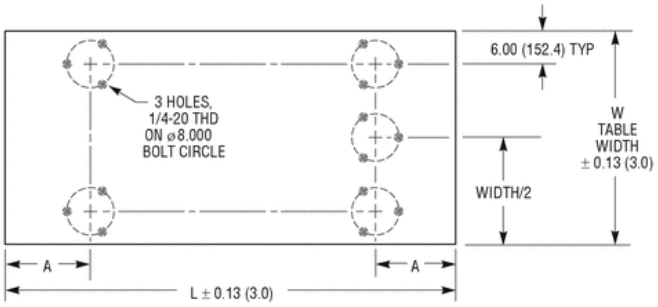

Isolator Mounting Hole Dimensions

WIDTH (W)	LENGTH (L)	DIMENSION (A)
in.	ft	in.
36.0	20.0	53.0
48.0	18.0	47.0
59.1	16.0	42.0
	14.0	37.0
	12.0	32.0
	10.0	27.0
	8.0	22.0
	6.0	16.0

Model	**RS2000-48-18**
Mounting Hole Type	1/4-20
Mounting Hole Pattern	1 in. grid
Length	8 ft.
Width	4 ft.
Thickness	18 in.
Working Surface	400 series ferromagnetic stainless steel
Surface Flatness	±0.1 mm
Deflection Under Load	$<5.0 \times 10^{-5}$ in. ($<1.3 \times 10^{-3}$ mm)
Maximum Dynamic Deflection Coefficient	0.8×10^{-3}
Core Design	Trussed Honeycomb, Vertically Bonded Closed Cell Construction, 0.010 in. Steel sheet materials, 0.030 in. triple core interface
Broadband Damping	Constrained layer core, damped working surface and composite edge finish
Hole/Core Sealing	Easy clean conical cup 0.75 in. (19 mm) deep, Non-corrosive high impact polymer material
Top and Bottom Skins	3/16 in. (4.8 mm) thick with integrated damping layer

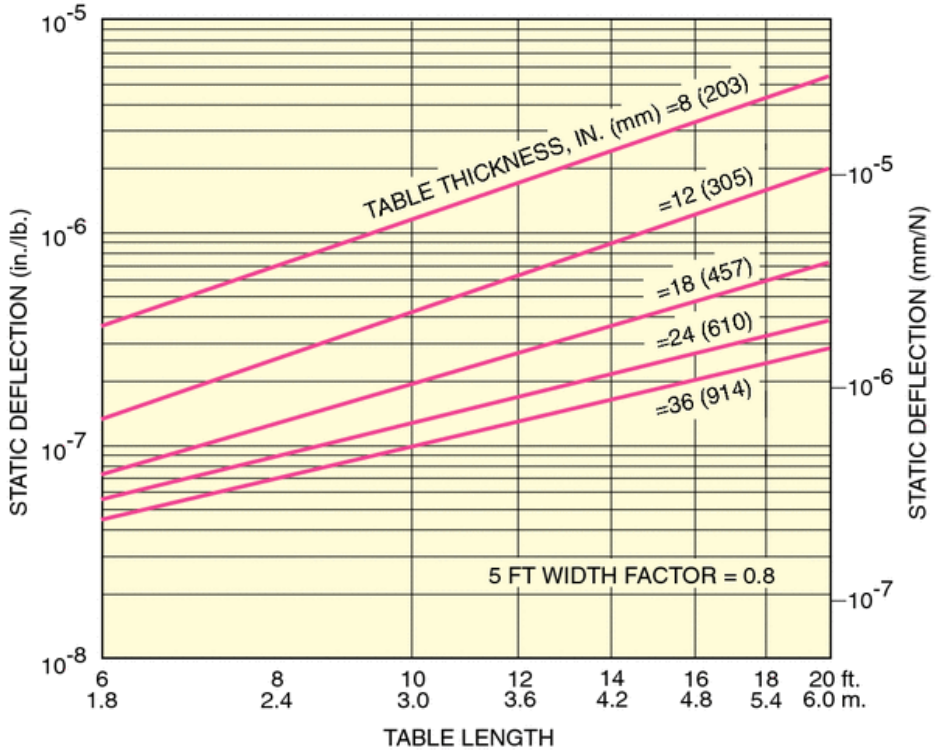
STATIC DEFLECTION (in./lb.)
10^{-5}
10^{-6}
10^{-7}
10^{-8}
TABLE THICKNESS, IN. (mm) =8 (203)
=12 (305)
=18 (457)
=24 (610)
=36 (914)
5 FT WIDTH FACTOR = 0.8
STATIC DEFLECTION (mm/N)
10^{-5}
10^{-6}
10^{-7}
6 1.8
8 2.4
10 3.0
12 3.6
14 4.2
16 4.8
18 5.4
20 ft. 6.0 m.
TABLE LENGTH

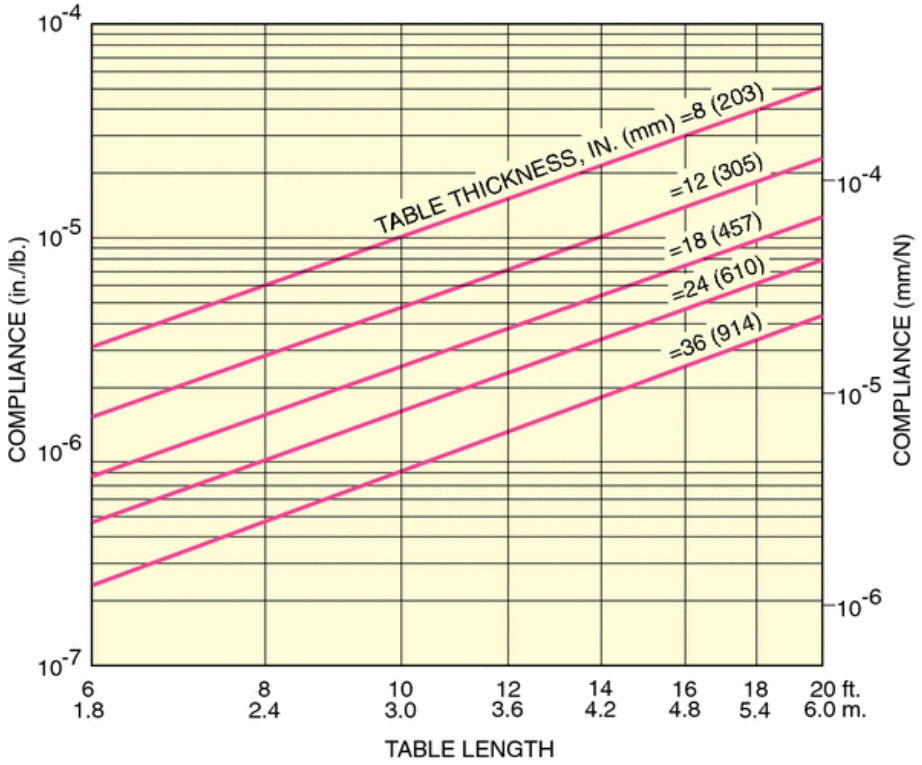
COMPLIANCE (in./lb.)
10^{-4}
10^{-5}
10^{-6}
10^{-7}
TABLE THICKNESS, IN. (mm) =8 (203)
=12 (305)
=18 (457)
=24 (610)
=36 (914)
COMPLIANCE (mm/N)
10^{-4}
10^{-5}
10^{-6}
6 1.8
8 2.4
10 3.0
12 3.6
14 4.2
16 4.8
18 5.4
20 ft. 6.0 m.
TABLE LENGTH

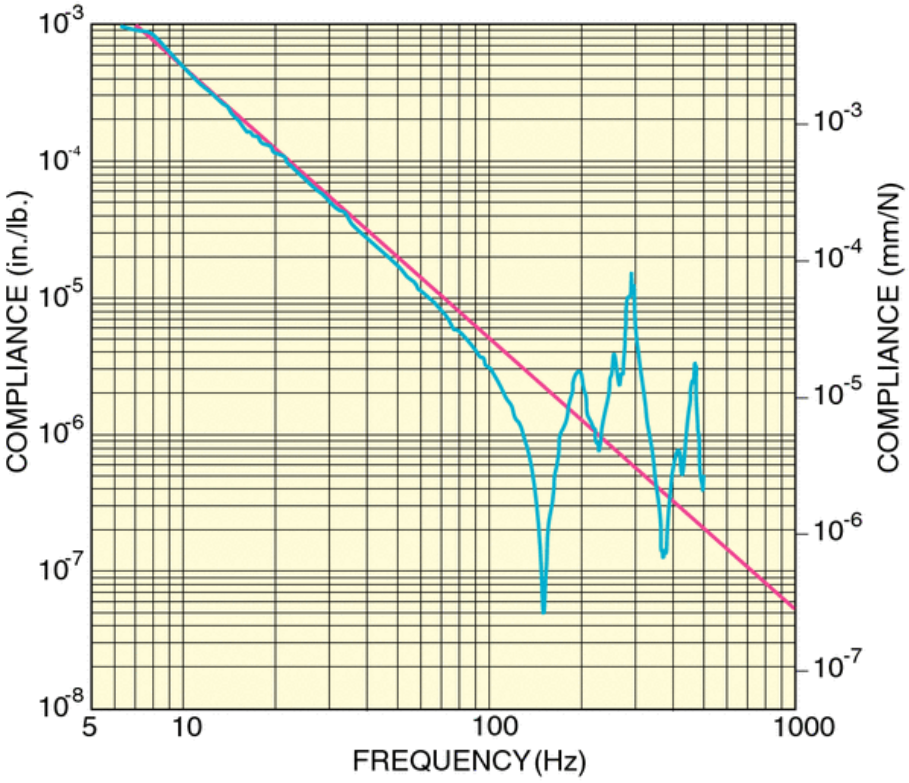
COMPLIANCE (in./lb.)
COMPLIANCE (mm/N)
FREQUENCY (Hz)

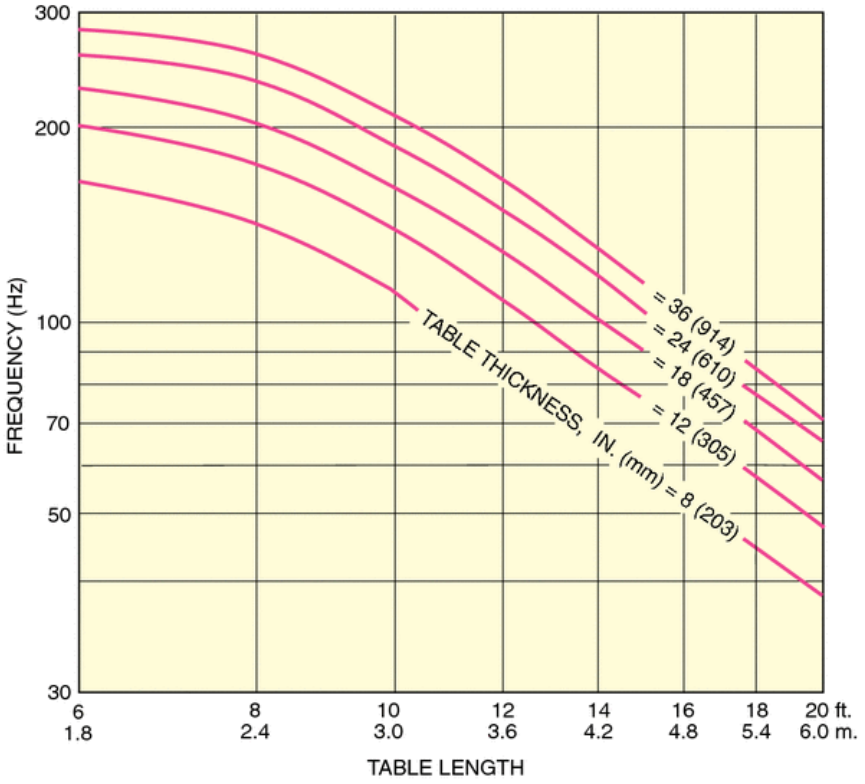
FREQUENCY (Hz)
TABLE THICKNESS, IN. (mm)
= 36 (914)
= 24 (610)
= 18 (457)
= 12 (305)
= 8 (203)
TABLE LENGTH

APPENDIX I: Newport Pneumatic Isolators

Specifications

Table Tops:	
Flatness:	±0.005in. (0.13mm)*
Compliance:	Consult your Newport Catalog or Newport directly for the specific compliance and other pertinent table top specifications of your particular table top model.
Isolators:	Stabilizer™ I-2000
Vertical Resonant Frequency:	<1.1 Hz at 80 psi
Horizontal Resonant Frequency:	<1.5 Hz
Recommended Load Range: (per 4 isolators)	660 to 8,000 lb (300 to 3,600 kg)
Automatic Leveling Accuracy:	±0.010 inch (0.25 mm) standard, higher accuracy available on special order
Vertical Adjustment Range:	1.3 inches (33 mm)
Settling Time: (after 5-lb. weight removal)	<1.5 sec.
Typical Air Pressure Range:	10 to 85 psi (0.7 to 6.0 kg/cm^2)

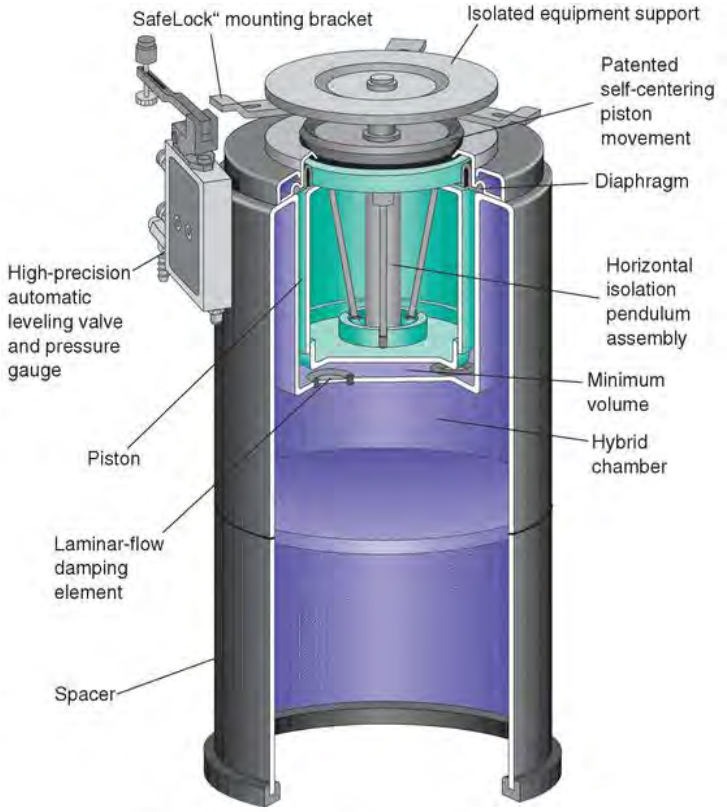

Isolation System Transmissibility

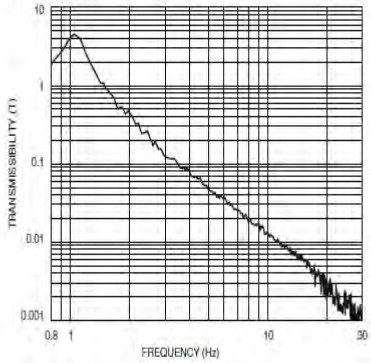

Vertical Transmissibility (at maximum recommended load)

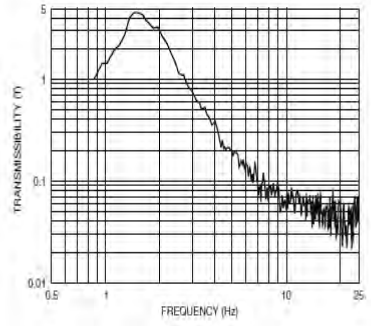


Clamp
(3 per Isolator)
Wrench Holes
Level
Adjustment
Screw
Leveling Valve
(3 per system)
Newport

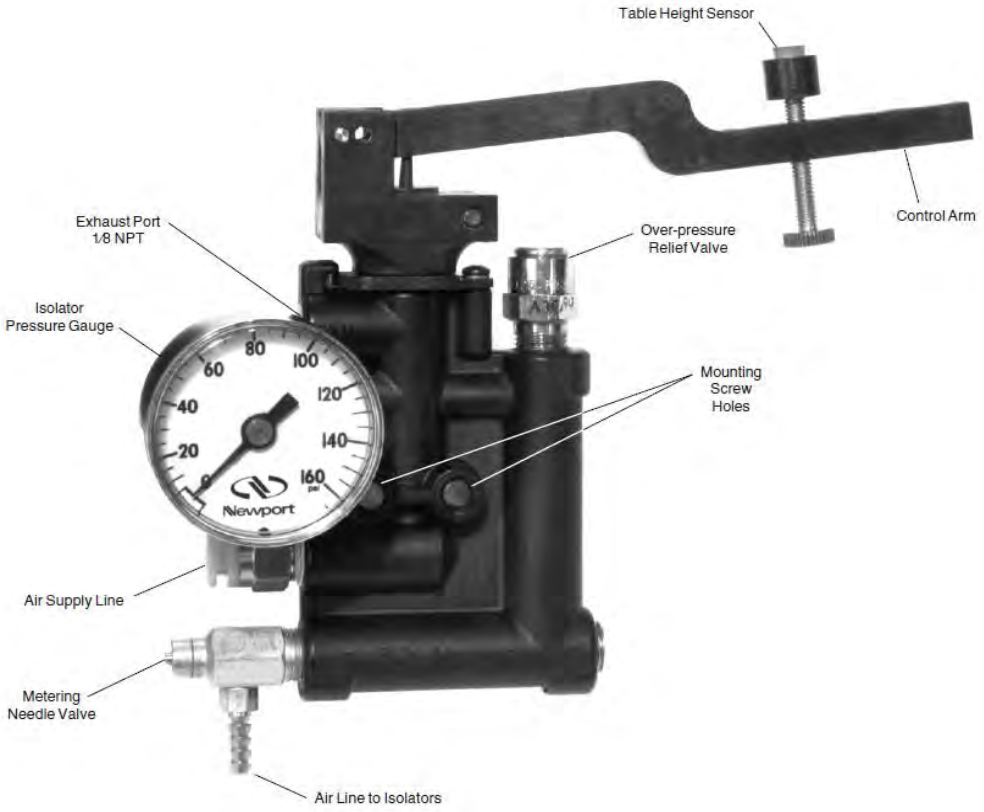
Table Height Sensor
Control Arm
Exhaust Port
1/8 NPT
Over-pressure
Relief Valve
Isolator
Pressure Gauge
Mounting
Screw
Holes
Air Supply Line
Metering
Needle Valve
Air Line to Isolators
Newport

APPENDIX J: Laser Diode

Class	5mW, Class IIIa
Typical Power Output	~75% of max. output power
Beam Diameter	3.8 x 0.9mm, typical collimated beam
Beam Divergence	0.45 x 0.95 mrad, typical collimated beam
Line Width, Focused Spot	<0.001" (25 microns) user adjustable
Focusing Distance	Face of module to past collimation
Dimensions	
Module only	0.750" Diameter +0/-0.005"
Projection Head	0.734" Diameter
Bore Sighting (Beam vs. Housing Alignment)	<3 mrad, collimated beam
Temperature Range	+10°C to +48°C
Frequency Drift	0.25nm / °C
ESD Protection	+8,000 volts
Diode MTBF, calc.	50 - 100,000 hrs, varies with model
Current Draw	65 - 150 mA, varies with model
Input Voltage	5 - 6V DC
Weight	~65 grams
Housing Material	Black Anodized Aluminum
*Class IIIb Models	CDRH certified with key box

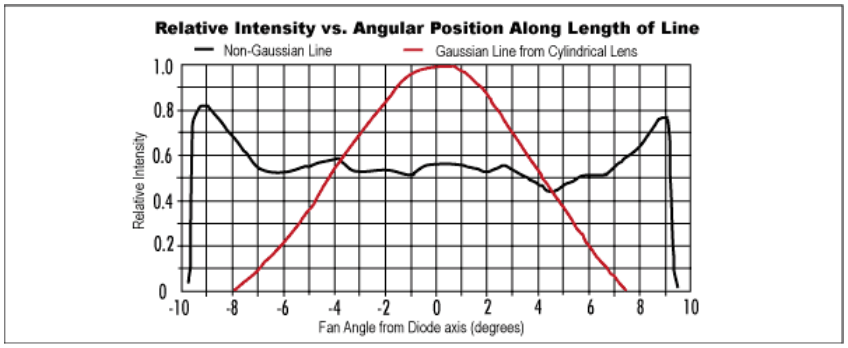

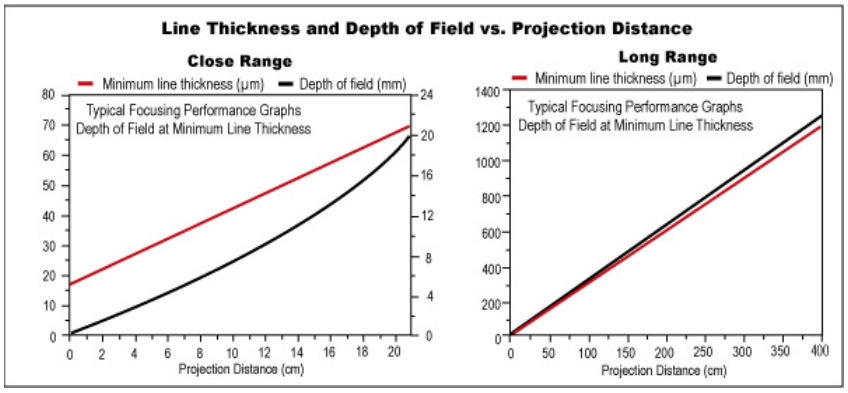

APPENDIX K: Kistler Accelerometer Model 8690C5

Acceleration - ATP

KISTLER
measure. analyze. innovate.

PiezoBeam™

Type 8690C...

Light Weight, Voltage Mode Triaxial Accelerometer

High sensitivity triaxial accelerometers that simultaneously measure vibration in three, mutually perpendicular axis (x, y and z).

Designed primarily for modal analysis applications, the triaxial accelerometer can also find selective use as a general purpose vibration sensor.

- Low impedance, voltage mode
- High sensitivity
- Low cost, lightweight triaxial design
- High accuracy and stability
- Choice of ranges and sensitivities
- Excellent thermal stability
- Conforming to CE

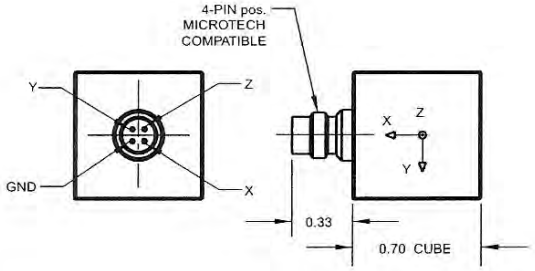

Description
Internal of the PiezoBeam accelerometer is a uniquely configured sensing element consisting of a ceramic beam supported by a center post that when bending occurs as a result of being subjected to vibration, the cantilevered beam element yields an electrical charge. The charge signal is converted by the internal charge amplifier to a proportional high level voltage signal at a output impedance of less than 500 ohms.

The lightweight units reduce mass loading on thin-walled structures in multichannel general vibration measurements or modal applications. This series of triaxial sensors, with an integral four-pin connector, is designed for simplified installation in confined areas. Each unit may be mounted on any of three surfaces.

The 8690C triaxial series offer outstanding phase response, thermal stability, as well as wide frequency range. They are constructed of hard, anodized aluminum which provides ground isolation and environmentally sealed with epoxy.

The accelerometers will operate directly from the internal power source found in most FFT analyzers, from several Kistler Piezotron™ power supply couplers or any industry standard IEPE (Integrated Electronic Piezo Electric)compatible power source.

Application
This light weight, triaxial accelerometer series is ideally suited for multiple channel modal vibration measurement on aerospace vehicle, air frame, flight flutter and automotive structural testing.

Technical Data

Type	Units	8690C5	8690C10	8690C50
Acceleration Range	g	±5	±10	±50
Acceleration Limit	g_{pk}	±8	±16	±80
Threshold nom.	μV_{rms}	120	140	100
	μg_{rms}	120	280	1000
Sensitivity ±5 % (at 100Hz, 3 g_{rms})	mV/g	1000	500	100
Resonant Frequency mounted, nom.	kHz	9	22	22
Frequency Response ±5%	Hz	1... 3000	1... 5000	1...6000
Phase Shift, < 5°	Hz	4...2000	4...2000	4...4000
Amplitude Non-linearity	%FSO	±1	±1	±1
Time Constant nom.	s	1	1	1
Transverse Sensitivity	%	<1	<1	<1
Long Term Stability	%	±1	±1	±1
Environmental:				
Base Strain Sensitivity @ 250 με	g/με	<0.001	<0.001	<0.001
Shock Limit (0.2ms pulse width)	g_{pk}	5000	10000	10000
Temperature Coefficient of Sensitivity	%/°F	- 0.02	+0.04	+0.04
Temperature Range Operating (4mA supply current)	°F	32 ...150	32 ...150	32 ...150
Temperature Range Operating Storage	°F	- 10 ... 200	- 10 ... 200	- 10 ... 200
Output				
Bias	VDC	11	11	11
Impedance	Ω	<500	<500	<500
Current, (4mA supply)	mA	2	2	2
Voltage full scale	V	±5	±5	±5
Source				
Constant Current	mA	2 ... 20	2 ... 20	2 ... 20
Voltage	VDC	20 ... 30	20 ... 30	20 ... 30
Construction				
Sensing Element	type	ceramic bimorph/ bender	ceramic bimorph/ bender	ceramic bimorph/ bender
Housing	material	Al, hard anodized	Al, hard anodized	Al, hard anodized
Sealing housing/connector	type	Epoxy	Epoxy	Epoxy
Connector	type	4-pin pos. Microtech Equivalent	4-pin pos. Microtech Equivalent	4-pin pos. Microtech Equivalent
Ground Isolation	MΩ	10	10	10
Weight	grams	11.2	11.2	11.2
Mounting	type	adhesive/wax	adhesive/wax	adhesive/wax

1 g = 9.80665 m/s², 1 inch = 25.4 mm, 1 gram = 0.03527 oz, 1 lbf-in = 0.1129 Nm

Mounting
The cube shape configuration of the triaxial accelerometer allows for the unit to be attached to the test surface using any available side. Attachment can be by wax or by adhesive. Reliable and accurate measurements require that the mounting surface be clean and flat. The Operating Instruction Manual for the 8690C series provides detailed information regarding mounting surface preparation.

Ordering Information

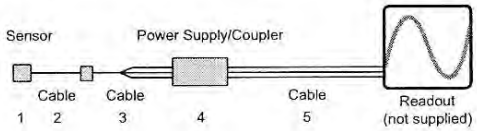

X = specify range; 5g, 10g, 50g
sp = specify cable length in meters

1 - 8690C(X)	triaxial accelerometer, specify range
2 - 1578Asp	optional extension cable, 4-pin pos. Microtech equivalent to 4-pin neg. Microtech equivalent
3 - 1756B(Y)	cable, 4-pin Microtech neg., to 3x BNC pos., length Y = 0.5, 3, 10 meters
4 - 5100	coupler series, or
5134	four-channel coupler
5 - 1511sp	output cable BNC pos. to BNC pos.

Supplied Accessories

8432	mounting wax

Optional Accessories

8476	mounting clip, black derlin

APPENDIX L: MATLAB Scripts

```
%% M-file to calibrate FFD_9
%*****************************
%LAST USED: 04-24-2011
%STATUS: FUNCTIONAL
%% Evaluate This Cell Before Building Model:
Ts=0.001;
%sample time
fintime = 7;        %Length of data run.

calibrate=0;
%-----------------------------------------
% Shaker input (sinusiod, max 4 signals)
shakeramp = [0      0        0       0];
shakerfreq= [0      0        0       0];
shakerphase = [0   0   0   0];
shakeramp2 = [0     0        0       0];
shakerfreq2= [0      0        0       0];
shakerphase2 = [0   0   0   0];
shaker_start=0;
shaker_end=fintime;
shaker_start2=1.00;
shaker_end2=fintime;
dist_targ = 4.62; %m
dist_FSM = (0.365+0.427)*1; %m
% dist_FSM = 0.2275; %m
w = 0.0635; %m
h = 0.1175; %m
d= 0.3048; %m
trackstart=0.1;
OT5FBX = 1;
OT5FBY = 1;
A_x_ffd_sel = 1; A_y_ffd_sel = 1;
chirp_on = 0; IA_chirp_gain=1;
IA_init_freq = 1;  IA_final_freq = 1000; IA_targ_time = 120;
noise_power=0.00;  noise_power2=0.00;
xzero = 0; yzero = 0;
xzero2 = 0; yzero2 = 0;
kr = 20.194; kp = 20.671; ky = 19.930;
Filter_Mean=0;
Run_Mean = 1;
a_Run_Mean = 1;
FSM_position=[0,0,0];
PSD_or_Rate_Sensors = 1;
Algorithm_or_radice_calc = 1;
Tgt_Pos_or_Req_Theta = 1;
trigger=1;
mirror_angle = 45;  mirror_angle = mirror_angle*pi/180*1000;
cal_ot1x = 0;   cal_ot1y = 0;
cal_ot2x = 0;   cal_ot2y = 0;
```

```
cal_ot3x = 0;   cal_ot3y = 0;
cal_ot4x = 0;   cal_ot4y = 0;
cal_ot5x = 0;   cal_ot5y = 0;
% cal_ot6z = 0;   cal_ot6x = 0;
% cal_ot7z = 0;   cal_ot7x = 0;
cal_tgtx = 0;   cal_tgty = 0;
%Rate Sensors
cal_pitch_rate = 0;
cal_roll_rate = 0;
cal_yaw_rate = 0;
%Accelerometers
r_OA=0.1225; % m
r_OB=0.118;% m
r_OC=0.1235; % m
cal_Ox = 0;
cal_Oy = 0;
cal_Oz = 0;
cal_Ay = 0;
cal_Az = 0;
cal_Bx = 0;
cal_Bz = 0;
cal_Cx = 0;
cal_Cy = 0;
%----------------------------------------
%  PID gains for PI Controller (Control A)
    fsm1px = 0.04*0.45;
    fsm1ix = fsm1px*1.2/0.001;
    fsm1dx = 0;
    fsm1py = 0.1*0.45;
    fsm1iy = fsm1py*1.2/0.001;
    fsm1dy = 0;
avg_m1xc = 0;
avg_m1yc = 0;
% PI test mode for critical gains
    PI_tune_step_value= 0; %step value
    x_PI_tune = 3; %time for x axis step
    y_PI_tune = 3; %time for y axis step



    % Target tracking curve fit parameters
%Target tracking slope x
Mx = 0; %(curve fit=0.9)
%Target tracking offset x
Bx = 0; %(curve fit = 3378.6/500)
%Y
%Target tracking slope y
My = 0; %(curve fit=0.9)
%Target tracking offset y
By = 0; %(curve fit = 3378.6/500)

    %PID parameters for target tracking
targtrackxprop=0.0003;
```

```
targtrackxint=2;
targtrackxderiv=0;
targtrackyprop=0.0001;
targtrackyint=1;
targtrackyderiv=0;
%-----------------------------------------
%   Test Parameters for sinusoid (max 4 signals)
    x_test_amp= [0.05*0        0     0       0];
    x_test_freq=[10          0       0       0];
    y_test_amp= [0.05*0        0       0       0];
    y_test_freq=[10          0       0       0];
%-----------------------------------------
%   Test Parameters
%   time in sec, value in mrad (max = 13.1 mrad)
    y_step_time = 0.5; y_step_value = -0.3;
    y_step_value = y_step_value*10/26.2; %convert to volts
    x_step_time = 0.5;
    x_step_value = 0.3; x_step_value = x_step_value*10/26.2;
    imp_delay = 1;
    imp_delay=round(imp_delay/Ts);  %delay time to impulse in sec
    imp_mag = -0.3;
    imp_mag = imp_mag*10/26.2+0.03*0;  % impulse mag in mrad
    init_freq = 1;
    final_freq = 1000; targ_time = 120;  %Chirp Parameters
    chirp_gain = 0.262;  chirp_gain=chirp_gain*10/26.2;
%-----------------------------------------
% LMS parameters for LMS Controller (Control B)
mux=0.010; leakx=1.0; % x axis adaption rate and leakage factor
muy=0.030; leaky=1.0; % y axis adaption rate and leakage factor
w0x = 0; w0y = 0; % initial tap gains
biasx=-0.005*0;  biasy=0.002*1; % estimate of bias correction
ax_to_mx=1; ay_to_my=14; % estimate of gain correction for FSM to accel
ot2y_to_m2y = -1/10;
mu_y_error = 0.05; leak_y_error = 1.0;
adapt_y_error = 0.0;
mu_x_error = 0.05; leak_x_error = 1.0;
x_ref_sel=2;    y_ref_sel=2;   zz=1;
x_error_sel=2;  y_error_sel=2;
accel_lag = 1.05;
OT2y_lag = 1;
rmeanx = 0;  rmeany = 0;
%Additional LMS parameters for Prediction
adapt_y_error = 0.0;
mu_y_error = 0.05; leak_y_error = 1.0;
mu_x_error = 0.05; leak_x_error = 1.0;
%-----------------------------------------
%Plot Parameters
    plot_time=2.0;    %length of plot in seconds
    delay_time=shaker_start+1;   %delay before start of example plot
    adapt=2+delay_time+plot_time;  %modify adaption to be after delay
    x_plot_bias=200;    y_plot_bias=200; %amt to bias example signal
    pbiasy = 300; pbiasx = 300;
    pidstart = (adapt-0.1)+1*0; % PID control start, sec, before adaption
    req_theta_start=pidstart;
```

```
    % parallel controllers cmd - 1=single, 2 = parallel A and B
    par_cntlrsA = 1; par_cntlrsB = 1;
%-----------------------------------------
%  STOP EVALUATION HERE!
%-----------------------------------------
%%   Load Model
%-----------------------------------------
% First Calibration
tg=xpctarget.xpc;
C1 = (get(tg,'Application'));C2='FFD_9';C3 = get(tg,'Connected');
C4 = 'Yes';
TF1=strcmp(C1, C2);TF2=strcmp(C3, C4);
if ~TF1;
    unload(tg);
    load(tg,'FFD_9');
    tg=xpctarget.xpc;
end
if ~TF2
    error('Connection with target cannot be established - aborting');
end
reply=input('connect model (if not connected),...set Jitter Control OFF,
Target Tracking OFF,...press enter    ')
set_param('FFD_9', 'SimulationCommand', 'update')
    tg.StopTime=999;
+tg
reply1=input('press enter when beam is centered on all three detectors   ');
pause(2.5)
-tg
clear tt oo
tt=tg.Time;
last2 = 2/Ts;  endtt = length(tg.Time);
f2 = endtt - last2;
oo = tg.Output(f2:end,:);

%OT Calibrations
cal_ot1x = mean(oo(:,3));
cal_ot1y = mean(oo(:,4));
cal_ot2x = mean(oo(:,5));
cal_ot2y = mean(oo(:,6));
cal_ot3x = mean(oo(:,7));
cal_ot3y = mean(oo(:,8));
cal_ot4x = mean(oo(:,9));
cal_ot4y = mean(oo(:,10));
cal_ot5x = mean(oo(:,11));
cal_ot5y = mean(oo(:,12));

%ARS Calibrations
cal_pitch_rate = mean(oo(:,16));
cal_roll_rate = mean(oo(:,17));
cal_yaw_rate = mean(oo(:,18));

%Accelerometer Calibrations
cal_Ox = mean(oo(:,28));
cal_Oy = mean(oo(:,29));
```

```
cal_Oz = mean(oo(:,30));
cal_Ay = mean(oo(:,31));
cal_Az = mean(oo(:,32));
cal_Bx = mean(oo(:,33));
cal_Bz = mean(oo(:,34));
cal_Cx = mean(oo(:,35));
cal_Cy = mean(oo(:,36));


%Target Calibrations
ot5x=tg.Output(:,11);
ot5y=tg.Output(:,12);
%mirror zero calibration
xzero= mean(oo(:,40));
yzero= mean(oo(:,41));
xzero2= mean(oo(:,42));
yzero2= mean(oo(:,43));
%----------------------------------------
% 2nd Calibration
cal_tgty = 0;   cal_tgtx = 0;
tg=xpctarget.xpc;
C1 = (get(tg,'Application'));C2='FFD_9';C3 = get(tg,'Connected');
C4 = 'Yes';
TF1=strcmp(C1, C2);TF2=strcmp(C3, C4);
if ~TF1;
    unload(tg);
    load(tg,'FFD_9');
    tg=xpctarget.xpc;
end
if ~TF2
    error('Connection with target cannot be established - aborting');
end
%reply=input('connect model (if not connected) and press enter')
set_param('FFD_9', 'SimulationCommand', 'update')
    tg.StopTime=999;
+tg
%reply1=input('press enter when beam is centered on all three detectors');
pause(2.5)
-tg
clear tt2 oo2
tt2=tg.Time;
last2 = 2/Ts;  endtt2 = length(tg.Time);
f2 = endtt2 - last2;
oo2 = tg.Output(f2:end,:);
ot5x_calc=tg.Output(:,50);
ot5y_calc=tg.Output(:,51);
cal_tgtx=mean(oo2(:,50));
cal_tgty=mean(oo2(:,51));
%----------------------------------------
% Check Calibration Constants with Plot
figure(1)
    subplot(2,1,1)
    plot(tt,ot5y*500,tt2,(ot5y_calc*500)),grid,
    line([0 2],[cal_ot5y*500 cal_ot5y*500])
```

```
    line([0 2],[cal_tgty*500 cal_tgty*500],'color','r')
    title('Calculation based on FSM and plate motion')
    xlabel('sec'),ylabel('y axis, \mum')
    legend('Actual','Calc')
    subplot(2,1,2)
    plot(tt,ot5x*500,tt2,(ot5x_calc*500)),grid
    line([0 2],[cal_ot5x*500 cal_ot5x*500])
    line([0 2],[cal_tgtx*500 cal_tgtx*500],'color','r')
    xlabel('sec'),ylabel('x axis, \mum')
    legend('Actual','Calc')

beep


%% M-file to Run FFD_9
%*******************************
%LAST USED: 03-22-2011
%  STATUS: Functional=X
%   FB:
%       FSMA: PI                X
%             LMS
%       FSMB: PI
%             LMS
%   FFD:
%       FSMA: PI: PSD           X
%                 ARS          ~X (need to tune better)
%             LMS: PSD
%                  ARS
%       FSMB: PI: PSD
%                 ARS
%             LMS: PSD
%                  ARS
%    Target Tracking X OT5 FB  X (may want to tune better)
%    Target Tracking Y OT5 FB  X (may want to tune better)
 %   Target Tracking X OT4
%    Target Tracking Y
%
%% Use this for saving data (May need to update variables!)
%*******************************
% Check to make sure date for save file is correct!
%*******************************
%for ii = 1:1;  %using this for running the same experiment numerous times
ptime = input('input pause time in sec   ');
%ptime = 0; %This is a pause time
% pltfrf = 0;         %   Set to one to run FRF
% if isempty(ptime)
%     ptime=0;
% end
%% Basic Run Parameters
calibrate=1;            %Set to '1' to use Calibration Constants
Ts=0.001;               %sample time
Fs=1/Ts;                %sample Freguency
```

```
fintime = 35;            %Length of data run

%-----------------------------------------
% Actuator input (sinusoid, max 4 signals)
%   amp in volts, freq in Hz
%-----------------------------------------
sfreq = 10;              %Actuator First Frequency
aa = 0;                  %Make '1' to Run all Frequncies for Actuator 1
bb = 0;                  %Make '1' to Run all Frequencies for Actuator 2
%-----------------------------------------
%Actuator 1 (Pitch/Yaw)
shakeramp = [3*1    2*aa       2*aa       1*aa];
shakerfreq= [sfreq       13         29         47]; %[sfreq       13
27         47];
shakerphase = [0   0   0   0];
shaker_start=1.00;         %start time of vibrations in secs
shaker_end=fintime;
noise_power=0.02*aa;  %noise power for Band Limited White Noise
                      %(usually use about 0.01)
%-----------------------------------------
%Actuator 2 (Roll)
shakeramp2 = [3*bb  2*bb       1*bb       1*bb];
shakerfreq2= [17      23         41       51]; %[17      23         41
51];
shakerphase2 = [pi/4*0   pi/3*0   0   0];
shaker_start2=shaker_start;         %start time of vibrations in secs
shaker_end2=fintime;
noise_power2=0.02*bb;  %noise power for Band Limited White Noise
                       %(usually use about 0.01)
%-----------------------------------------
%Chirp Parameters (set chirp_on to 1 for chirp signal, 0 to input freq)
chirp_on = 0; IA_chirp_gain=0.8;
IA_init_freq = 1;  IA_final_freq = 150; IA_targ_time = 101;  %Chirp
Parameters
%-----------------------------------------
%Distance from Last FSM face to Target
dist_targ = 4.9*1.1; %m
% dist_targ = 4.62; %m
%Distance from Laser Source to FSM

dist_FSM = (0.365+0.427)*1.00; %m
% dist_FSM = 0.2275*0; %m
%-----------------------------------------
% Distance from Plate's "Center of Rotation" to FSM
    w = 0.0635; %m       (originally 0.0635)
    h = 0.1175; %m   (originally 0.1175)
    d= 0.3048; %m        (originally 0.3048)
%-----------------------------------------
FSM_position = [0,0,0];
%-----------------------------------------
Run_Mean = 0;       %Set to '1' to Subtract Running Mean from Rate Sensor
Data
a_Run_Mean = 0;     %Set to '1' to Subtract Running Mean from Accelerometer
Data
```

```
Filter_Mean = 1;    %Set to '1' to Subtract the jitter free "drift" signal
from ARS data

% Target tracking curve fit parameters

%X
%Target tracking slope x
Mx = -0.9212; %(curve fit=-0.9212)
%Target tracking offset x
Bx = -5.11; %(curve fit = -3.714)

%Y
%Target tracking slope y
My = 0; %(curve fit=)
%Target tracking offset y
By = 0; %(curve fit = )


% target tracking PID parameters
% targtrackxprop=0.022; %0.022 for filtered .033
% targtrackxint=0.27;  %0.27 for filtered 0.9
% targtrackxderiv=0.003; %0.003  0.0055

targtrackxprop=0.02;
targtrackxint=2;
targtrackxderiv=0;

% targtrackxprop=0.02;
% targtrackxint=2;
% targtrackxderiv=0;

targtrackyprop=0.01;
targtrackyint=1;
targtrackyderiv=0;

%-----------------------------------------
trigger=2;  %Trigger for Beam Profile, 1=Trigger ON, 2=Trigger OFF

%% Plot Selection
%   1 = plot, 0 = don't plot
%-----------------------------------------
%                       Title of plot
acc          =0;    %   Accelerometer Output
OT_plot      =0;    %   OT1,OT2 and OT3 PSD position in \mu','m and FSM pos
in volts
volt_fig     =0;    %   FSM position in mrad
OT3_pos      =0;    %   OT3 pos on detector with OT3 x and y vs. time
OT1_pos      =0;    %   OT1 pos on detector vs. time
OT2_pos      =0;    %   OT2 pos on detector vs. time
OT4_pos      =0;    %   OT4 pos on detector vs. time
OT5_pos      =1;    %   OT5 pos on detector vs. time
OT_plot_compare=0;  %   OT5 and prediction vs. time
```

```
percent_imp  =1;     %   Percent improvement in Target position
powerplot    =0;     %   RMS laser power
fsm_cmd      =0;     %   FSM command voltage
psd_plt_x    =0;     %   Periodogram of accels/displacement x dir
psd_plt_y    =1;     %   Periodogram of accels/displacement x/y dir
psd_plt_z    =0;     %   Periodogram of accels/displacement z dir

test_inp     = 0;    %   Set to one to plot test input signal
stats        = 1;    %   Set to calculate statistics for output
rot          = 0;    %   Set to plot rotation rates
rot_cal      = 0;    %   Set to plot calibrated rotation rates
rotations    = 0;    %   Set to plot Rotations from PSDs and Rate Sensors
jitter       = 1;    %   Set to plot jitter angle
temp         =0;    %   Set to plot temperatures

%% Control Selection:
%----------------------------------------
% Select Rotations from either PSDs or Rate Sensors for use with Control
    % 1 = PSD Calc
    % 2 = Rate Sensors (Integration Only)
    % 3 = Rate Sensors with Prediction Algorithm
    % 4 = Rate Sensor with Accels and Prediction Algorithm
    PSD_or_Rate_Sensors =1;

%----------------------------------------
%   Select Target Position Control or Required FSM Theta Control
       % 1 = Tgt Position with PI
       % 2 = Req Theta
    Tgt_Pos_or_Req_Theta = 1;

%----------------------------------------
%   Select FeedBack or FeedForward Control for use with Target Position
%       Control Above (1 must be selected above)
%    1 = FeedBack;  2 = FeedForward
     Back_or_Forward = 1;
        A_x_ffd_sel = Back_or_Forward; %(x axis at tgt)
        A_y_ffd_sel = Back_or_Forward; %(y axis at tgt)
%----------------------------------------
%   Select Target tracking source
    %1=OFF(Beacon Laser on OT4)   2=ON (OT5 feedback)
    OT5FBX = 2;
    OT5FBY = 2;
   trackstart=2.5; %delay before tracking starts

%% Control Parameters:
%----------------------------------------
%   PID gains for PI Controller (Control A)
    %(Kcr_x=0.0158, Pcr_x=0.002 and y crit gain = 0.031)

if Back_or_Forward == 1;
    %FB ideal gains:
    fsm1px = 0.04*0.45;
    fsm1ix = fsm1px*1.2/0.001;
```

```
    fsm1dx = 0;
    fsm1py = 0.1*0.45;
    fsm1iy = fsm1py*1.2/0.001;
    fsm1dy = 0;
 elseif Back_or_Forward == 2;
    if PSD_or_Rate_Sensors == 1;
    %PSM ideal gains:
    fsm1px = 0.03*0.45;
    fsm1ix = fsm1px*1.4/0.001;
    fsm1dx = 0;
    fsm1py = 0.04*0.45;
    fsm1iy = fsm1py*1.5/0.001;
    fsm1dy = 0;
    else
    %ARS ideal                    PSM ideal                  FB ideal
    fsm1px = 0.007*0.45;          %0.03*0.45                %0.04*0.45
    fsm1ix = fsm1px*1.9/0.001;    %fsm1px*1.4/0.001         %fsm1px*1.2/0.001
    fsm1dx = 0;
    fsm1py = 0.005*0.45;          %0.04*0.45                %0.1*0.45
    fsm1iy = fsm1py*3.1/0.001;    %fsm1py*1.5/0.001         %fsm1py*1.2/0.001
    fsm1dy = 0;
    end
end

%     fsm1px = 0.0079*on_off; %0.016*0.45*za*1.1;   %0.04*0.45*za
%     fsm1ix = 11.4048;
%     fsm1dx = 0;                %0
%     fsm1py = 0.031*0.45*on_off;     %0.1*0.45*za
%     fsm1iy = fsm1py*1.2/0.001*on_off;
%     fsm1dy = 0;

    % Use these for tuning the PI Controller
    PI_tune_step_value= 0; %step value
    x_PI_tune = 3; %time for x axis step
    y_PI_tune = 3; %time for y axis step
%-----------------------------------------
%   LMS parameters for LMS Controller (Control B)
%     mux=0.012;      leakx=1;      % x axis adaption rate and leakage factor
%     muy=0.020;      leaky=1;      % y axis adaption rate and leakage factor
    mux=0.05;      leakx=1;      % x axis adaption rate and leakage factor
    muy=0.010;      leaky=1;      % y axis adaption rate and leakage factor
    w0x = 0;        w0y = 0;        % initial tap gains
    biasx=-0.005*1;   biasy=0.05*1;     % estimate of bias correction
    ax_to_mx=1;       ay_to_my=14;   % estimate of gain correction for FSM to
accel
    ot2y_to_m2y = -1/10;
    mu_y_error = 0.05; leak_y_error = 1.0;
    adapt_y_error = 0.0;
    mu_x_error = 0.05; leak_x_error = 1.0;
%-----------------------------------------
%   Reference Signal Selection
%   1=OT-1, 2=Accel-2 (a2x and a2y), 3 = rate sensor (pitch, roll)
    x_ref_sel=1;    y_ref_sel=1;
    zz=1;  % number of delays for the predictor ref signal
```

```
%-----------------------------------------
%   Error source selection
%   1=mirror postion, 2=OT3 position, 3=OT2 position
    x_error_sel=2;  y_error_sel=2;
    accel_lag = 1.05;
    OT2y_lag = 1;
%-----------------------------------------
% parallel controllers cmd - 1=single, 2 = parallel A and B
    par_cntlrsA = 1; par_cntlrsB = 1;
%-----------------------------------------
%   Test Parameters for sinusoid (max 4 signals)
%   amplitude in Volts, frequency in Hz
    x_test_amp= [0.1*1        0     0       0];
    x_test_freq=[1          0       0       0];
    y_test_amp= [0.1*1        0       0       0];
    y_test_freq=[15          0       0       0];
%   time in sec, value in mrad (max = 13.1 mrad)
    y_step_time = 1;
    y_step_value = 0.1; y_step_value = y_step_value*10/26.2; %convert to
volts
    x_step_time = 1;
    x_step_value = 0.1; x_step_value = x_step_value*10/26.2;
    imp_delay = 1;  imp_delay=round(imp_delay/Ts);  %delay time to impulse in
sec
    imp_mag = -0.3;  imp_mag = imp_mag*10/26.2+0.03*0;  % impulse mag in mrad
    init_freq = 1;  final_freq = 1000; targ_time = 120;  %Chirp Parameters
    chirp_gain = 0.262;  chirp_gain=chirp_gain*10/26.2;
    stepOTxstart = 1;
    stepOTystart = 1;


%% Plot Parameters
%-----------------------------------------
    plot_time=1.5; %length of plot in seconds
    delay_time=shaker_start+0.1;  %delay before start of example plot
    adapt=0.5+delay_time+plot_time; %modify adaption to be after delay
    x_plot_bias=350;    y_plot_bias=750; %amt to bias example signal
    pbiasy = 900; pbiasx = 300;
    pidstart = adapt; % PID control start, sec, before adaption
    req_theta_start=pidstart; %Required Theta Control start

%% Run Model
%-----------------------------------------
pause(ptime);
set_param('FFD_9', 'SimulationCommand', 'update')
    tg.StopTime=fintime;
tg = xpctarget.xpc
+tg
pause(fintime+0.5);
-tg
clear tt oo
tt=tg.Time;
```

```
%% Get Vairables for Plotting and Analysis:

% FSM position in volts
    m1x=tg.Output(:,46);
    m1y=tg.Output(:,47);
    m2x=tg.Output(:,48);
    m2y=tg.Output(:,49);
    %----------------------------------------
% OnTrak position in micrometers
%   Corrected to Platform coordinate system
%   (except OT2x and OT3x are +/-z direction)
%   Negative value for OT mounted on platform
%   since upward motion results in downward
%   displacement
    ot1x=-500*tg.Output(:,3);   %pt1 x
    ot1y=-500*tg.Output(:,4);   %pt1 y
    ot2x=500*tg.Output(:,5);    %pt2 x
    ot2y=-500*tg.Output(:,6);   %pt2 y
    ot3x=-500*tg.Output(:,7);  %pt3 x
    ot3y=-500*tg.Output(:,8);   %pt3 y
    ot4x=500*tg.Output(:,9);   %pt1 x'
    ot4y=-500*tg.Output(:,10);  %pt1 z
    ot5x=-500*tg.Output(:,11);  % Target x pos
    ot5y=500*tg.Output(:,12);   % Target y pos
%     %ot6x=500*tg.Output(:,31);   %pt2 z'
%     %ot6y=500*tg.Output(:,33);   %pt2 x
%     %ot7x=-500*tg.Output(:,34);  %pt3 z'
%     %ot7y=-500*tg.Output(:,35);  %pt3 x
%     E1=tg.Output(:,24);  %was 34
%     E2=tg.Output(:,35);
%         c0=5.306462;
%         c1=-25.30863;
%         c2=-0.777941;
%         c3=-0.507258;
%         temp1= c0 + c1.*log(E1) + c2.*(log(E1)).^2 + c3.*(log(E1)).^3;
%         temp2= c0 + c1.*log(E2) + c2.*(log(E2)).^2 + c3.*(log(E2)).^3;
%----------------------------------------
% Angular Rate Sensors
    pitch_rate=tg.Output(:,16)./kp.*1e6;
    roll_rate=tg.Output(:,17)./kr.*1e6;
    yaw_rate=tg.Output(:,18)./ky.*1e6;
    pitch_rate_calibrated=tg.Output(:,19);
    roll_rate_calibrated=tg.Output(:,20);
    yaw_rate_calibrated=tg.Output(:,21);
    %PSD Calculated angles
    pitch_1=tg.Output(:,13);
    roll_1=tg.Output(:,14);
    yaw_1=tg.Output(:,15);
    %ARS integrated angles
    pitch_2=tg.Output(:,22);
    roll_2=tg.Output(:,23);
    yaw_2=tg.Output(:,24);
    %ARS predicted angles
    pitch_3=tg.Output(:,25);
```

```
    roll_3=tg.Output(:,26);
    yaw_3=tg.Output(:,27);
%Accelerometers
    % Accelerometer predicted angles
%     a_pitch_accel=tg.Output(:,67);
%     a_roll_accel=tg.Output(:,68);
%     a_yaw_accel=tg.Output(:,69);
%     a_pitch_rate=tg.Output(:,64);
%     a_roll_rate=tg.Output(:,65);
%     a_yaw_rate=tg.Output(:,66);
%     a_pitch_angle=tg.Output(:,61);
%     a_roll_angle=tg.Output(:,62);
%     a_yaw_angle=tg.Output(:,63);
%ARS+Accelerometer Angle Calculation Block
%     ARSaccel_pitch_angle=tg.Output(:,61);
%     ARSaccel_roll_angle=tg.Output(:,62);
%     ARSaccel_yaw_angle=tg.Output(:,63);
%-----------------------------------------
% Position at Target from Beam Prediction Algorithm
    x_pred = -500*tg.Output(:,50); %yes, the minus sign is supposed ot be
there
    y_pred = 500*tg.Output(:,51);
% Position at Target from Prof. Radice's Formula
%     x_pos_radice=500*tg.Output(:,50);
%     y_pos_radice=500*tg.Output(:,51);
%
%% Calculate Jitter at Target
%-----------------------------------------
shake=find(tt>=shaker_start);
shake=shake(1);
control=find(tt>=pidstart);
control=control(1)-1;
done=length(tt);

ot5r = ((ot5y.^2+ot5x.^2).^0.5); % miss dist in um
ot5j = ot5r./dist_targ;  % jitter in urad

%Use this if using Control with Mirror Command b/c it does not target (0,0)
if Tgt_Pos_or_Req_Theta == 2;
    ot5r = (((ot5y-mean(ot5y(1:shake))).^2 + (ot5x-
mean(ot5x(1:shake))).^2).^0.5);
    ot5j = ot5r./dist_targ;
end

% Mean Jitter Angle Before and after Control
Mean_jitter_before=mean(ot5j(shake:control));
Mean_jitter_after=mean(ot5j(control:done));
imp_mean_jitter=((Mean_jitter_before-
Mean_jitter_after)/Mean_jitter_before)*100;

%Running mean of mean jitter angle
rmean_jitter=smooth(ot5j,5,'moving');
```

```
% % Jitter in Calculated Signal
% if Tgt_Pos_or_Req_Theta == 1;
    ot5x_calc = x_pred;
    ot5y_calc = y_pred;
% end
% if Tgt_Pos_or_Req_Theta == 2;
%     ot5x_calc = x_pos_radice;
%     ot5y_calc = y_pos_radice;
% end
ot5r_calc=((ot5y_calc.^2 + ot5x_calc.^2).^.5);
ot5j_calc=ot5r_calc./dist_targ;
jitter_error=ot5j_calc-ot5j;
RMS_jitter_error=sum(sqrt(jitter_error(shake:done).^2))/length(jitter_error(s
hake:done));
% Percent Improvement with Control
%ot5j_shake=mean(ot5j(shake:control,:));
%ot5j_control=mean(ot5j(control:done,:));
%jstdin=sqrt(var(ot5j(shake:control)));
%jstdout=sqrt(var(ot5j(control:done)));
%ystdin=sqrt(var(ot5y(shake:control)));
%xstdin=sqrt(var(ot5x(shake:control)));
%ystdout=sqrt(var(ot5y(control:done)));
%xstdout=sqrt(var(ot5x(control:done)));
%impj=(1-(jstdout/jstdin))*100;
%impy=(1-(ystdout/ystdin))*100;
%impx=(1-(xstdout/xstdin))*100;

%%   Acceleration in volts
Ox = tg.Output(:,28);
Oy = tg.Output(:,29);
Oz = tg.Output(:,30);
Ay = tg.Output(:,31);
Az = tg.Output(:,32);
Bx = tg.Output(:,33);
Bz = tg.Output(:,34);
Cx = tg.Output(:,35);
Cy = tg.Output(:,36);

%----------------------------------------
%   Test output in volts.
    xtest=tg.Output(:,1);
    ytest=tg.Output(:,2);
%----------------------------------------
%   FSM command voltage and Misc inputs/outputs

%       FSM commanded positions(volts)
        m1xc=tg.Output(:,46);
        m1yc=tg.Output(:,47);
        m2xc=tg.Output(:,48);
        m2yc=tg.Output(:,49);
%       FSM actual positions (volts)
        FSMAVx=tg.Output(:,40);
        FSMAVy=tg.Output(:,41);
        FSMBVx=tg.Output(:,42);
```

```
        FSMBVy=tg.Output(:,43);

        IA_1_input=tg.Output(:,44);
        IA_2_input=tg.Output(:,45);
%
%         req_theta_x=tg.Output(:,52);
%         req_theta_y=tg.Output(:,53);


%% Calculation of plot samples
    frt1=size(tg.Output);
    calc_sample=frt1(1,1)-(round(plot_time/Ts+0.1/Ts));  % start of plot
    start_sample=round(0.5/Ts);
    plot_sample=calc_sample+round(plot_time/Ts);         % end of plot
    exsamp=round(delay_time/Ts);
exsamp_end=round(plot_time/Ts+delay_time/Ts);
    tt1=tt(calc_sample:plot_sample);
    ot5xplt=ot5x(calc_sample:plot_sample);
    ot5yplt=ot5y(calc_sample:plot_sample);
    ot5xex=ot5x(exsamp:exsamp_end); ot5xex=ot5xex-mean(ot5xex)+x_plot_bias;
    ot5yex=ot5y(exsamp:exsamp_end); ot5yex=ot5yex-mean(ot5yex)+y_plot_bias;
    title_ctr='LMS';
    title_error='OT3';

%%   Statistics
if stats==1;
    ystdin=sqrt(var(ot5yex));               %standard deviation of input
    xstdin=sqrt(var(ot5xex));

    ystd=sqrt(var(ot5yplt));                %standard deviation of output
    xstd=sqrt(var(ot5xplt));

    impx=(1-(xstd/xstdin))*100;             %percent improvement in st.dev.
    impy=(1-(ystd/ystdin))*100;

    meanx=round(1000*mean(ot5xplt));        %mean position at OT3 in
nanometers
    meany=round(1000*mean(ot5yplt));

%     mean_start_power =
round(1000*mean(laser_power(start_sample:round((shaker_start/Ts-10)))));
%     mean_dist_power =
round(1000*mean(laser_power((exsamp+round(0.25/Ts)):exsamp_end)));
%     mean_rec_power =
round(1000*mean(laser_power(calc_sample:plot_sample)));
    ot5ym = ot5y-mean(ot5y);
    ot5xm = ot5x-mean(ot5x);

    rot_error_pitch= (mean(pitch_1(1000:6000)))-
mean(pitch_3(1000:6000))/mean(pitch_1(1000:6000)); %error between PSD and ARS
platform rotation calcs-referenced to PSD
```

```
    rot_error_roll=(mean(roll_1(1000:6000))-
mean(roll_3(1000:6000)))/mean(roll_1(1000:6000));
    rot_error_yaw=(mean(yaw_1(1000:6000))-
mean(yaw_3(1000:6000)))/mean(yaw_1(1000:6000));
end

%% Calculate Frequency Spectrum
if psd_plt_x==1;
%     [Pa1x,ff]=periodogram(a1x,nfft,'onesided',window,Fs);
Pa1x=10*log10(Pa1x);
%     [Pa1y,ff]=periodogram(a1y,nfft,'onesided',window,Fs);
Pa1y=10*log10(Pa1y);
%     [Pa1z,ff]=periodogram(a1z,nfft,'onesided',window,Fs);
Pa1z=10*log10(Pa1z);
%     [Pa2x,ff]=periodogram(a2x,nfft,'onesided',window,Fs);
Pa2x=10*log10(Pa2x);
%     [Pa2y,ff]=periodogram(a2y,nfft,'onesided',window,Fs);
Pa2y=10*log10(Pa2y);
%     [Pa2z,ff]=periodogram(a2z,nfft,'onesided',window,Fs);
%     Pa2z=10*log10(Pa2z);

[Pot1x,ff]=periodogram(ot1x,nfft,'onesided',window,Fs);Pot1x=10*log10(Pot1x);

[Pot1y,ff]=periodogram(ot1y,nfft,'onesided',window,Fs);Pot1y=10*log10(Pot1y);

[Pot3x,ff]=periodogram(ot3x,nfft,'onesided',window,Fs);Pot3x=10*log10(Pot3x);

[Pot3y,ff]=periodogram(ot3y,nfft,'onesided',window,Fs);Pot3y=10*log10(Pot3y);

[Pot2x,ff]=periodogram(ot2x,nfft,'onesided',window,Fs);Pot2x=10*log10(Pot2x);

[Pot2y,ff]=periodogram(ot2y,nfft,'onesided',window,Fs);Pot2y=10*log10(Pot2y);

[Pot5x,ff]=periodogram(ot5x,nfft,'onesided',window,Fs);Pot5x=10*log10(Pot5x);

[Pot5y,ff]=periodogram(ot5y,nfft,'onesided',window,Fs);Pot5y=10*log10(Pot5y);
end

%% Plots:
%-------------------------------------------------------------------------
if volt_fig==1
%     vmeanstx = roundn(mean(m1x(round(0.9/Ts):round(1.0/Ts))),-2);
%     vmeansty = roundn(mean(m1y(round(0.9/Ts):round(1.0/Ts))),-2);
%     vmeanspx = roundn(mean(m1x((round(1.4/Ts)):round(1.6/Ts))),-2);
%     vmeanspy = roundn(mean(m1y((round(1.4/Ts)):round(1.6/Ts))),-2);
%     vmeanstx2 = roundn(mean(m2x(round(0.9/Ts):round(1.0/Ts))),-2);
%     vmeansty2 = roundn(mean(m2y(round(0.9/Ts):round(1.0/Ts))),-2);
%     vmeanspx2 = roundn(mean(m2x((round(1.4/Ts)):round(1.6/Ts))),-2);
%     vmeanspy2 = roundn(mean(m2y((round(1.4/Ts)):round(1.6/Ts))),-2);

figure(2)
    m1xp = m1x.*2.62; m1yp = m1y.*2.62;
    subplot(2,1,1)
```

```
plot(tt,m1xp,tt,req_theta_y.*1000,tt,m1xc*2.62),grid,zoom,legend('Act','Req',
'Cmd')
    ylabel('fsm x pos, mrad')
    title('FSM pos vs. time')
    subplot(2,1,2)

plot(tt,m1yp,tt,req_theta_x.*1000,tt,m1yc*2.62),grid,zoom,legend('Act','Req',
'Cmd')
    ylabel('fsm y pos, mrad')
    xlabel('time,sec')
end
%-------------------------------------------------------------------------
if OT_plot==1;
%figure('Name','OT Plot','NumberTitle','on')
figure(3)
    subplot(2,1,1)
    plot(tt,(ot1y-mean(ot1y)),tt,(ot2y-mean(ot2y)),tt,(ot3y-mean(ot3y)),...
        tt,(ot4y-mean(ot4y)),tt,(ot5y-mean(ot5y))),grid,zoom
    legend('ot1y','ot2y','ot3y','ot4y','ot5y')
    ylabel(['\mu','m '])
    title(['OT1,OT2,OT3 and OT4 PSD position in \mu','m '])
    subplot(2,1,2)
    plot(tt,(ot1x-mean(ot1x)),tt,(ot2x-mean(ot2x)),tt,(ot3x-mean(ot3x)),...
        tt,(ot4x-mean(ot4x)),tt,(ot5x-mean(ot5x))),grid,zoom
    legend('ot1x','ot2x','ot3x','ot4x','ot5x')
    %axis([tt(calc_sample) tt(plot_sample) -inf inf ])
    %axis([tt(calc_sample) tt(plot_sample) -50 250 ])
    ylabel(['\mu','m '])
    xlabel('time,sec')
end
%-------------------------------------------------------------------------
if OT3_pos==1;
%figure('Name','OT 3','NumberTitle','on')
figure(4)
    subplot(2,1,1)
    plot(tt,ot3x),grid,zoom
     ylabel(['x pos, \mu','m'])
     title('OT3 pos vs. time')

     subplot(2,1,2)
     plot(tt,ot3y),grid,zoom
     ylabel(['y pos, \mu','m'])
     xlabel('time,sec')
end
%-------------------------------------------------------------------------
% if acc==1
% %figure('Name','Accels','NumberTitle','on')
% figure(5)
%     subplot(3,1,1)
%     plot(tt,(a1x-mean(a1x)),tt,(a2x-mean(a2x)),tt,(a3x-
mean(a3x))),grid,zoom
%     xlabel('time,sec')
%     ylabel('Acceleration, g_x')
```

```
%     legend('A1x','A2x','A3x')
%     title('Accelerometer Output')
%     subplot(3,1,2)
%     plot(tt,(a1y-mean(a1y)),tt,(a2y-mean(a2y)),tt,(a3y-
mean(a3y))),grid,zoom
%     xlabel('time,sec')
%     ylabel('Acceleration, g_y')
%     legend('A1y','A2y','A3y')
%     %title('Accelerometer Output')
%     subplot(3,1,3)
%     plot(tt,(a1z-mean(a1z)),tt,(a2z-mean(a2z)),tt,(a3z-
mean(a3z))),grid,zoom
%     xlabel('time,sec')
%     ylabel('Acceleration, g_z')
%     legend('A1z','A2z','A3z')
%     title('Accelerometer Output')
% end
%-------------------------------------------------------------------------
if percent_imp==1;
%figure('Name','% imp','NumberTitle','on')
figure(6)
subplot(2,1,1)
    plot(tt1,ot5yex,tt1,ot5yplt),grid,zoom
    title(['36 stage ',char(title_ctr),' Controller: Improvement: X  ',...
            num2str(impx),' %, Y  ',num2str(impy),' %   Mean X :
',num2str(meanx),' nm  Y : ',num2str(meany),...
            ' nm ',char(title_error)])
    %text(0.01,20,' X Axis','FontWeight','bold')
    %title('35 Hz vibration signal - amplitude 1.3 V')
    legend('input jitter','controlled beam')
    ylabel(['y-pos, \mu','m'])
    %axis([tt(calc_sample) tt(plot_sample) -inf inf ])
    axis([tt(calc_sample) tt(plot_sample) -100 y_plot_bias+pbiasy ])
    subplot(2,1,2)
    plot(tt1,ot5xex,tt1,ot5xplt),grid,zoom
    title(['Std Dev of error: X Axis input - ',num2str(xstdin),'\mu, Output -
',num2str(xstd),...
            '\mu; Y Axis input - ',num2str(ystdin),'\mu, Output -
',num2str(ystd),'\mu'])
    %text(0.01,20,' Y Axis','FontWeight','bold')
    legend('input jitter','controlled beam')
    %axis([tt(calc_sample) tt(plot_sample) -inf inf ])
    axis([tt(calc_sample) tt(plot_sample) -100 x_plot_bias+pbiasx ])
    ylabel(['x pos, \mu','m'])
    xlabel('time,sec')
end
%-------------------------------------------------------------------------
if powerplot==1;
%figure('Name','Laser Pwr','NumberTitle','on')
figure(7)
    ystart=mean_start_power-0.10*mean_start_power;
    yend=mean_start_power+0.02*mean_start_power;
    laser_smooth=smooth(laser_power,150);
    plot(tt,laser_smooth*1000),grid,zoom
```

```
    %plot(tt,laser_power*1000),grid,zoom
    axis([-inf inf  ystart yend ])
    title(['Laser power - ','starting power: ',num2str(mean_start_power),...
        '\mu W; disturbed power: ',num2str(mean_dist_power),'\mu W;
recovered power: '...
        num2str(mean_rec_power),'\mu W (using a 150 pt moving avg filter)'])
    ylabel(['power, \mu','W'])
    xlabel('time,secs')
    line([shaker_start shaker_start],[ystart yend],'color','r')
    line([adapt adapt],[ystart yend],'color','g')
    text(shaker_start,yend-5,['Start vibration
\rightarrow'],'HorizontalAlignment','right','VerticalAlignment','bottom','Fon
tWeight','bold')
    text(adapt,yend-5,['\leftarrow Controller start
'],'HorizontalAlignment','left','VerticalAlignment','bottom','FontWeight','bo
ld')
end
%-------------------------------------------------------------------------
if fsm_cmd==1;
%figure('Name','FSM Cmd','NumberTitle','on')
figure(8)
    subplot(2,1,1)
        plot(tt,m1xc,tt,m1yc),grid,zoom
        legend('FSMAcmdx','FSMAcmdy')
        xlabel('time,secs')
        ylabel('FSMA cmd, volts')
        title('FSMA command voltage')
    subplot(2,1,2)
        plot(tt,m2xc,tt,m2yc),grid,zoom
        legend('FSMBx','FSMBy')
        xlabel('time,secs')
        ylabel('FSMB cmd, volts')
        title('FSMB command voltage')
end
%-------------------------------------------------------------------------
if psd_plt_x==1;
%figure('Name','Accelx OTx PSD','NumberTitle','on')
figure(9)
    subplot(2,1,1)
        plot(ff,Pa1x,ff,Pa2x),grid,zoom
        title('Spectral Density a1x and a2x - Accel. in X direction')
        xlabel('frequency, Hz')
        ylabel('dB/Hz')
        legend('accel 1','accel 2')
    subplot(2,1,2)
        plot(ff,Pot1x),grid,zoom
        title('Spectral Density OT1x - displacement in X direction')
        xlabel('frequency, Hz')
        ylabel('dB/Hz')
        legend('Source')
end
%-------------------------------------------------------------------------
if psd_plt_y==1;
window = 8192/2; nfft=[];       %   Window and size of FFT
```

```
%     [Pa2x,ff]=periodogram(a2x,nfft,'onesided',window,Fs);
Pa2x=10*log10(Pa2x);
%     [Pa2y,ff]=periodogram(a2y,nfft,'onesided',window,Fs);
Pa2y=10*log10(Pa2y);
%
[Pot5y,ff]=periodogram(ot5y,nfft,'onesided',window,Fs);Pot5y=10*log10(Pot5y);
%
[Pot5x,ff]=periodogram(ot5x,nfft,'onesided',window,Fs);Pot5x=10*log10(Pot5x);
    noverlap = [];
%     [Pa2x,ff]=pwelch(a2x(5/Ts:end),window,noverlap,nfft,Fs);
Pa2x=10*log10(Pa2x);
%     [Pa2y,ff]=pwelch(a2y(5/Ts:end),window,noverlap,nfft,Fs);
Pa2y=10*log10(Pa2y);
    %  Subtract calibration if FFD
    %if (x_ffd_sel|A_ffd_sel)==1;
    [Pot5y,ff]=pwelch((ot5y(3/Ts:end)-
(cal_tgty*500)),window,noverlap,nfft,Fs);Pot5y=10*log10(Pot5y);
    [Pot5x,ff]=pwelch((ot5x(3/Ts:end)-
(cal_tgtx*500)),window,noverlap,nfft,Fs);Pot5x=10*log10(Pot5x);
%     if h_Pot5x == [];h_Pot5x = Pot5x;end;
%     if h_Pot5y == [];h_Pot5y = Pot5y;end;
    %else
%
[Pot5y,ff]=pwelch((ot5y(5/Ts:end)),window,noverlap,nfft,Fs);Pot5y=10*log10(Po
t5y);
%
[Pot5x,ff]=pwelch((ot5x(5/Ts:end)),window,noverlap,nfft,Fs);Pot5x=10*log10(Po
t5x);
%     end
%figure('Name','OT 1,2 PSD','NumberTitle','on')
figure(10)
    subplot(2,1,1)
        plot(ff,h_Pot5x,ff,Pot5x,ff,h_arsx,ff,h_psdx),grid,zoom
        %plot(ff,Pot3x,ff,Pa1x),grid,zoom
        %title('Spectral Density OT1 and OT2 - Accel. in Y direction')
        title(['Power Spectral Density using Welchs method with window length
= ',num2str(window),' - OT5x '])
        xlabel('frequency, Hz')
        ylabel('dB/Hz')
        legend('Uncontrolled','Controlled','ARS','PSD')
        axis([0 100 -inf inf]);
    subplot(2,1,2)
        %plot(ff,Pot3x,ff,Pot3y),grid,zoom
        plot(ff,h_Pot5y,ff,Pot5y,ff,h_arsy,ff,h_psdy),grid,zoom
        title('Power Spectral Density using Welchs method - OT5y ')
        xlabel('frequency, Hz')
        ylabel('dB/Hz')
        legend('Uncontrolled','Controlled','ARS','PSD')
        axis([0 100 -inf inf]);
end
%-------------------------------------------------------------------------
if psd_plt_z==1;
figure(11)
    plot(ff,Pa1y,ff,Pa2y),grid,zoom
```

```
    title('Spectral Density a1y and a2y - Accel. in Z direction')
    xlabel('frequency, Hz')
    ylabel('dB/Hz')
    legend('accel 1','accel 2')
end
%-------------------------------------------------------------------------
if OT1_pos==1;
%figure('Name','OT 1','NumberTitle','on')
figure(12)
    subplot(2,1,1)
    plot(tt,ot1x),grid,zoom
     ylabel(['x pos, \mu','m'])
     %xlabel('x pos, micrometers')
     title('OT1 pos on detector vs. time')
     %axis([-1 1 -1 1]);
     %axis equal
     subplot(2,1,2)
    plot(tt,ot1y),grid,zoom
     ylabel(['y pos, \mu','m'])
     xlabel('time,sec')
     %legend('ot3y','ot3x')
     %axis([-1 1 -1 1]);
end
%-------------------------------------------------------------------------
if OT2_pos==1;
    meanstx = roundn(mean(ot2x(round(0.9/Ts):round(1.0/Ts))),-2);
    meansty = roundn(mean(ot2y(round(0.9/Ts):round(1.0/Ts))),-2);
    meanspx = roundn(mean(ot2x((round(1.03/Ts)):round(1.1/Ts))),-2);
    meanspy = roundn(mean(ot2y((round(1.03/Ts)):round(1.1/Ts))),-2);
%figure('Name','OT 2','NumberTitle','on')
figure(13)
    subplot(2,1,1)
    plot(tt,ot2x),grid,zoom
     ylabel(['x pos, \mu','m'])
     %xlabel('x pos, micrometers')
     title('OT2 pos on detector vs. time')
     %axis([-inf inf 50 75]);
     %axis equal
     %title(['Step Response: X Axis start : ',num2str(meanstx),'\mu, end :
',num2str(meanspx),...
      %      '\mu; Y Axis start : ',num2str(meansty),'\mu, end :
',num2str(meanspy),'\mu'])
     subplot(2,1,2)
    plot(tt,ot2y),grid,zoom
     ylabel(['y pos, \mu','m'])
     xlabel('time,sec')
     %legend('ot3y','ot3x')
     %axis([-1 1 -1 1]);

end
%-------------------------------------------------------------------------
if OT4_pos==1;
%figure('Name','OT 4','NumberTitle','on')
figure(14)
```

```
    subplot(2,1,1)
    plot(tt,ot4x/500),grid,zoom
     ylabel(['x pos, \mu','m'])
     %xlabel('x pos, micrometers')
     title('OT4 pos on detector vs. time')
     %axis([-1 1 -1 1]);
     %axis equal
     subplot(2,1,2)
    plot(tt,ot4y),grid,zoom
     ylabel(['y pos, \mu','m'])
     xlabel('time,sec')
     %legend('ot3y','ot3x')
     %axis([-1 1 -1 1]);
end
%-------------------------------------------------------------------------
if OT5_pos==1;
%figure('Name','OT 5','NumberTitle','on')
figure(15)
    subplot(2,1,1)
%     plot(tt,-ot5x/500),grid,zoom
plot(tt,ot5x),grid,zoom
    %title(['Target X pos vs. time - ','Std Dev: X Axis -
',num2str(xstdin),'\mum'])
     ylabel(['x pos, \mu','m'])
     %legend('ot5x','x_pred')
     %xlabel('x pos, micrometers')
     %title('OT5 pos on detector vs. time')
     %axis([-1 1 -1 1]);
     %axis equal
     subplot(2,1,2)
    plot(tt,ot5y),grid,zoom
    %title(['Target Y pos vs. time - ','Std Dev: Y Axis -
',num2str(ystdin),'\mum'])
     ylabel(['y pos, \mu','m'])
     xlabel('time,sec')
     %legend('ot5y','y_pred')
     %axis([-1 1 -1 1]);

end
%-------------------------------------------------------------------------
if OT_plot_compare==1;
figure(16)
    subplot(2,1,1)
    plot(tt,ot5x,tt,x_pred),grid,zoom
    legend('measured x','predicted x')
    ylabel(['\mu','m '])
    title(['Beam Position at Target Measured vs Predicted in \mu','m '])
    subplot(2,1,2)
    plot(tt,ot5y,tt,y_pred),grid,zoom
    legend('measured y','predicted y')
    ylabel(['\mu','m '])
    xlabel('time,sec')
end
%-------------------------------------------------------------------------
```

```
if test_inp==1;
figure(17)
    plot(tt,xtest,tt,ytest),grid,zoom
    %plot(tt,-100*IA_1_input,tt,ot5y),grid,zoom
    legend('xtest','ytest')
    xlabel('time,secs')
    ylabel('test input, 1000 \muvolts, and displacement, \mu m')
    title('input - output')
end
%-------------------------------------------------------------------------
if rot==1;
figure(18)
    plot(tt,pitch_rate,tt,roll_rate,tt,yaw_rate),grid,zoom
    legend('pitch rate','roll rate','yaw rate')
    xlabel('time,secs')
    ylabel('\murads/sec')
    title('Rotational Rates')
end
%-------------------------------------------------------------------------
if rotations==1;
figure(19),
    subplot(3,1,1)
    plot(tt,pitch_1,tt,pitch_2,tt,pitch_3),grid,zoom
    legend('pitch PSD','pitch integ ARS','pitch pred ARS')
    xlabel('time,secs')
    ylabel('\murads')
    title({'Plate Rotations','',[' ARS Rotation Measurement Error: Pitch
',...
            num2str(rot_error_pitch),' %, Roll  ',num2str(rot_error_roll),...
            ' %, Yaw  ',num2str(rot_error_yaw),' %']});
        subplot(3,1,2)
    plot(tt,roll_1,tt,roll_2,tt,roll_3),grid,zoom
    legend('roll PSD','roll integ ARS','roll pred ARS')
    xlabel('time,secs')
    ylabel('\murads')
        subplot(3,1,3)
    plot(tt,yaw_1,tt,yaw_2,tt,yaw_3),grid,zoom
    legend('yaw PSD','yaw integ ARS','yaw pred ARS')
    xlabel('time,secs')
    ylabel('\murads')
end
%-------------------------------------------------------------------------
if rot_cal==1;
figure(20),title('Plate Rotation Rates')
    subplot(3,1,1)
    plot(tt,pitch_rate_calibrated),grid,zoom
    legend('pitch rate')
    xlabel('time,secs')
    ylabel('\murads/sec')
        subplot(3,1,2)
    plot(tt,roll_rate_calibrated),grid,zoom
    legend('roll rate')
    xlabel('time,secs')
    ylabel('\murads/sec')
```

```
        subplot(3,1,3)
    plot(tt,yaw_rate_calibrated),grid,zoom
    legend('yaw rate')
    xlabel('time,secs')
    ylabel('\murads/sec')
end
%-------------------------------------------------------------------------
if jitter==1,'Color',[0 0.502 0]
    figure(21)
    plot(tt,ot5j,tt,rmean_jitter),grid,legend('Jitter Angle')
    title(['Percent Improvement in Mean Jitter Angle =
',num2str(imp_mean_jitter,4),'%'...
        ' , ',num2str(Mean_jitter_after,4),' \murad'])
    xlabel('sec'),ylabel('\murad'),axis([-inf inf -inf inf]);
end
%-------------------------------------------------------------------------
if temp==1
    figure(22)
    plot(tt,temp1,tt,temp2),grid,legend('temp1','temp2')
    xlabel('sec'),ylabel('deg C')
end

% figure(23)
% plot(tt,filterin,tt,filterout),grid,zoom
% legend('filter in','filter out')
% xlabel('sec')
% ylabel('Volts')
%plot accelerometers
% figure(99)
% subplot(3,1,1)
% plot(tt,a_pitch_accel,tt,a_roll_accel,tt,a_yaw_accel)
% legend ('pitch accel','roll accel','yaw accel')
% subplot(3,1,2)
% plot(tt,a_pitch_rate,tt,a_roll_rate,tt,a_yaw_rate)
% legend ('pitch rate','roll rate','yaw rate')
% subplot(3,1,3)
% plot(tt,a_pitch_angle,tt,a_roll_angle,tt,a_yaw_angle)
% legend ('pitch angle','roll angle','yaw angle')
% figure(99)
% subplot(3,1,1)
% plot(tt,ARSaccel_pitch_angle,tt,pitch_3,tt,pitch_1)
% legend ('ARS+accel pitch','ARS pitch','PSD pitch')
% subplot(3,1,2)
% plot(tt,ARSaccel_roll_angle,tt,roll_3,tt,roll_1)
% legend ('ARS+accel roll','ARS roll','PSD roll')
% subplot(3,1,3)
% plot(tt,ARSaccel_yaw_angle,tt,yaw_3,tt,yaw_1)
% legend ('ARS+accel yaw','ARS yaw','PSD yaw')

% figure(19),
%     subplot(3,1,1)
%     plot(tt,pitch_3),grid,zoom
%     legend('pitch ARS')
%     xlabel('time,secs')
```

```
%     ylabel('\murads')
%     title('Plate Rotations');
%         subplot(3,1,2)
%     plot(tt,roll_3),grid,zoom
%     legend('roll ARS')
%     xlabel('time,secs')
%     ylabel('\murads')
%         subplot(3,1,3)
%     plot(tt,yaw_3),grid,zoom
%     legend('yaw ARS')
%     xlabel('time,secs')
%     ylabel('\murads')

% figure (97)
% subplot(2,1,1)
%     plot(tt,m2x),grid,zoom
%     legend('m2x')
%     xlabel('time,secs')
%     ylabel('\murads')
%     title('mirrors');
%         subplot(2,1,2)
%     plot(tt,m2y),grid,zoom
%     legend('m2y')
%     xlabel('time,secs')
%     ylabel('\murads')
%
%     figure (98)
% subplot(2,1,1)
%     plot(tt,m1x),grid,zoom
%     legend('m1x')
%     xlabel('time,secs')
%     ylabel('\murads')
%     title('mirrors');
%         subplot(2,1,2)
%     plot(tt,m1y),grid,zoom
%     legend('m1y')
%     xlabel('time,secs')
%     ylabel('\murads')

% figure(99)
%     subplot(2,1,1)
%         plot(tt,FSMAVx,tt,FSMAVy),grid,zoom
%         legend('FSMAVx','FSMAVy')
%         xlabel('time,secs')
%         ylabel('FSMA actual position, volts')
%         title('FSMA actual position voltage')
%     subplot(2,1,2)
%         plot(tt,FSMBVx,tt,FSMBVy),grid,zoom
%         legend('FSMBVx','FSMBVy')
%         xlabel('time,secs')
%         ylabel('FSMB actual position, volts')
%         title('FSMB actual position voltage')
% figure(101)
%     plot(tt,FSMBVx,tt,filterout,tt,filterin),grid,zoom
```

```
%     legend('FSMBVx','filter out','filterin')
%     xlabel('time, sec');ylabel('volts')
%% Post Process and Data Save (May Need to update Variables!)
% if pltfrf==1;
%     FRF_from_data2
% end
% %-------------------------------------------------------------------------
%Save Experimental Data
%savefile     = 1;   %   Set to one to save data

% %Change this folder location to where you want the data saved to!
% c1= 'C:\Documents and Settings\VIBES\My
Documents\Roberts\Summer2010\23AUG_c\ex';
%
% % savefile = input('Do you wish to save this data? y/n [n]: ','s');
% % if savefile=='y';
%     %reply1 = input('input experiment number   ','s');
%     %reply2 = input('input run number   ','s');
%     c2= '1';  c3='_run'; c4=num2str(ii);c5='.mat';c6='.fig';
%     strsave = strcat(c1,c2,c3,c4,c5);
%     if exist(strsave,'file')
%         reply3 = input('THIS FILE EXISTS - OK TO OVERWRITE?  y/n [n]:
','s');
%         if isempty(reply3);reply3='n';end
%         if reply3 ~= 'y';
%             beep
%             reply1 = input('input experiment number   ','s');
%             reply2 = input('input run number   ','s');
%             c2= reply1;  c4=reply2;
%             strsave = strcat(c1,c2,c3,c4,c5);
%         end
%     end
%     save(strsave,...
%
'tt','ot1y','ot1x','ot2y','ot2x','ot3y','ot3x','pitch_1','roll_1',...
%
'yaw_1','ot5y','ot5x','ot5j','temp1','temp2','pitch_rate','roll_rate',...
%         'yaw_rate')
%         'tt','ot5y','ot5x','ot3y','ot2y','ot1y','ot3x','ot2x','ot1x',...
%         'm1x','m1y','ot5ym','ot5xm','xtest','ytest','m2xc','m2yc',...
%
'y_pred','x_pred','ot4y','ot4x','a1x','a1y','a1z','a2x','a2y','a2z'...
%
,'a3x','a3y','a3z','cal_tgtx','cal_tgty','ot6x','ot6y','ot7x','ot7y',...
%         'pitch','roll','yaw')
       %'ot5ym','ot5xm','ot3ym','ot2ym','ot1ym','ot3xm','ot2xm','ot1xm',...
       %'delta_z','delta_x','delta_y','ot4ym','ot4xm'
%      savefig = input('Do you wish to save these figures (6,11,16)? y/n [n]:
','s');
%      if savefig=='y';
%          c7 = '_fig11';c8 = '_fig6';c9 = '_fig16';
%          figure(11);strsave2 =
strcat(c1,c2,c3,c4,c7,c6);saveas(gcf,strsave2);
```

```
%          figure(6);strsave2 =
strcat(c1,c2,c3,c4,c8,c6);saveas(gcf,strsave2)
%          figure(16);strsave2 =
strcat(c1,c2,c3,c4,c9,c6);saveas(gcf,strsave2)
%      end

% end
% %-------------------------------------------------------------------------
%end
% save noise_floor2.mat;

ot5r = (((ot5y-cal_ot5y*500).^2+(ot5x-cal_ot5x*(-500)).^2).^0.5); % miss dist
in um
ot5j = ot5r./dist_targ;  % jitter in urad
rmean_jitter=smooth(ot5j,300,'moving');

 figure(102)
 subplot(2,1,1)
 plot (tt,ot5x-((-500)*cal_ot5x))
 subplot(2,1,2)
 plot (tt,ot5y-cal_ot5y*500)

 figure(103)
 plot(tt,ot5r)

 %load systemARS10.mat
 figure(106)
 plot(tt,rmean_jitter);grid
%  hold on
%  load systemPSM10.mat
%  plot(tt,rmean_jitter);grid

beep;
home;
```

APPENDIX M: Soloist Script

```
' ------------------------------------------------
' ------------ LinearMotion.ab -------------
' ------------------------------------------------
'
' This program performs linear motion in
' simple point-to-point moves.
'
' For blended moves using velocity profiling,
' see the VelocityProfile.ab example.
'
' ------------------------------------------------

PROGRAM

   DIM Distance AS INTEGER

   Distance = 30

   ' Acknowledge any faults.
   FAULTACK

   ' Enable the axis.
   ENABLE

   ' Set the curve factor.
   ' This value ranges anywhere from 0 to 100.
   ' Any value outside this range is a runtime error.
   ' If the scurve is zero, the ramp up and ramp
   ' down is linear. If the value is 100,
   ' the ramp up and ramp down is parabolic.
   ' Any value between these values is the percentage
   ' of the ramp up and ramp down that is parabolic.
   SCURVE 100

   ' Execute the linear move with the given distance
   ' and speed. This type of linear move ramps up to
   ' travel the specified distance and ramps down to zero.
   LINEAR D 1*Distance F 5

   ' Move the double the distance in the opposite direction.
```

```
    LINEAR D (Distance * -2) F 5
          '
          'Return to start position
    LINEAR D 1*Distance F 5

'    ' A faster move.
'    LINEAR D Distance F 50
'
'    ' Move back again.
'    LINEAR D (Distance * -1) F 50

    ' Disable axis.
    DISABLE



END PROGRAM
```

APPENDIX N: Additional Simulink Blocks

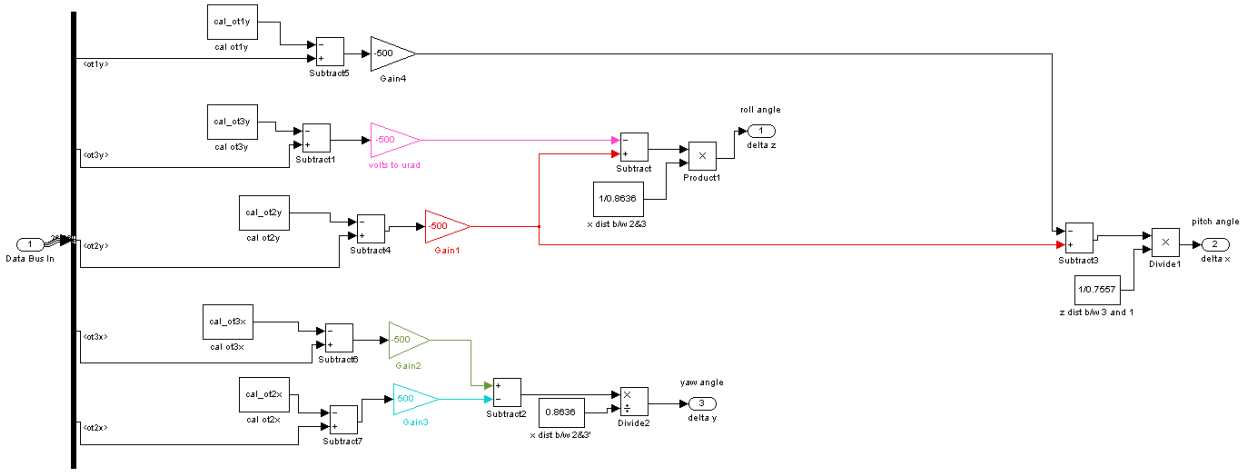

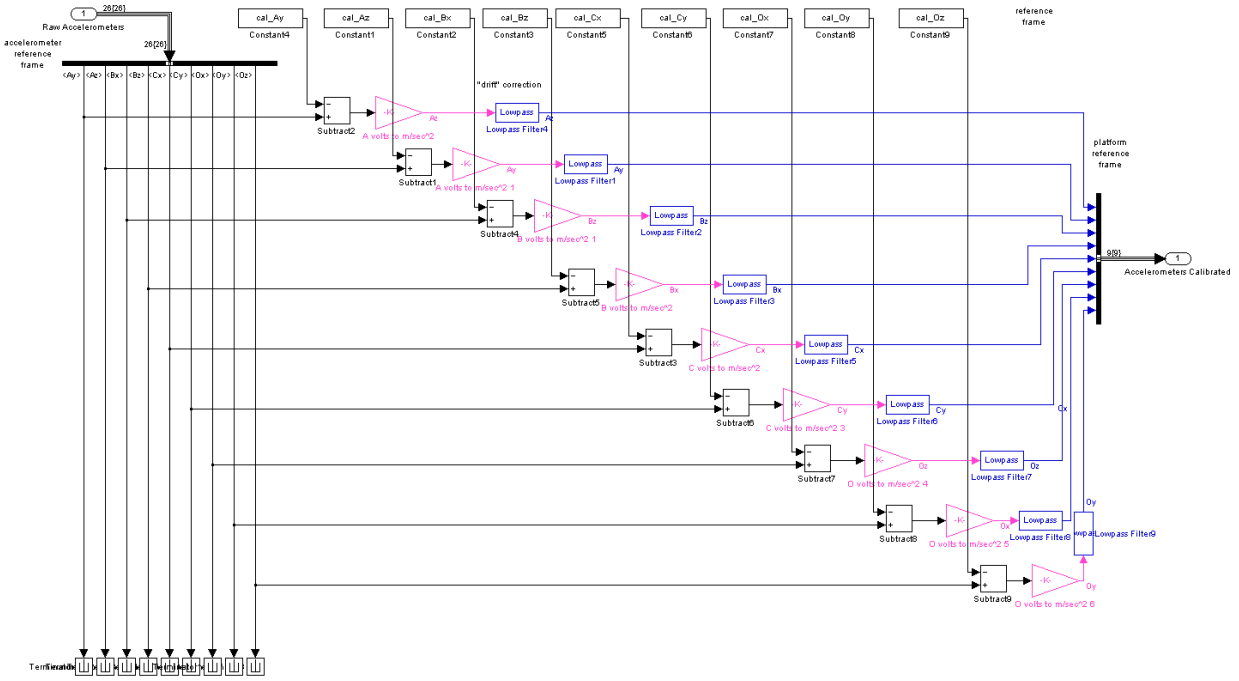

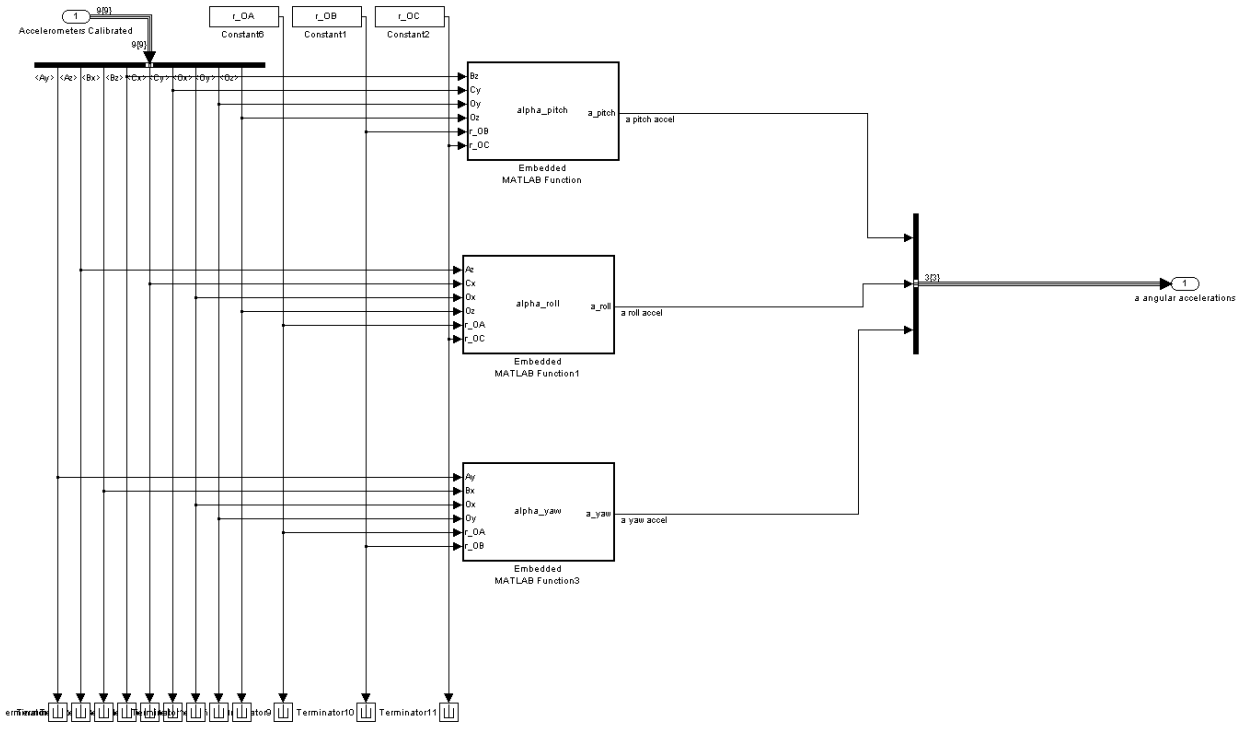
1
Accelerometers Calibrated
9[9]
r_OA
Constant6
r_OB
Constant1
r_OC
Constant2
<Ay> <Az> <Bx> <Bz> <Cx> <Cy> <Ox> <Oy> <Oz>
Bz
Cy
Oy
Oz
r_OB
r_OC
alpha_pitch
a_pitch
a pitch accel
Embedded
MATLAB Function
Az
Cx
Ox
Oz
r_OA
r_OC
alpha_roll
a_roll
a roll accel
Embedded
MATLAB Function1
Ay
Bx
Ox
Oy
r_OA
r_OB
alpha_yaw
a_yaw
a yaw accel
Embedded
MATLAB Function3
3[3]
1
a angular accelerations
Terminator10
Terminator11

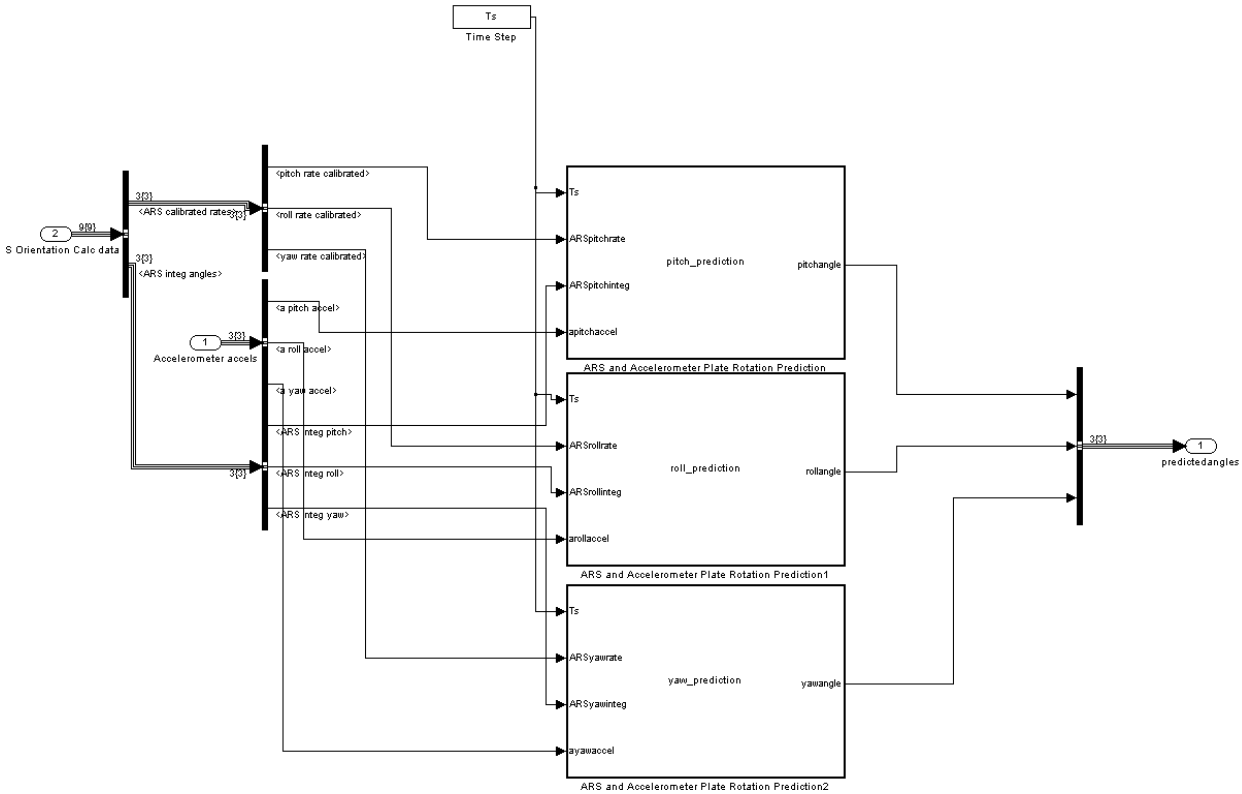
Ts
Time Step
2
9[9]
S Orientation Calc data
3[3]
<ARS calibrated rates>
<ARS integ angles>
<pitch rate calibrated>
<roll rate calibrated>
<yaw rate calibrated>
<a pitch accel>
1
Accelerometer accels
<a roll accel>
<a yaw accel>
<ARS integ pitch>
<ARS integ roll>
<ARS integ yaw>
Ts
ARSpitchrate
ARSpitchinteg
apitchaccel
pitch_prediction
pitchangle
ARS and Accelerometer Plate Rotation Prediction
ARSrollrate
ARSrollinteg
arollaccel
roll_prediction
rollangle
ARS and Accelerometer Plate Rotation Prediction1
ARSyawrate
ARSyawinteg
ayawaccel
yaw_prediction
yawangle
ARS and Accelerometer Plate Rotation Prediction2
predictedangles

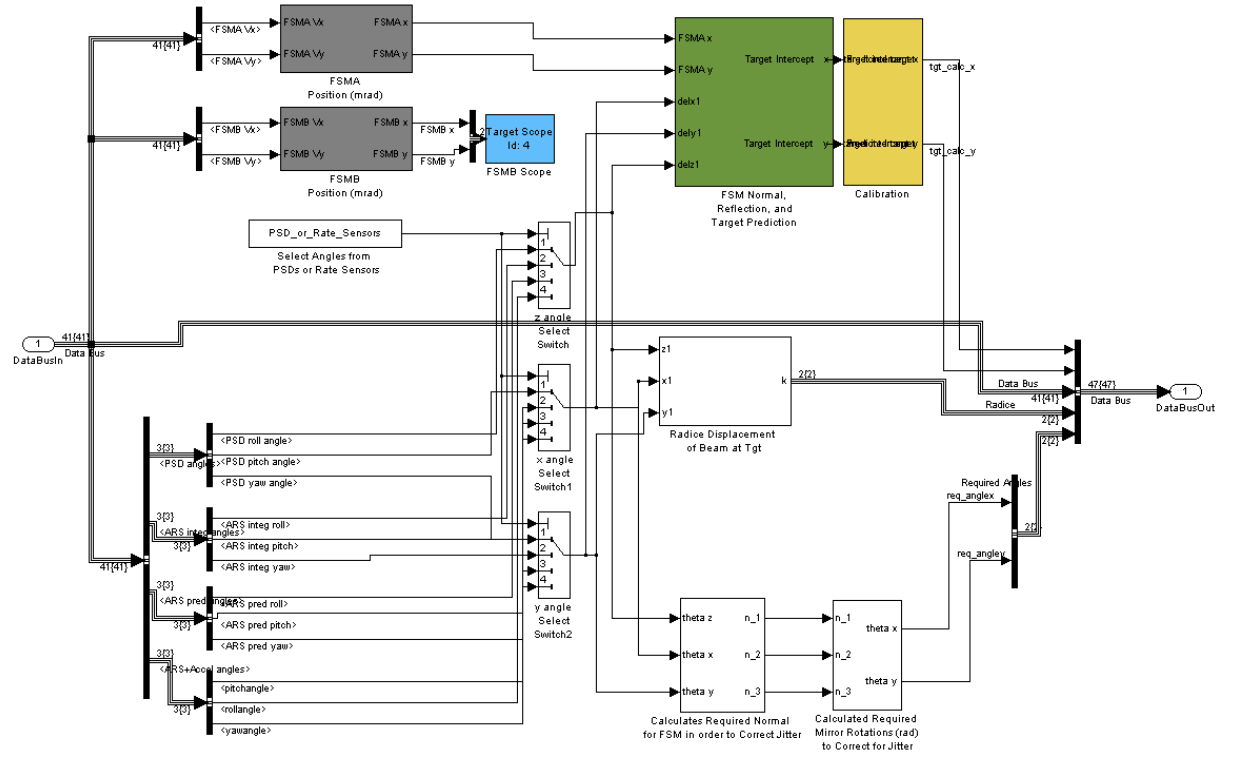
FSMA
Position (mrad)
FSMB
Position (mrad)
Target Scope
Id: 4
FSMB Scope
FSM Normal,
Reflection, and
Target Prediction
Calibration
tgt_calc_x
tgt_calc_y
PSD_or_Rate_Sensors
Select Angles from
PSDs or Rate Sensors
z angle
Select
Switch
x angle
Select
Switch1
y angle
Select
Switch2
DataBusIn
DataBusOut
Data Bus
Radice
Radice Displacement
of Beam at Tgt
Required Angles
req_anglex
req_angley
Calculates Required Normal
for FSM in order to Correct Jitter
Calculated Required
Mirror Rotations (rad)
to Correct for Jitter

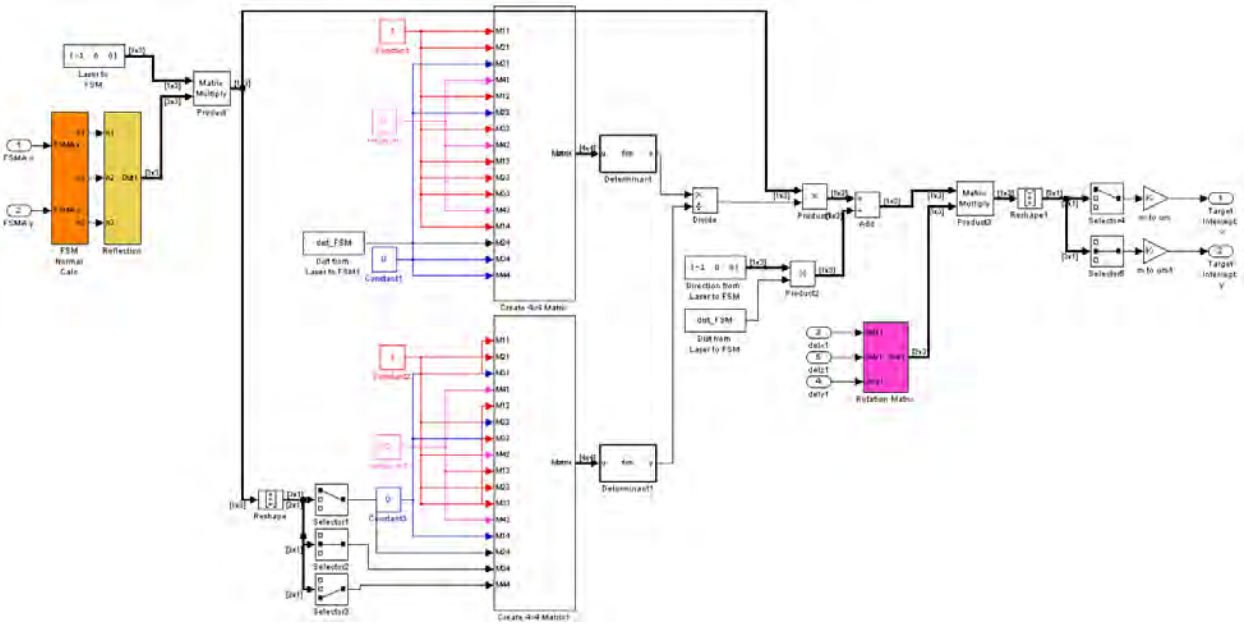

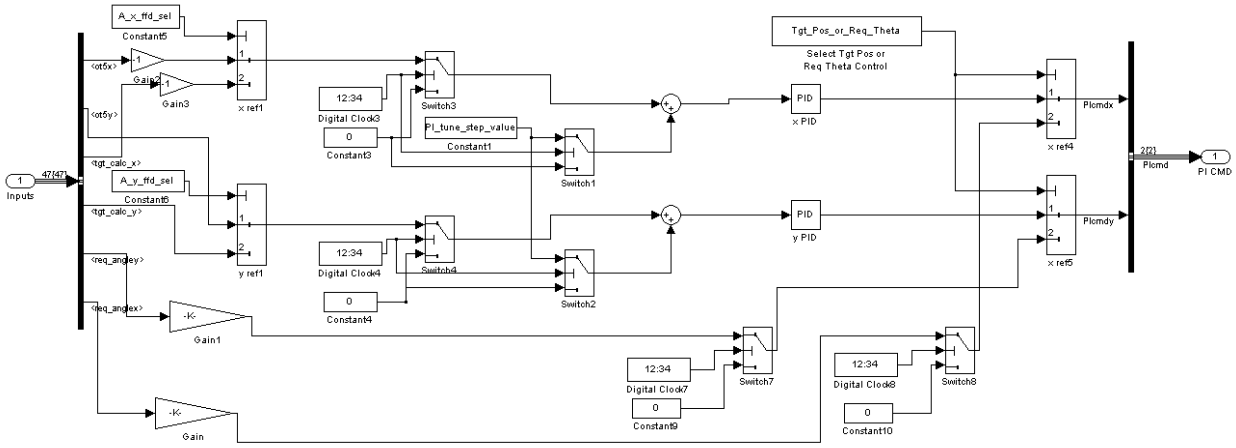
A_x_ffd_sel
Constant5
<ot5x>
Gain2
Gain3
x ref1
<ot5y>
<tgt_calc_x>
A_y_ffd_sel
Constant6
<tgt_calc_y>
y ref1
<req_angley>
<req_anglex>
-K-
Gain1
-K-
Gain
1
47[47]
Inputs
12:34
Digital Clock3
0
Constant3
Switch3
PI_tune_step_value
Constant1
Switch1
12:34
Digital Clock4
0
Constant4
Switch4
Switch2
Tgt_Pos_or_Req_Theta
Select Tgt Pos or
Req Theta Control
PID
x PID
PID
y PID
12:34
Digital Clock7
0
Constant9
Switch7
12:34
Digital Clock8
0
Constant10
Switch8
x ref4
Plcmdx
x ref5
Plcmdy
2[2]
Plcmd
1
PI CMD